The Modelling and Simulation of Passive Bistatic Radar

Yik Ling Lim

Thesis submitted for the degree of

Master of Philosophy

School of Electrical and Electronic Engineering

The University of Adelaide

South Australia 5005

March 2013

Contents

Abstract

Passive radar systems use illuminations by transmitters of opportunity, such as digital audio broadcasts (DAB), to detect and track targets. In bistatic radar systems, the transmitting and receiving antennas are separate and widely spaced. In an era of strong demand for enhanced surveillance, proponents of passive bistatic radar (PBR) technology assert that it offers many benefits, in particular the use of already existing transmitters. PBR systems suffer from high system complexity however. This presents challenges for PBR designers and researchers, as testing ideas experimentally is prohibitively expensive.

Direct signal interference (DSI) is a major problem in all passive radar systems and occurs when the direct signals transmitted by the illuminators are stronger than the target return signals. This can lead to a large reduction in the dynamic range that is available for target detection. DAB networks are particularly problematic because there are often a large number of illuminators present that are transmitting virtually identical signals at the same frequency.

This thesis describes the development of a realistic model/simulator for a general PBR system that can be used to develop radar algorithms, DSI mitigation techniques and optimise the design of radar systems. The simulator can be applied to multi-transmitter/multi-receiver systems, which allows researchers to test ideas without building equipment.

In this thesis, a brief introduction is given to PBR, including its history, challenges and an overview of radar modelling and simulation. A rudimentary PBR model is then described and verified by comparison of a simulated radar signal produced by the model with that of an off-the-air radar signal.

The rudimentary model is made more realistic by the addition of more sophisticated propagation effects, namely, diffraction, multipath and depolarisation. Further enhancements are made with the development of radar cross section and antenna gain components. The model is then used to simulate a number of realistic scenarios involving typical aircraft flight paths around the University of Bath in the UK.

Finally, the model is applied to the testing of a DSI mitigation technique, namely, shielding by topography, using the Bath region as a test case. The success of the simulation results suggests that the technique can be used in the Adelaide area of South Australia.

The simulator serves as a virtual multi-static environment for developing applications such as a tracker. A tracker would need to function in a variety of situations, and its operation would be affected by factors such as terrain and DSI. A detailed knowledge of the propagation environment would be necessary for the development of such a tracker, and the simulator can provide this knowledge.

Statement of Originality

This work contains no material which has been accepted for the award of any other degree or diploma in any university or other tertiary institution to Yik Ling Lim and, to the best of my knowledge and belief, contains no material previously published or written by another person, except where due reference has been made in the text.

I give consent to this copy of my thesis when deposited in the University Library, being made available for loan and photocopying, subject to the provisions of the Copyright Act 1968.

I also give permission for the digital version of my thesis to be made available on the Web, via the University's digital research repository, the Library catalogue, the Australasian Digital Theses Program (ADTP) and also through web search engines, unless permission has been granted by the University to restrict access for a period of time.

Signed: …….. **Date:** …….

Acknowledgements

I wish to sincerely thank my supervisors A/Prof Coleman and Dr Tamath Rainsford for their guidance and support, and the staff of the School of Electrical and Electronic Engineering and the University of Adelaide for their help throughout this project.

I would also like to express my deep gratitude for the assistance of Dr Robert Watson and the staff at the University of Bath in the collection of vital DAB data. Many thanks to Dave Darlington and the staff of the British Broadcasting Corporation for providing invaluable antenna data.

I gratefully acknowledge the funding provided by the Australian Postgraduate Award, the University of Adelaide School of Electrical and Electronic Engineering, the D R Stranks Postgraduate Travelling Fellowship, the Research Abroad Scholarship, the IEEE South Australia Section Student Travel Assistance Fund and the Walter and Dorothy Duncan Trust Student Travel Grant.

Last but not least, my heartfelt thanks to my family and friends for their unwavering love and support.

List of Figures

List of Tables

List of Abbreviations

ADC	Analog-to-digital converter
AOA	Angle of arrival
ARD	Amplitude range-Doppler
CBD	Central business district
CFAR	Constant false alarm rate
COFDM	Coded orthogonal frequency division multiplexing
CW	Continuous wave
DAB	Digital audio broadcast
DR	Dynamic range
DSI	Direct signal interference
DTED	Detailed terrain elevation data
DTV-T	Digital television – terrestrial
DVB	Digital video broadcast
FM	Frequency modulation
GPS	Global positioning system
GSM	Global system for mobile
LOS	Line-of-sight
NEC	Numerical electromagnetics code
PBR	Passive bistatic radar
PE	Parabolic equation
RC	Radar channel
RCS	Radar cross section
SIR	Signal to interference ratio
UHF	Ultra high frequency
UK	United Kingdom
VHF	Very high frequency

1 Introduction

1.1 Overview of Passive Radar

Unlike an active radar system, a passive radar system does not have a dedicated transmitter. Such radar systems use illuminations by transmitters of opportunity, such as commercial broadcasts and communications signals, to detect and track targets. To calculate the bistatic range of a target, the receiver measures the time difference of arrival between the signal arriving via reflection from the target and the signal arriving directly from the transmitter. A passive radar will also typically determine the location, heading and speed of the target. These quantities are calculated using the bistatic Doppler shift and direction of arrival of the echo signal.

In a passive radar system, the time of transmission of the pulse and the transmitted waveform are often not known. A dedicated receiver channel (called the "reference channel") is therefore needed to monitor each transmitter being used, and to dynamically sample the transmitted waveform. A typical passive radar first receives the direct signal from the transmitter(s) and surveillance region using low-noise, linear, digital receivers. Digital beamforming is then carried out to calculate the direction of arrival of signals and to perform spatial rejection of strong in-band interference. Any unwanted direct signal returns in the surveillance channel(s) are cancelled with adaptive filtering. Transmitter-specific signal conditioning then follows. To find the target bistatic range and Doppler, the reference channel is correlated with the surveillance channels. Next, a constant false alarm rate (CFAR) scheme is employed for cross-correlation of detection. Association and tracking of target returns in the range/Doppler space are then performed. Finally, the last estimate of a target's location, heading and speed is calculated by association and fusion of line tracks from each transmitter.

In bistatic radar systems, the transmitting and receiving antennas are separate and widely spaced. This is in contrast to monostatic radar, which uses a single transmit/receive antenna [1]. In a monostatic radar system, the co-located transmit/receive antenna first functions as a transmitter, sending a pulsed signal to the target. The signal is reflected and sent back as an echo signal to the antenna, which then acts as a receiver. By measuring the time taken for the pulse to travel to the target and back, the range of the target can be determined. In a bistatic radar system, the transmitter and receiver are located a distance apart that is comparable to the expected target distance [2]. The transmitted signal from the transmitter reaches the target and the reflected echo signal travels to the receiver. In addition, there is a direct signal between the transmitter and receiver. Figure 1 shows the difference between the monostatic and bistatic cases.

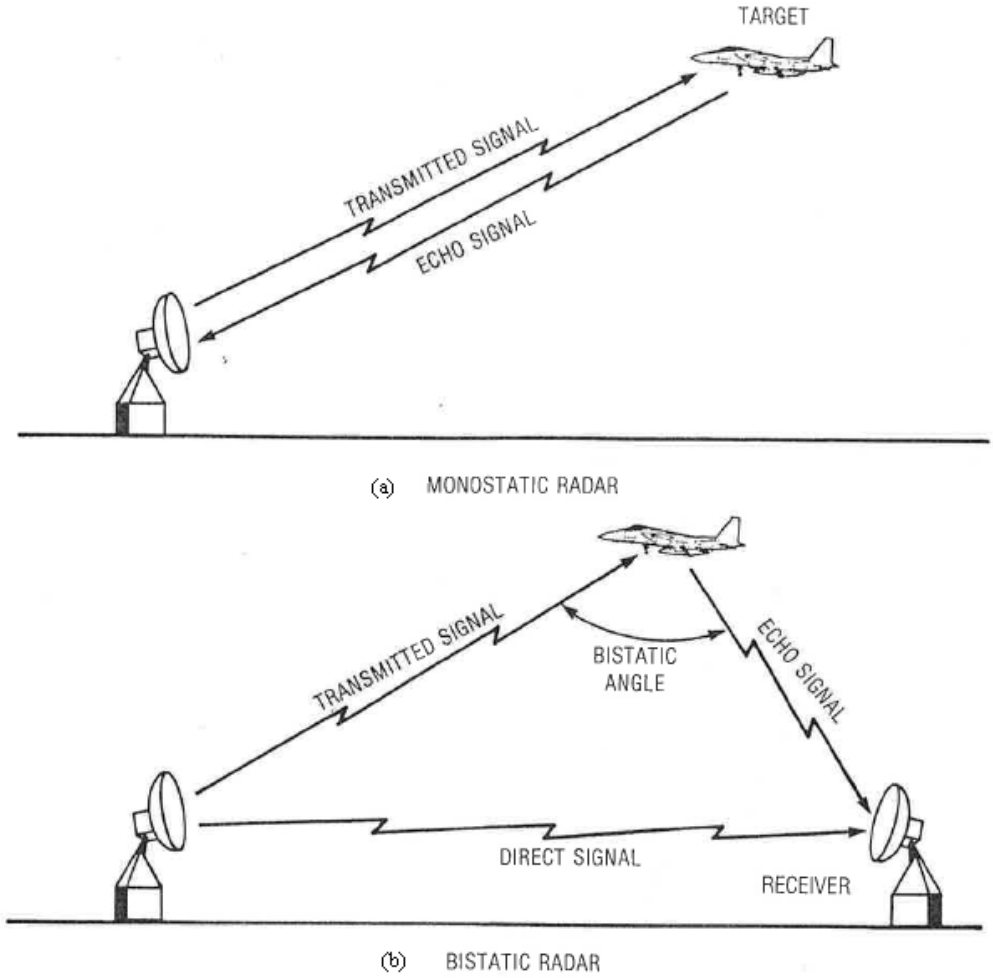

Figure 1 - (a) Monostatic radar uses a single transmit/receive antenna (b) Bistatic radar has separate transmitting and receiving antennas that are widely spaced

In an era of strong demand for enhanced surveillance, particularly in military applications, proponents of passive bistatic radar (PBR) technology assert that it offers a range of benefits, including frequency diversity and new electronic countermeasures challenges. It has been claimed that PBR systems are difficult to locate (hence can be used in covert operations) and present improved detection of low-observable targets [3]. The counter-stealth capability of PBR arises from the fact that target shaping to decrease target monostatic radar cross section (RCS) will in general not decrease the bistatic RCS [4]. PBR systems have enhanced resilience to electronic countermeasures because the waveform being used and the location of the receiver are potentially unknown. There are many analogue and digital very high frequency (VHF) radio and ultra high frequency (UHF) television transmissions available at high power and such frequencies may be utilised to detect stealthy targets. This is because, in addition to the advantage enjoyed by the bistatic geometry, the methods of target radar signature reduction employed are less effective at low frequencies than at microwave frequencies [5].

Other advantages of PBR cited include lower costs for procurement, operation and maintenance (due to the absence of a transmitter and moving parts, and the lack of a need to allocate an appropriate frequency band for the radar) [6], rapid updates (typically once a second), difficulty of jamming, and resistance

to anti-radiation missiles. Because of geometrical effects, it is possible that the target will have improved RCS. Furthermore, multiple receivers can be used, with each one forming a bistatic radar with the single transmitter. This provides the opportunity for tailored coverage and a richer source of information to enable more accurate location, high resolution imaging and target reconstruction [7]. The use of systems based on unmanned air vehicles has become more common, making PBR systems attractive. Also, the extra degrees of freedom offered by PBR makes it simpler to extract information from bistatic clutter in remote sensing applications [8].

As with any technology, there is a price associated with its advantages. In the case of PBR, the price is an increase in system complexity and processing. Opponents of PBR technology list other disadvantages as immaturity, the complexity of deployment, two-dimensional operation, and dependence on third-party illuminators. The geometry of bistatic systems is more complicated than that of monostatic systems. There is also a need to incorporate some form of synchronisation between transmitter and receiver, in respect of transmitter azimuth angle, instant of pulse transmission, and (for coherent processing) transmit signal phase. For receivers that use transmitters scanning in azimuth, there will probably be 'pulse chasing' processing involved [4]. The global positioning system (GPS) has made many of the synchronisation and geolocation problems that were previously very difficult more soluble [8]. Beam pointing is more difficult to implement. There is decreased low-level coverage because of the requirement for line-of-sight (LOS) communication between several locations. In addition, the location of the transmitter and the form of the transmission to be exploited are no longer under the control of the radar designer.

Some applications of PBR are air-space surveillance, maritime surveillance, atmospheric studies, ionospheric studies, oceanography, mapping lightning channels in thunderstorms and monitoring radioactive pollution. There have also been reports of algorithm development for interferometry, target tracking and target classification [7].

1.2 A Brief History of Passive Radar

The first passive radar experiments were performed in 1935 in Daventry, the United Kingdom, by Robert Watson-Watt, who demonstrated the detection of a Heyford bomber at a range of about eight miles using reflections of the British Broadcasting Corporation (BBC) shortwave broadcast six miles away [9].

During the early 1930s, the technology that allows an antenna to be switched from transmit to receive mode did not yet exist. As a result, early radars were all bistatic and many countries developed bistatic systems in their air defence networks during this period. For example, the British used the Chain Home system; the French developed a bistatic Continuous Wave (CW) radar in a "fence" (or "barrier") system; the Soviet Union deployed a bistatic CW system designated the RUS-1; and the Japanese used a bistatic CW radar called "Type A".

The Germans deployed a passive bistatic system, called the Kleine Heidelberg device, to detect aircraft over the southern part of the North Sea during World War II. This system operated at seven sites as bistatic receivers, and used the British Chain Home radars as non-cooperative illuminators.

The development of the synchroniser in 1936 saw the rise in popularity of monostatic systems. This was because monostatic systems removed the geometric complexities due to the separate transmitter and receiver sites, making the implementation of monostatic systems much more straightforward. Bistatic systems were not considered again until the early 1950s, with the discovery of some interesting properties of the scattered radar energy.

In 1955, the United States developed a bistatic system called the AN/FPS-23 fluttar radar for the North American Distant Early Warning (DEW) Line. The CW fixed-beam bistatic fence radar detected low-flying bombers that penetrated the DEW line, and covered the low-altitude gaps between SENTINEL monostatic surveillance radars. Fluttar radars were in use on the DEW line for about five years.

There was some amateur radio interest in passive radar in the 1960s, but apart from that, the technology was largely neglected for about 50 years after the Daventry experiments.

In the 1980s, interest in passive radar technology was resurrected with the increase in availability of low-cost computing power and powerful digital receiver technology. Designers could now exploit a range of broadcast signals using digital signal processing techniques. In addition, cross-correlation techniques could be applied to obtain enough signal processing gain for target detection and the estimation of target bistatic range and Doppler shift.

By the early 1990s, there was another resurgence of interest in passive radar. This was due to the accessibility of cheap analogue-to-digital converters with high enough sample rates and dynamic range to analyse the Doppler shifted echoes of the sound and vision carriers of analogue TV signals [9].

Several nations have had classified passive radar development programmes. In 1998, Lockheed-Martin Mission Systems was the first to announce a commercial system, with the launch of the Silent Sentry system. This system exploits Frequency Modulation (FM) radio and analogue television transmitters. A number of other commercial organisations have publicly announced the development of passive radar systems. These include BAE Systems' CELLDAR, which uses Global System for Mobile (GSM) communications basestations, and Thales Air Systems' Homeland Alerter, an FM radio-based system [10].

The first decade of the 21st century saw an upsurge in passive radar development with the emergence of hardware such as high-speed processors and high dynamic-range receivers. This coincided with shrinking research and defence budgets [9]. The need for enhanced surveillance was still substantial however. The low-cost nature of passive radar systems attracted the attention of numerous university laboratories and other agencies with limited budgets.

This is because passive radar requires less hardware and more computational power and algorithmic sophistication.

Throughout the world, there is increasing interest in research on passive radar systems. Active research and development is being undertaken at major research hubs in the United States (including work at the Air Force Research Labs, Raytheon, University of Washington, Georgia Tech/Georgia Tech Research Institute and the University of Illinois), in the NATO C3 Agency in The Netherlands, in the United Kingdom (at Roke Manor Research, QinetiQ, University of Birmingham, University College London and BAE Systems), France (including the government labs of ONERA), Germany (including the labs at FGAN-FHR), and Poland (including Warsaw University of Technology). There is also active research on this technology in a number of government or university laboratories in China, Iran, Russia and South Africa.

More information about recent developments in passive radar research can be found in [5], [7]-[22].

It is likely that practical PBR systems will continue to be developed and used. First, spectral congestion is ever-increasing, and military operations will most probably be carried out close to centres of population. The many broadcast and communications signals at these centres of population will be an advantage for passive radar. In addition, the VHF and UHF frequencies used by high power FM radio and television transmissions are ideal for PBR. Second, numerous synchronisation and timing problems that previously constrained the performance of passive radar systems have been removed by the deployment of the GPS satellite navigation systems. Third, PBR receivers are potentially simple and inexpensive, as mentioned earlier. Fourth, the advancement of signal processing power has made many of the signal digitisation and processing operations feasible in real time. If Moore's law is correct, these improvements will continue for many years [4].

1.3 Challenges of Passive Bistatic Radar

1.3.1 The Bistatic Configuration

The bistatic configuration of PBR gives rise to a number of challenges. Compared to monostatic radar, bistatic radar has greater system complexity, and therefore is more difficult to deploy, due to its geometry. Bistatic target detection and location are more complicated than those of a monostatic radar. As in the case of a monostatic radar, target detection involves the illumination of the target by the transmitter, and the detection and processing of target echoes by the receiver. In matched filter operation, a known signal is sent out and the reflected signal is correlated with the known signal. This process is used to detect common elements of the known signal in the reflected signal. The receiver therefore needs to know the transmitted waveform. For coherent receiver operation, the receiver also needs to know the phase of the transmitted waveform.

As with a monostatic radar, to locate a target, the bistatic receiver typically determines angles of arrival (AOA) and estimates the range of the target echo. Measurement of bistatic AOA are usually made in the azimuth and elevation plane that has its centre at the receiver site. To estimate bistatic range, the total signal propagation time from transmitter to target to receiver is used to derive a range sum estimate, ($R_T + R_R$), where R_T is the transmitter-to-target range and R_R is the target-to-receiver range. In a monostatic radar, $R_T = R_R$. In a bistatic radar, however, $R_T \neq R_R$ for most cases. Figure 2 shows a typical example. Before the bistatic radar can calculate R_T or R_R, it must solve the transmitter-target-receiver triangle, or bistatic triangle. An estimate of the transmitter location with respect to the receiver is typically needed in the solution [2].

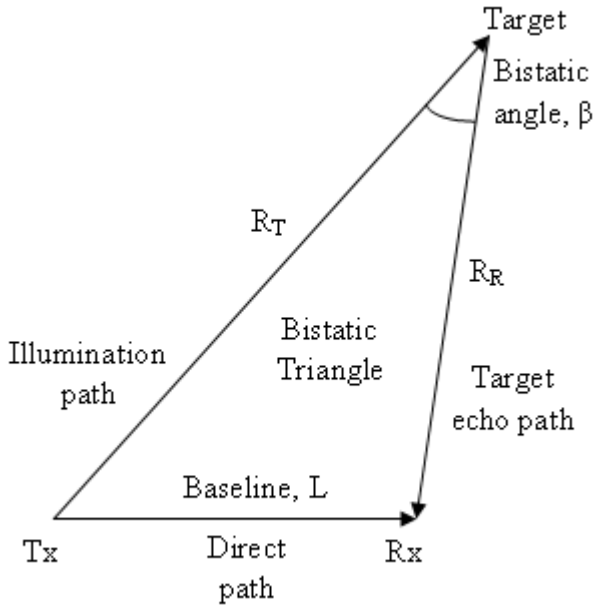

Figure 2 - Bistatic geometry and typical requirements for bistatic radar operation

All bistatic radars have three distinguishing features: the need to couple data between the transmitter and receiver; the geometry, defined by the bistatic triangle; and the strategies devised by a bistatic radar to either reduce the unfavourable consequences of the geometry or occasionally make use of the helpful effects of the geometry [2]. These are the main issues surrounding the bistatic configuration.

1.3.2 Direct Signal Interference

A typical PBR configuration is shown in Figure 3, in which an aircraft is illuminated by a number of digital audio broadcast (DAB) transmitters, labelled Broadcast Tx1 and Broadcast Tx2. At the radar receiver (labelled Rx), we wish to obtain the reflection (shown as filled lines) from the target. The target range can then be deduced from the time of flight. Unfortunately, the direct signals (shown as dotted lines) transmitted by the illuminators are often much stronger than the target return signals. This phenomenon is known as direct signal interference (DSI). The performance of the PBR system can only

be estimated if the signal to interference ratio (SIR) can be reliably and accurately predicted. The SIR is an important system performance parameter as it is often the dominant factor and provides a measure for the receiver dynamic range needed [23].

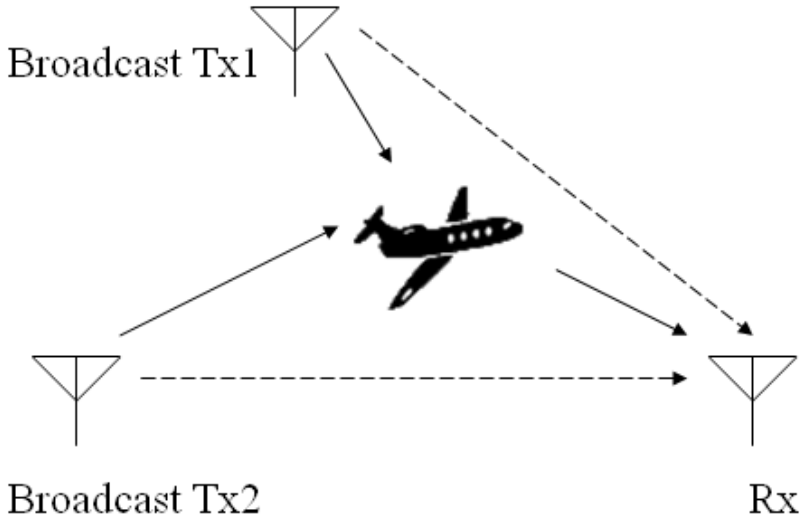

Figure 3 - Passive bistatic radar configuration

DSI can be so strong that the target returns are masked, that is, the target signals are buried under the range and Doppler sidelobes of the DSI in the receiver circuit [24]. The sidelobes are several orders of magnitude larger than the target echoes that are sought. As a result, there is a decrease in the available dynamic range of the data acquisition card in the receiver for the detection of targets. The target echoes are also limited by the reference voltage input, and the bit number allocated to the target information is very small, leading to difficulties in subsequent digital signal processing [25]. The receiver needs to be complex in order to mitigate the DSI and to extract the original transmitted waveform.

Much work has been done on mitigating DSI in PBR systems. Traditionally, the problem has been addressed by using an adaptive antenna, steering a null towards the illuminator of opportunity, or siting the receive antenna so that it is physically shielded from DSI using topography, buildings or shrouds [24].

Saini et al. investigated two tracking methods for suppressing DSI for a digital television – terrestrial (DTV-T) based radar: using dynamic compensation and using an adaptive antenna. They were able to achieve DSI suppression of 30 to 40 dB for the case of a fast rotating radar channel (RC) antenna, which can complement an adaptive antenna. Configuring the RC antenna to be in cross-polarisation to the DTV-T transmitter added another 10 to 15 dB to the DSI reduction. In total, the methods achieved 40 to 50 dB of DSI suppression [26].

Much attention has been focused on software cancellation of DSI, with the cancellation carried out in the digital domain and many adaptive methods used to filter out interferences. Wan et al. proposed a hardware solution to mitigate the DSI prior to the analog-to-digital converter (ADC) for FM radio-based passive radar. The solution produced about 35 dB of DSI reduction [25].

Howland experimented with spectral cancellation of the direct path signal. He recognised that removing DSI by using angular nulling with the antenna and adaptive echo cancellation in the receiver was restricted by the receiver dynamic range, and that the main performance limitation of a PBR system is determined by the ADC technology. He has developed a two-stage adaptive noise canceller. The first stage is an adaptive M-stage lattice predictor, with prediction order $M = 50$, and the second stage is an adaptive tapped delay line. The DSI reduction was found to be approximately 75 dB [24].

It is probable that a combination of techniques will be needed in most cases to reduce DSI to an acceptable level.

1.3.3 Digital Broadcast Signals

At the commencement of the present project, researchers at the School of Electrical and Electronic Engineering at the University of Adelaide had developed a PBR system that captures transmitted DAB signals and converts the signals into radar detections and aircraft tracks [27]. A practical radar detection system had been built to the proof-of-concept stage and a crude, but functioning, tracker was in place.

At that stage, the University of Adelaide was leading the field of digital broadcast-based passive radar. The advantage of using digital broadcast signals lies in the fact that they facilitate higher bandwidths. As a result, researchers at the University of Adelaide have been able to develop a radar with very good accuracy. In the area of DSI mitigation, cross-polarisation has been the major breakthrough. Since Australia did not introduce a DAB system until June 2009, and the United Kingdom (UK) had a well-established DAB system, preliminary experiments on the hardware of the radar system were performed at the University of Bath, UK.

Whilst a number of other passive radar systems are currently under development, the project was the first to successfully exploit digital broadcast signals, namely DAB and digital video broadcast (DVB) signals. Unlike the analogue signals used in other passive radar systems, digital broadcast signals give an almost ideal ambiguity function. In pulsed radar signal processing, an ambiguity function is a two-dimensional function of time delay and Doppler frequency showing the distortion of a returned pulse due to the receiver matched filter due to the Doppler shift of the return from a moving target. The almost ideal ambiguity function resulting from digital broadcast signals makes them highly desirable as radar signals. However, the use of digital broadcast signals also presents the challenge of distinguishing between the different illuminations of a target, since all the illuminations are at the same frequency. The only difference between illuminations of the same target is the time delay between their detections. For applications such as tracking, additional algorithms would be needed.

1.4 Motivation

The main research area to be addressed in this thesis is the development of a realistic PBR simulator that can be used to develop radar algorithms and also optimise the design of radar systems. In particular, an effective PBR simulator must be able to simulate multitransmitter/multireceiver systems. This problem needs to be solved in order for researchers to test ideas without building equipment.

Developing a radar signal simulator provides an environment in which problems, such as developing target tracking algorithms for a multitransmitter/multireceiver passive radar system, can be solved. A tracker would need to function in a variety of situations, and its operation would be affected by factors such as terrain and DSI. A detailed knowledge of the propagation environment would be necessary for the development of such a tracker, and a simulator can assist in providing this knowledge.

Regarding the optimisation of the radar design, we need to answer questions such as:

- Where should the radar be located?
- What is the best way to avoid DSI?
- What is the best radar architecture?
- What is the optimum combination (for example, a circular array with a nulling capability, a linear array with a nulling capability)?

To answer the above questions experimentally would be prohibitive in cost.

Another area investigated in this project concerns radar signal data. Although the radar in its state at the beginning of the project provided considerable data for the improvement of the radar algorithms, this data was not comprehensive and it was necessary to be able to generate data that could test all aspects of the signal processing, detection and tracking. In particular, since the final radar consists of a network of simpler radars, we needed to be able to generate data from such a system. (At the beginning of the project, the radar had only a single receiver and hence could only provide Doppler and range. A system of such radars was required to gain the position of targets.) A simulator can provide data to develop the required radar software.

The simulator will be a major research tool and can be used to develop passive radar in general as it is not limited to DAB illuminators.

The goals of this thesis are as follows:

- to discuss the theory behind the simulator
- to describe the various stages of the development of the simulator
- to explain the verification of the simulator
- to demonstrate the success of the simulator
- to link the lessons learned from the aforementioned objectives with radar modelling and simulation in general

1.5 Literature Review of Radar Modelling and Simulation

This section gives a critical review of existing work on radar modelling and simulation and puts it in the context of the present project.

A review of the literature on radar modelling and simulation reveals that there is much interest in this work. Modelling and simulation is a means of facilitating the planning, design and evaluation of systems, and is important in the appraisal of system modification and transformation strategies.

For sea echo observation, Airiau and Khenchaf [28] proposed a model of the sea echo received by a moving polarimetric bistatic radar. An expression for the received signal was derived for the general case of the transmitter, target and receiver all moving. The radiation of the antenna, the influence of the sea on the polarisation of the transmitted wave, and the effect of the moving objects were factored in. The model can be used for any target, including the sea surface, provided that the target scattering matrix is known. Although the model accounts for the effect of the sea on the transmitted wave, the model does not take into account the effects of the signal propagation through the air. No mention is made of diffraction around or reflection off objects that lie between the transmitter and the receiver. The radar system of the present project is based on developed land, so these effects need to be considered in its modelling and simulation.

Scott [29] has developed a methodology for implementing radar system simulation and modelling frameworks. A number of tools have been built that allow the user to model complete radar modes and carry out performance prediction studies. Platform and target motion, analogue and digital electronic components and complex signal processing algorithms can be modelled. A common data file format enables the same framework to be used to process real or synthetic multi-channel datasets without recompiling or rebuilding the modelling framework. The tools were designed for synthetic aperture radar (SAR) and ground moving target identification (GMTI) modes for both monostatic and bistatic operation. The radar of the present project is not a SAR and involves airborne targets. The tools described by Scott are of limited use for the present project and do not include the propagation effects that play a major role in the project.

Radar modelling and simulation have also been applied to studies in clutter reduction. Han et al. [30] have proposed a bistatic clutter geometrical model that describes the mathematical relationship between bistatic radars and clutter scatterers in a variety of geometrical scenarios. Liu et al. [31] have described a clutter model for bistatic spaceborne radar. Clutter for spaceborne radar has markedly different characteristics from those of airborne radar. This is due to the high speed of satellites, which generates a much larger Doppler band, the rotation of the earth, which causes clutter characteristics to vary with time and range, and the curvature of the earth's surface. The effects of clutter will not be considered in the present project.

In recent years, research into radar simulation has concentrated mainly on SAR systems [32]-[41]. The work is not of much relevance to the location and tracking of remote targets by traditional radar systems however.

Paichard et al. [42] sought to address this shortcoming by designing the Flexible Simulator for Multistatic Radars (FERS), which can be used to simulate raw returns in radar systems with arbitrary waveforms and arbitrary numbers of receivers, transmitters and scatterers, and is applicable to passive radar systems. The target returns are modelled as copies of the transmitted signals which have been altered by the effects of transmission, environmental interactions (including propagation and target interaction), and reception. In 2009, Inggs et al. [23] presented a conference paper that described the use of the AREPS propagation suite of the US Navy in the modelling of this radar system planning tool. AREPS calculates propagation loss by taking into account environmental propagation effects such as multipath, diffraction and refractive index lapse rate. Paichard et al. describe how the propagation delay is broken down into two effects: a phase shift on the carrier (phase delay) and a time shift of the envelope of the transmitted signal (group delay), with the assumption that the transmitted signal is made up of a complex band-limited signal that is mixed with a carrier at a constant frequency. Paichard et al. claim that the Doppler shift induced by a target is modelled accurately when both of these delays are considered.

More recently, Brooker and Inggs [43] have developed a signal level simulator for multistatic and netted radar systems. The simulator accounts for the effects of propagation through the atmosphere, delay and attenuation, on the transmitted signals. The present project is concerned with building a simulator for scenarios involving hilly terrain and built-up areas however. Propagation effects on transmitted signals caused by their interaction with obstacles, specifically, diffraction, multipath and depolarisation, need to be considered in detail for the present study. In addition, the Brooker and Inggs paper states that the simulator only supports point scatterers with arbitrary RCSs at the time of publication. The present study requires the inclusion of a target RCS model that is more sophisticated than a point scatterer. The target RCS model used in the present study is that of a small executive jet.

Weiss [44] has also produced a simulator, implemented in Matlab, that generates datasets for optimising the results of tracking algorithms. The datasets are created by combining real radar datasets with artificially produced data. The simulator is concerned mainly with sea scenarios rather than land scenarios however, and so does not go into the detailed modelling of diffraction, multipath and depolarisation that is needed in the present study.

Berry et al. [45] have devised a generic phased array radar model for detailed radar performance assessment that includes the modelling of diffraction around obstacles and multipath effects due to forward scatter reflection from surfaces causing signal cancellation. Ideas for the present study could be gleaned from this model, but the radar in the present study is not a phased array radar, and the modelling of depolarisation of reflected signals is not mentioned, so the paper is not of great use in the present study.

The model of the radar system of the present project introduces some novel techniques, including the application of Fermat's Principle of Least Time. The model has added sophistication and is fast and efficient compared to previous models.

1.6 Thesis Overview

Following on from this introduction, this thesis is structured into five chapters.

Chapter 2 describes the basic modelling of the radar system. We start with the simplest model, which uses the bistatic radar and Friis equations to calculate target returns and DSI. This model is enhanced by modelling antennas with electromagnetic response simulation software. The radar signal is modelled using random sequences, and the effect of a moving target is added. The model is tested using Amplitude Range Doppler (ARD) displays.

In Chapter 2, the goals of discussing the theory behind the simulator and describing the earliest stage of the development of the simulator are achieved. The basic model is successfully tested, meeting the simulator verification objective at the most basic stage.

In Chapter 3, more advanced propagation effects are explored. These include multipath and diffraction of the signal around obstacles. The modelling elements are verified individually before being incorporated into the simulator, and the effects of the refinements on DSI are investigated.

Chapter 3 meets the objective of describing the second stage of the development of the simulator and its verification.

Chapter 4 examines the problem of bistatic radar cross section (RCS). The cross sections for various targets are modelled using electromagnetic response simulation software. Antennas are also modelled, and the implications for radar modelling are discussed.

During the course of Chapter 4, the goal of linking the work in the present project to radar modelling and simulation in general is accomplished.

In Chapter 5, the simulation of several realistic scenarios is carried out. One application of the modelling, DSI mitigation, is presented, and the success of the model through the simulation of collected data is demonstrated. Chapter 5 verifies that the simulator is working, meeting the verification objective, and achieves the goal of producing and showing the capability of a successful simulator.

Chapter 6 concludes the work by summarising the elements that need to be included in a radar signal simulator and discussing possible extensions to the project.

2 Basic Modelling

This chapter describes the basic modelling and simulation of a PBR system. The purpose of modelling and simulation in PBR system development is discussed. A rudimentary model for a general PBR system is then described. The details of the functions, inputs and outputs of the individual components of the model are given. Model verification is performed using a real-world application of the simulator. Refinements are then made in later chapters to the model to obtain greater accuracy and hence a more realistic modelling and simulation tool.

2.1 The Purpose of Modelling and Simulation

Modelling and simulation is a means of facilitating the planning, design and evaluation of systems, and the appraisal of system modification and transformation strategies. The process of modelling produces an object (i.e., a model) that is a representation of a system, and is a specification of behaviour generation. This specification is developed by the modelling process. The model is then used as a vehicle for experimentation. This experimentation with the model is referred to as simulation [46].

The possible reasons for performing a modelling and simulation study are numerous and varied. Among the most common are engineering design, prototyping and concept evaluation, performance evaluation, evaluation of plans for transformation or change, evaluation of decision or action alternatives, support for acquisition or procurement decisions, forecasting, sensitivity analysis, risk or safety assessment, and education and training. A model replaces the system that it represents in experimental studies. In many cases, it is preferable to experiment with a model rather than the actual system. For example, direct experimentation with an existing system can be too costly, time-consuming, dangerous or disruptive, irreversible, or morally or ethically unacceptable [46].

In the context of radar systems, modelling and simulation serves as an important tool in a variety of ways. During the design phase of a radar system, modelling allows designers to determine the requirements of a radar. Knowing the optimum values of factors involved in the radar system, such as transmitter and receiver positions, enables designers to plan a new radar system for best performance. Simulation goes one step further and provides synthetic, but realistic, output of the radar receiver. In this data, all the system factors, including aircraft position and radar position, are under the control of designers. The exact details of the target, such as target velocity and radar cross section, are known, and specific scenarios to test the radar system can be devised. System parameters can be optimised without the need for costly experiments. In short, modelling and simulation assists in the design, prototyping and concept evaluation of new radar systems before they are built.

Modelling and simulation can also provide support for the performance evaluation of existing radar systems. While data can be collected directly from

an existing system, the amount gathered is often limited due to the expensive and time-consuming nature of direct experimentation. Simulated data, however, can be produced in large quantities in a much shorter period of time, making simulation a more cost-effective option in terms of time and other resources.

If an existing radar system needs to be changed or transformed in some way, modelling and simulation can help to evaluate the plans without disrupting the activity of the system or putting the safety of its users at risk. In some instances, the modifications to the radar system are irreversible. Entire scenarios with changes ranging in impact on the system from trivial to severe can be played out on the simulator and evaluated without disturbing or affecting the actual system in any way. Similarly, the simulator can be used in the appraisal of decision or action alternatives, including acquisition or procurement decisions.

There is always the possibility of changes to a planned or existing radar system. For example, the specification for the system could change suddenly, such as an unexpected increase in the volume of air traffic in the vicinity of a particular airport. In a similar vein to the previously mentioned design of new radar systems and the assessment of plans to change existing systems, simulation can aid in forecasting, sensitivity analysis and risk or safety assessment of radar systems through the manipulation of system parameters. Hypothetical scenarios can be explored in detail before any changes to the radar system are applied.

Modelling and simulation can also be effective in education and training. Flight simulators establish a virtual, but realistic, environment for trainee pilots to practise critical skills before facing the dangers of flying the actual aircraft. The environment is safely removed from the reality, but simulates all the relevant features, of the cockpit. Similarly, the modelling of a radar system and the simulation of radar signals provides a theoretical ‘playpen’ for the trainee radar engineer to explore different radar configurations and signal processing techniques before any physical changes are applied to the actual radar system or any actual radar signals are used.

Finally, the synthetic data generated by the radar signal simulator can be used in the development of aircraft detection and tracking algorithms.

2.2 Overview of the Rudimentary Model

A typical PBR configuration was shown in Chapter 1 and is reproduced here in Figure 4. The aircraft is illuminated by a number of DAB transmitters, but the DSI can be so strong that the target returns are masked. As a result, there is a decrease in the available dynamic range of the receiver for the detection of targets. Consequently, DSI mitigation is a major challenge in the design of modern passive radar systems.

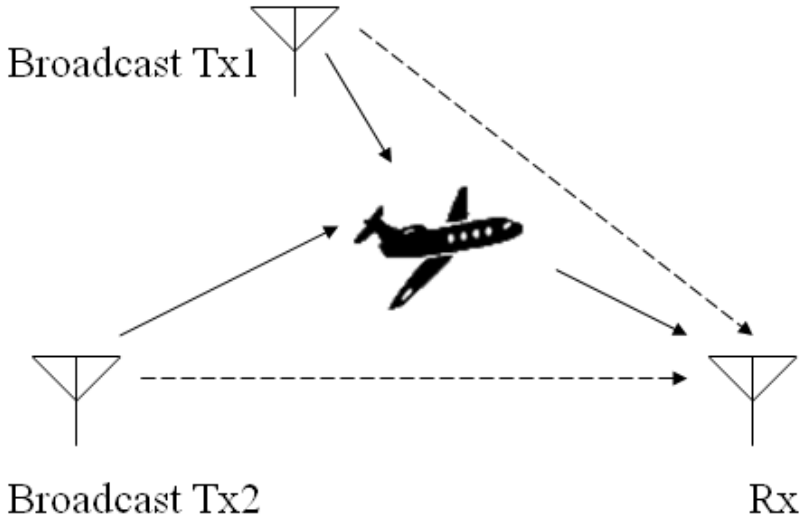

Figure 4 - Passive bistatic radar configuration

As mentioned in Chapter 1, this thesis describes the development of a simulator that models a PBR system. The simulator can be used to test techniques in DSI mitigation and to develop detection and tracking algorithms.

The block diagram of the simulator is shown in Figure 5. As shown in the diagram, the simulator is made up of individual units. These units are described separately later in this chapter.

The first stage of the development of the simulator involved a rudimentary model that gives the most basic approximation to the PBR system. At the first level of modelling, the simulator simulates the transmitted signals and the received signals from reflections at the target and DSI. The output of the simulator is an ARD display. An ARD display is essentially a pictorial representation of the cross-correlation between the originally transmitted signal and the signal in the radar receiver. The amplitude of a particular cross-correlation value in the two-dimensional array indicates the probability that the target is at a certain location for a pair of given range and Doppler values. This information can then be used by an aircraft tracker, as the Doppler gives information about speed and the range gives information about position. Details of how the simulator functions are given below.

The signal transmitted by each DAB illuminator is first simulated. These signals are virtually identical and synchronised. The signals that arrive at the receiver, either via the target or directly from the transmitters, are then calculated. The calculations are performed by the Target Power Unit and the DSI Power Unit, respectively. The Antenna Gain Unit and the Radar Cross Section (RCS) Unit produce outputs that are used in the calculations of the two Power Units.

During the journey from the transmitter to the receiver, the signals suffer transmission losses. The effects of these losses are introduced to the individual signals by the Propagation Loss Unit.

The individual signals are then added together to get the total signal entering the receiver. This function is performed by the Signal Generation Unit, and the output is termed the Synthesised Signal. The Synthesised Signal can be used to test signal processing, detection and tracking algorithms with precise knowledge of target position. In addition, the simulator can be used to perform experiments with alternative configurations of the radar system.

The Synthesised Signal is autocorrelated by the Autocorrelation Unit. An actual off-the-air received DAB signal, called the Off-the-Air Signal, is also autocorrelated by the Autocorrelation Unit. The two autocorrelations are compared to determine how well the Synthesised Signal approximates the Off-the-Air Signal.

At the final stage, the Synthesised Signal is fed into an ARD generator to form an ARD display. The ARD display can be used as the basis for an aircraft tracker.

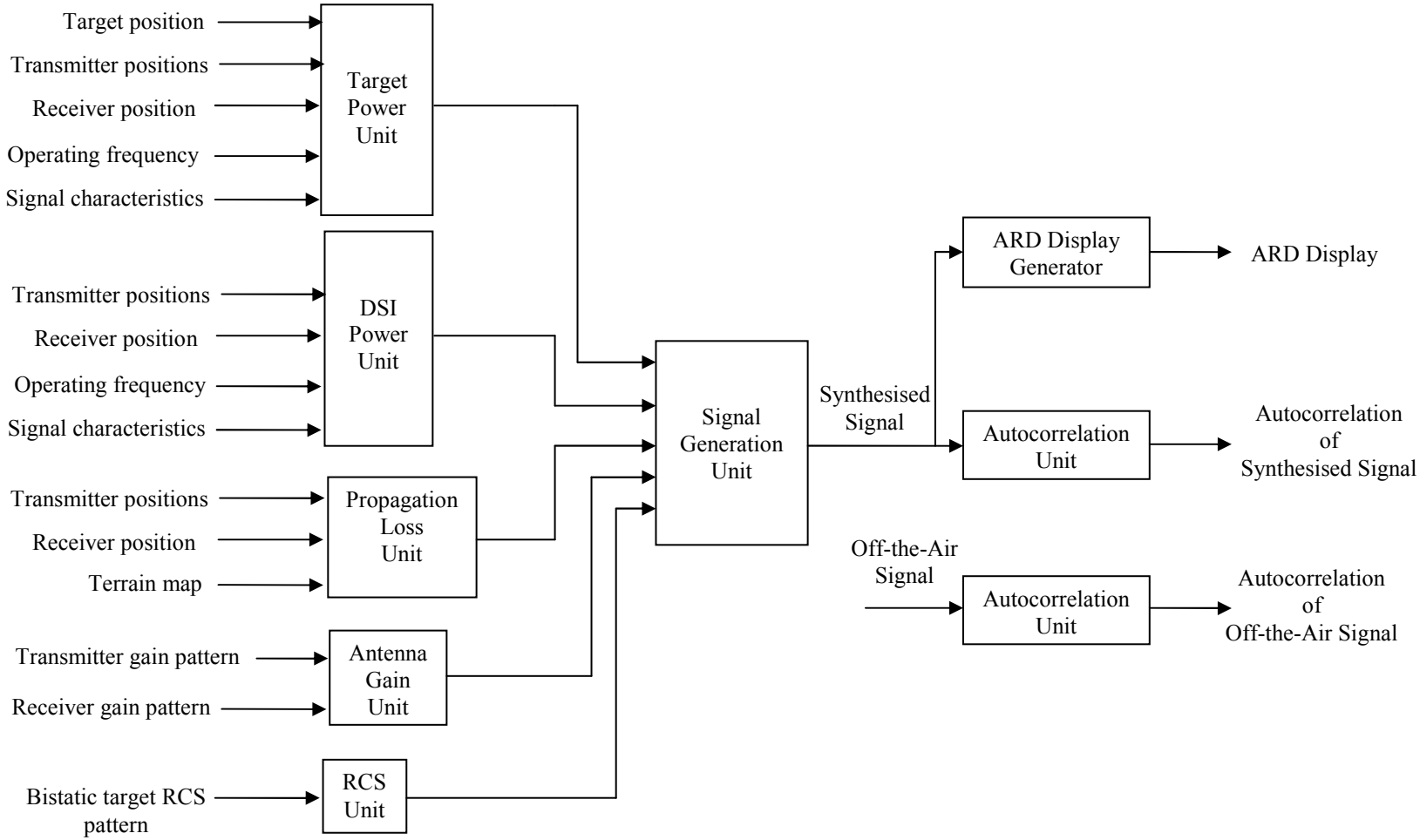

Figure 5 - Block diagram of simulator

2.3 Description of the Rudimentary Model Elements

2.3.1 Target Power Unit

The Target Power Unit calculates the power of a target return at the radar receiver. This Unit takes as its input the positions (latitude and longitude coordinates) and heights of the target, transmitters and receiver, as well as the operating frequency and the characteristics of the signal. The latitude and longitude coordinates are used to determine the distance from the illuminator to the target and the distance from the target to the receiver.

The target return power at the radar receiver is given by the bistatic radar equation

$$P_{TARGET} = P_T G_T G_R \left(\frac{\lambda}{4\pi R_{IT} R_{TR}} \right)^2 \frac{\sigma}{4\pi} \qquad (1)$$

where R_{IT} is the distance from the illuminator to the target, R_{TR} is the distance from the target to the receiver, σ is the radar cross section of the target, P_T is the illuminator power, G_T is the gain of the illuminator antenna, G_R is the gain of the receiver antenna and λ is the wavelength. The wavelength is obtained by dividing the speed of light by the operating frequency (220 MHz in the case of DAB based radar), giving approximately 1.36m.

For the rudimentary model, the radar equation is used only for line-of-sight signals, that is, non-line-of-sight signals (those masked by obstacles or terrain) are set to zero.

The Target Power Unit also finds the time shift for the target contribution to the received signal. This time shift is calculated by dividing the distance travelled by the target return signal by the speed of light.

The Target Power Unit is needed in the later simulation of the receiver output signal. This Unit factors in the contributions made by the signals that travel from the illuminators to the target and are subsequently reflected by the target.

2.3.2 DSI Power Unit

The DSI Power Unit determines the DSI power at the radar receiver. The inputs to this Unit are the positions (latitude and longitude coordinates) and heights of the transmitters and receiver, as well as the operating frequency and the characteristics of the signal.

The power of the DSI at the radar receiver is given by the Friis equation

$$P_{DSI} = P_T G_T G_R \left(\frac{\lambda}{4\pi R_{IR}} \right)^2 \qquad (2)$$

where R_{IR} is the distance from the radar receiver to the illuminator.

In the rudimentary model, the Friis equation is used only for line-of-sight signals (other signals are set to zero).

In addition, the DSI Power Unit calculates the time shift for the DSI contribution to the received signal. This time shift is found by dividing the distance travelled by the DSI signal by the speed of light.

The DSI Power Unit is used in the generation of the simulated receiver output signal at a later stage. This Unit factors in the contributions made by the signals that travel directly from the illuminators to the radar receiver.

2.3.3 Propagation Loss Unit

The Propagation Loss Unit accounts for reductions to the signals above those caused by spreading loss (which is accounted for by the Friis and radar equations). To obtain an accurate representation of the signals, it is necessary to deduct power from the original transmitted signals due to the effects of diffraction and reflections.

In the rudimentary model, this Unit does not perform a function (the Unit adds a loss of 0 dB), and the effects of ground topography will be introduced in a later chapter.

2.3.4 Antenna Gain Unit

The Antenna Gain Unit models the gains of the transmit and receive antennas. Gain describes the directional efficiency of an antenna and is important since most antennas (especially the radar receiver antenna) are highly directional.

In the rudimentary model, this Unit takes the gain patterns of the transmitters and receiver to be direction independent and gives them a value that is representative of the antenna look direction. More sophisticated modelling of antenna gain is described in a later chapter.

2.3.5 RCS Unit

The Radar Cross Section Unit takes in the target bistatic radar cross section. This value is used in the calculation of the power of target returns. The contributions made by the target reflections are incorporated into the final simulated receiver output signal. Therefore, like the Antenna Gain Unit, the RCS Unit determines the accuracy of the received signal simulation.

For the rudimentary model, the RCS Unit gives a representative value. More sophisticated modelling of the target RCS is discussed in Chapter 4.

2.3.6 Signal Generation Unit

The outputs of the Target Power, DSI Power and Propagation Loss Units are fed into the Signal Generation Unit. The Signal Generation Unit is responsible for producing the Synthesised Signal. The Synthesised Signal represents the signal that arrives at the receiving antenna. The signal generation process is detailed below.

Firstly, the signal that is transmitted from each DAB transmitter is simulated. This signal is a coded orthogonal frequency division multiplexing (COFDM) signal, as prescribed by the European Broadcasting Union. For the rudimentary model, the COFDM signal is represented by a sequence of random complex numbers in MATLAB (this has been found to give a good representation of the transmitted signal).

The total signal received at a receiver will then be a combination of direct signals received from the transmitters of the DAB network and the returns from targets. The amplitude and time shift of a particular contribution to the received signal is calculated using the DSI Power Unit (for the direct signals) and the Target Power Unit (for the target returns). In effect, this total signal consists of a sum of time delayed and amplitude shifted copies of the transmitted signal. The amplitude and time effects are dictated by transmitter location, target location, propagation effects, antenna patterns and target cross sections. These factors have been accounted for by the Units described earlier.

The Synthesised Signal is input to the Autocorrelation Unit.

2.3.7 Autocorrelation Unit

The Autocorrelation Unit performs an autocorrelation of its input signal.

The Synthesised Signal and Off-the-Air Signal at the transmitter are both autocorrelated. The synthesised autocorrelation can then be compared with the autocorrelation obtained from the off-the-air signal in order to gauge the effectiveness of the simulations.

2.3.8 ARD Display

As mentioned previously, in an ARD display, the range value indicates the distance that the signal has travelled from transmitter to target then to receiver, while the Doppler value shows the frequency shift of the signal due to the motion of the target. An ARD display represents, in two dimensions, the cross-correlation between the originally transmitted signal and the signal in the radar receiver with suitable weights to introduce Doppler. The amplitude of a particular cross-correlation value indicates the probability that the target is at a certain location for a given range and Doppler. This information can then be used to track targets.

2.4 Discussion of the Rudimentary Model

The radar and Friis equation models of the target returns and DSI, represented by the Target and DSI Power Units, are at the most basic level of modelling. These simple models do not take into account the propagation effects such as ground reflections and diffraction. For the purposes of developing algorithms for DSI mitigation, the effects of diffraction and multipath will need to be incorporated into a more sophisticated model.

2.5 Verification of the Rudimentary Model: An Example Application

Before the commencement of the present study, Australia had not yet introduced a DAB system. The UK had a well-established DAB system at that time, so in the work that preceded the present study, University of Adelaide researchers performed preliminary experiments on the hardware of the Adelaide passive radar system at the University of Bath in the UK.

As mentioned earlier, the objective of the present study was to develop a general PBR modelling and simulation tool. One way of verifying the accuracy of this tool was to determine how well the tool models the University of Adelaide radar located at Bath. In previous years, a large amount of data had been collected by this radar. The aims of the rudimentary model were to simulate the signals in the vicinity of the radar receiver, including the radar returns and the direct signal. Real off-the-air DAB signals were collected at the University of Bath to test the effectiveness of the rudimentary model in simulating real data.

Figure 6 shows the radar configuration in Bath. The red cross shows the location of the receiver. A target at Bristol airport is indicated by the red circle. The three blue crosses represent the DAB transmitters at Bath (1.1 km from the receiver), Mendip transmitter (25.1 km from the receiver) and Wenvoe (67 km from the receiver).

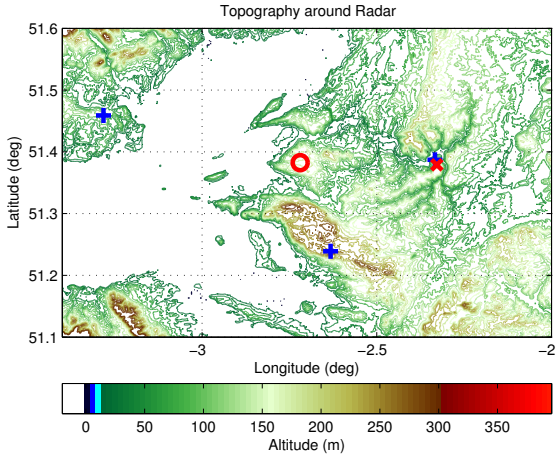

Figure 6 - The geometry of the radar at Bath

The illuminations of the DAB transmitters at Bath, Mendip and Wenvoe were taken into account in the simulations as these provided the strongest signals (other transmitters were present, but were far weaker). The receiver gain towards each of the illuminators was taken to be 2.2 dB because the receiver is a dipole antenna. The effective radiated power ($P_T G_T$) of the transmitters is 17.3 dBW for Bath, 32.7 dBW for Mendip and 34.3 dBW for Wenvoe. Finally a single target at Bristol airport was assumed, with its bistatic cross section taken to be 5 m^2. This is a cross polarisation cross section of a typical target when viewed in cross polarisation to that of the transmitters (vertical polarisation). The reason for cross polarisation in target observation was that it reduced by 20 dB the power that came from DSI. Off air measurements indicate a 20 dB reduction of DSI signals due to cross polarisation effects.

The autocorrelation of a signal is the cross-correlation of the signal with itself. In the context of signal processing, the cross-correlation of two waveforms can be thought of as a measure of their similarity as a function of a time lag applied to one of them. The autocorrelation of a signal s(t) is given by

$$(s * s)(t) = \int_{-\infty}^{\infty} s^*(\tau) s(t+\tau) d\tau \qquad (3)$$

where * (on the right hand side) denotes the complex conjugate. In an autocorrelation, there will always be a peak at a lag of zero unless the signal is the trivial zero signal. The time lags between zero and any other peaks in the autocorrelation indicate the time lags when peaks or troughs in the signal align and make large contributions to the autocorrelation s*s.

Figure 7 shows the autocorrelation of the Synthesised Signal (the zero Doppler line of the ARD). The autocorrelation shows the delay between the DSI signals arriving at the receiver from the illuminators.

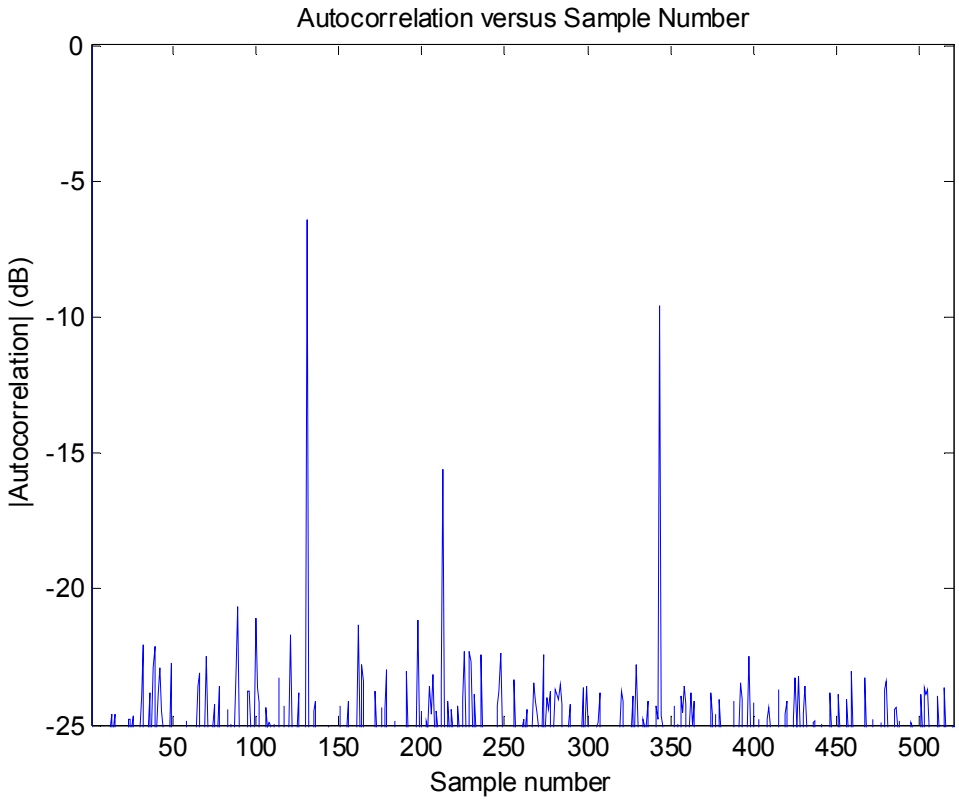

Figure 7 - Autocorrelation of Synthesised Signal (3 illuminators transmitting)

Figure 7 clearly shows the Bath, Mendip and Wenvoe signals. The sample number, effectively the time delay, allows us to determine the physical distance (delay divided by the speed of light). In the case of the autocorrelation, the peaks show the total signal correlated with itself (the signal at the origin), the Bath and Mendip signals' cross-correlation (at a delay of 131 time units), the Mendip and Wenvoe signals' cross-correlation (213 time units' delay) and the Bath and Wenvoe signals' cross-correlation (343 time units' delay).

Figure 8 gives the autocorrelation of the actual, off-the-air signal (the Off-the-Air Signal). The three main cross-correlations are due to the Bath, Mendip and Wenvoe, circled in the figure. Although the cross-correlations of Figure 7 can be found in this, there are several other cross-correlations that are not to be found and indicate discrepancies in the basic modelling that need to be addressed.

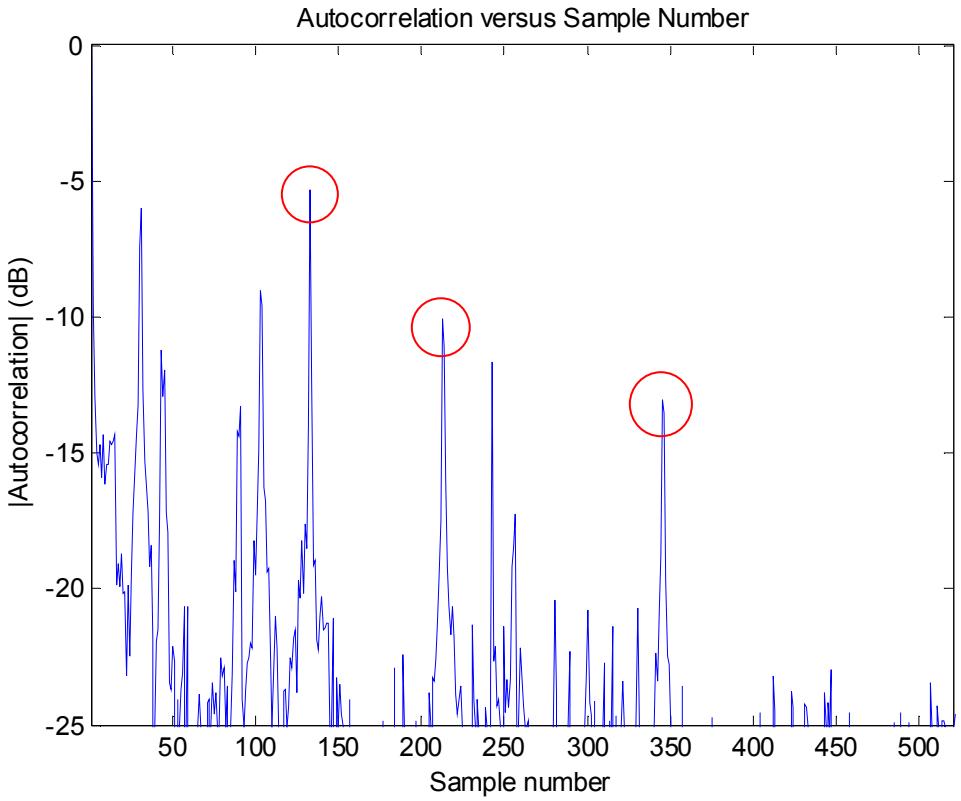

Figure 8 - Autocorrelation of Off-the-Air Signal

It will be noted that the autocorrelation of the Synthesised Signal clearly shows the direct signal from Mendip, Wenvoe and Bath. In addition, however, there are several other signals that are contaminating the output. These arise from the fact that the Off-the-Air Signal, which was obtained from an antenna directly pointing towards the illuminator, contains elements of many other illuminators in its signal. Further, there are far more than three illuminators in the actual scenario affecting the outcome. It is evident that the simulator needs to incorporate other weaker illuminators that have not been reduced by the antenna system. In the actual system, there are seven other transmitters that have not been included in the simulations of Figure 7. The actual system had nulling antennas in the direction of the major illuminators. As a result, the importance of the lesser illuminators has been increased.

The next stage of the modelling involves the addition of the effects of the other illuminators to the simulator. Illuminators at Abergavenny, Hannington, Membury, Naish Hill, Pur Down, Ridge Hill and Stockland Hill were added. The effective radiated power of the seven illuminators were taken to be 26.4 dBW, 31.9 dBW, 35.3 dBW, 30.7 dBW, 28.6 dBW, 38.9 dBW and 35.1 dBW, respectively. The receiver gain towards each of the seven illuminators is 2.2 dB. The autocorrelation produced when all seven illuminators were transmitting, in addition to those at Bath, Mendip and Wenvoe, is shown below in Figure 9.

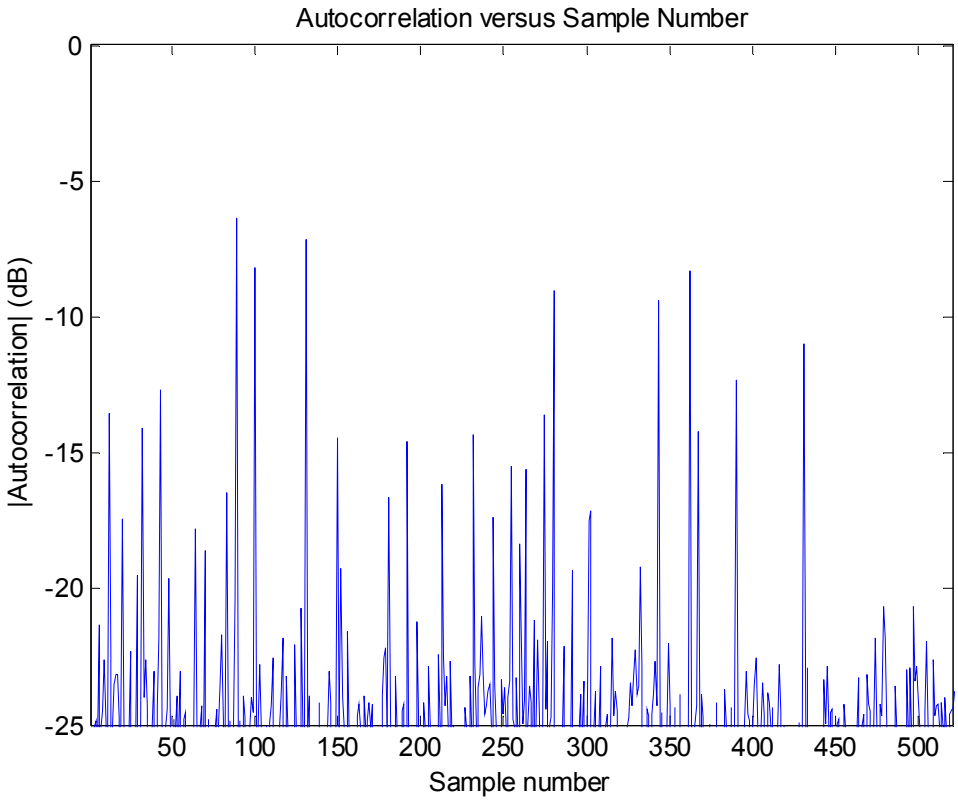

Figure 9 - Autocorrelation of Synthesised Signal (10 illuminators transmitting)

The lack of correspondence between the real Bath autocorrelation and the simulation motivates the need to include contributions from 'hidden' transmitters through diffraction and reflections.

With the simulated signals, and off-the-air signals, targets will still be well below the noise and a further stage of processing is required by the radar in order to make them visible. During this stage, direct signals from the illuminator, which are obtained from antennas directly pointing towards the illuminator, are combined with the signal from the target array in order to achieve further DSI reduction in the digital domain and hence reveal the target.

To verify that the simulator was functioning correctly for targets, a target with a large cross section (10000m^2) was added. Simulations were run with just one transmitter on at a time. Figure 10 shows the simulated autocorrelation against sample number with only the Abergavenny transmitter on. In the simulated autocorrelation graph, there is a large peak at the origin due to the direct signal, and a secondary peak at sample number 50 due to the target only. We expect the amplitude of the secondary peak to be close to the square root of the ratio of the target power to the DSI power and there was good agreement between the two values (0.14 and 0.15). The process was repeated for the other transmitters for which a secondary peak could be seen. Table 1 gives the results. The similarity between the two values for each of the cases listed gives confidence in the rudimentary model of the simulator working correctly.

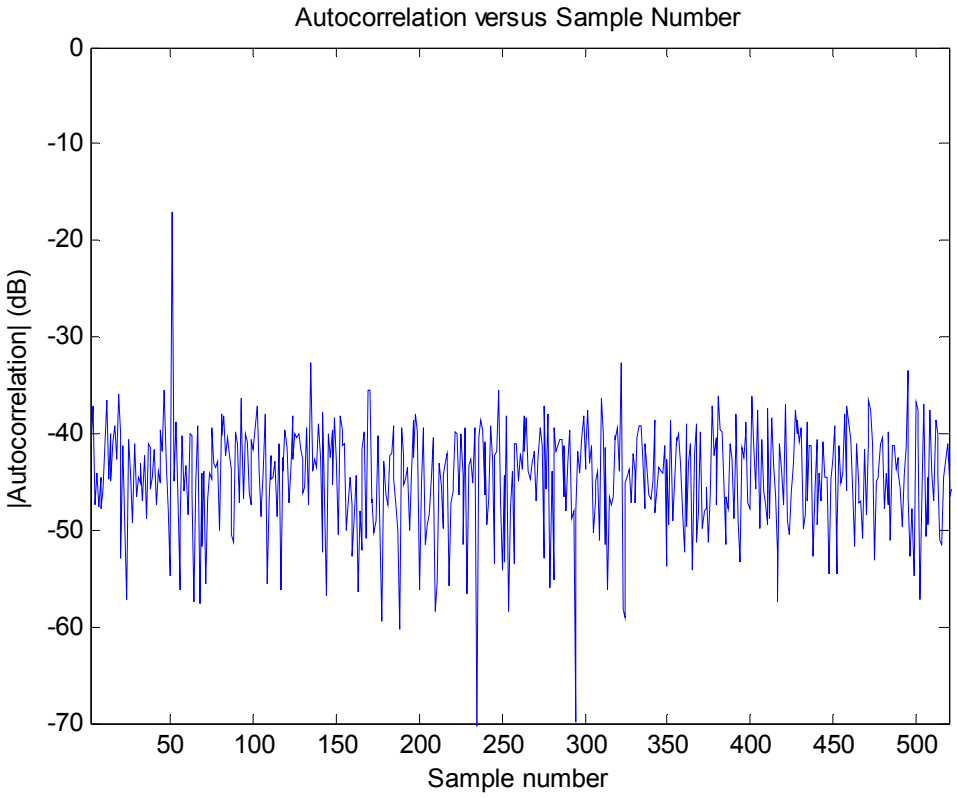

Figure 10 - Simulated autocorrelation with just the Abergavenny transmitter on

Table 1 - Results of simulating autocorrelations with single illuminators on

Illuminator	Amplitude of Secondary Peak (dB)	$\sqrt{(P_{Target}/P_{DSI})}$ (dB)
Hannington	-11.0	-11.0
Membury	-11.2	-11.4
Mendip	-8.2	-7.9
Pur Down	-13.4	-13.6
Ridge Hill	-8.5	-8.6
Stockland Hill	-9.2	-8.8

2.6 Simulation of Amplitude Range-Doppler (ARD) Displays

2.6.1 Modelling of Target Doppler

The motion of targets necessitates the inclusion of bistatic Doppler shifted frequencies in the modelling of the received signals. Bistatic Doppler shift is a specific example of the Doppler effect that is observed by a radar system with a separated transmitter and receiver. The Doppler shift is made up of the

component of motion of the target in the direction of the transmitter, plus the component of motion of the target in the direction of the receiver.

In the simulator, there are a number of stationary illuminators (10 for the Bath scenario) and one receiver. The target is assumed to have an initial location and be moving at a certain velocity. Each new target position is calculated using information about its previous position and current velocity. The bistatic range (the distance from each illuminator to the target then to the receiver) is calculated by summing the distance from the illuminator to the target R_{tx} and the distance from the target to the receiver R_{rx}. Ignoring relativistic effects, the Doppler shifted frequency is the time rate of change of the total path length of the scattered signal, normalised by the wavelength, and is given by

$$df = \frac{d(R_{tx} + R_{rx})}{dt} \frac{f}{c} \qquad (4)$$

The target, transmitter and receiver can be moving or stationary. The time between observations is assumed to be 1 time unit (dt = 1). A subroutine calculates the Doppler shift, given the change in bistatic range, the change in time, and the operating frequency (220 MHz for DAB-based radar). The Doppler cell size, or resolution, is the sampling rate divided by the number of samples. For the case of the Bath radar system, the sampling rate is 1.5625 MHz and the number of samples is 32 768, resulting in a Doppler resolution of 47.7 Hz. The Doppler cell number m is the ratio of the Doppler shift to the Doppler cell size, rounded to the nearest integer. This number is stored in a vector m. The range cell size, or resolution, is the speed of light divided by the DAB signal bandwidth. In the Bath system, the DAB signal bandwidth is 1.5625 MHz, which gives a range resolution of 192 m.

The original transmitted signal is modelled as a sequence of n random numbers. Most observations on the Bath system use n = 32768 samples (but greater length sequences can be used). For each contribution by the illuminators (target power or DSI power), a copy of the original signal is time shifted by the time delay and amplitude scaled by the amplitude of the contribution. For each target return, the signal is also multiplied by an exponential weighting factor that accounts for the Doppler shift. That is, each element in the signal s with index k is multiplied by $\exp\left(\frac{-j2\pi m_i k}{n}\right)$, where j is the imaginary unit and i is the index of vector m. The value of m_i is calculated as follows. The distance from the illuminator to the target then to the receiver $d_{TxTgtRx}$ is first calculated at a particular time instant. The process is repeated at the next time instant of interest. The time rate of change of the distance $d_{TxTgtRx}$ is used to calculate the Doppler shifted frequency, which is divided by the Doppler resolution to give m. The value of m_i corresponds to the value of m for illuminator i.

After further signal processing, an ARD display is generated by calling a function that takes in the original transmitted signal S, the received signal s, and the number of elements in each of these signals K. First, the calculation

$$x^k = s^k S^{k-l^*} \exp(\frac{j2\pi mk}{K}) \qquad (5)$$

is performed for k ranging from 1 to K, and m and l ranging for an appropriate number of integer steps. The ARD is then calculated as

$$ARD(l,m) = \left| \sum_{k=1}^{K} x^k \right| \qquad (6)$$

The ARD is then converted to decibels and displayed using a two-dimensional colour-coded display with Doppler on the vertical axis and range on the horizontal axis. The display uses colour to signify target intensity. Only the elements of the ARD matrix that are above the chosen detection threshold (10 dB above the average noise level) are plotted.

The choosing of a detection threshold involves the probability of false alarm. We wish to detect targets and DSI with a high probability of detection amid noise. A noise peak can be mistaken for a target or DSI detection, however, resulting in a false alarm. Due to the presence of noise in the radar system, there will always be a non-zero probability that the detection threshold will be exceeded, even if no target or DSI signal is present. Mathematical theory of thermal noise says that this probability can reach any finite value, small or large. In the statistics of thermal random-noise voltage, the value is at least equal to the saturation level of the detector. The probability that the detection threshold is exceeded in the absence of a signal is the probability of false alarm. We desire a low probability of false alarm.

The detection threshold needs to be low enough to detect the majority of target and DSI signals, but high enough to avoid a large proportion of false alarms. Radar designers usually seek to maximise the probability of detection for a given probability of false alarm.

The probability of false alarm P_{FA} is calculated by integrating the probability density function of the noise

$$\Pr(V_T < R < \infty) = \int_{V_T}^{\infty} \frac{R}{\beta^2} \exp\left(\frac{-R^2}{2\beta^2} \right) dR \qquad (7a)$$

and is related to the detection threshold V_T by

$$P_{FA} = \exp(\frac{-V_T^2}{2\beta^2}) \qquad (7b)$$

where β is the root mean square (RMS) value of the noise [47]. Rearranging gives

$$V_T = \sqrt{2\beta^2 \ln\left(\frac{1}{P_{FA}} \right)} \qquad (8)\,.$$

In terms of decibels,

$$V_T = 20\log_{10}\sqrt{2\ln\left(\frac{1}{P_{FA}}\right)} + 20\log_{10}(\beta) \qquad (9)$$

Now $20*\log_{10}(\beta) = 10*\log_{10}(\beta^2)$, which is just the average (or mean) noise power in decibels. So the detection threshold is the sum of the average noise power and the left term on the right hand side of equation (9). For a P_{FA} of 0.01, the left term on the right hand side of equation (9) is about 9.6 dB. Rounding up to the nearest integer gives a detection threshold of 10 dB above the average noise level. In other words, any signal that is 10 dB or more above the average noise level is taken as a target or DSI detection.

2.6.2 Testing of ARD Display Generator

To test that the ARD display generator was working correctly, a set of different scenarios was run through the simulator. In each scenario, it was expected that the features of the flight trajectory would correspond to those of the ARD display produced. Given a series of waypoints (target positions) and the corresponding velocities of the waypoints, the ARD displays generated should reflect the flight trajectory.

The first scenario has no targets present and all 10 illuminators of the Bath scenario transmitting. The receiver is located at the University of Bath. Figure 11 shows the ARD display. The transmitted radar signal was modelled as a sequence of 32768 complex random numbers. As expected, the ARD display showed the resulting DSI detections (shown circled) at zero Doppler, and all at the correct ranges (1.1 km, 17.9 km, 20.1 km, 26.1 km, 54.6 km, 66.8 km, 70.3 km, 71.4 km, 75.7 km and 83.6 km). Additional detections can be seen at zero and non-zero Doppler due to noise. There are always spurious responses present, and the likelihood of unintended targets producing some of these is not known. Responses that do not form consistent tracks are unlikely to be targets however.

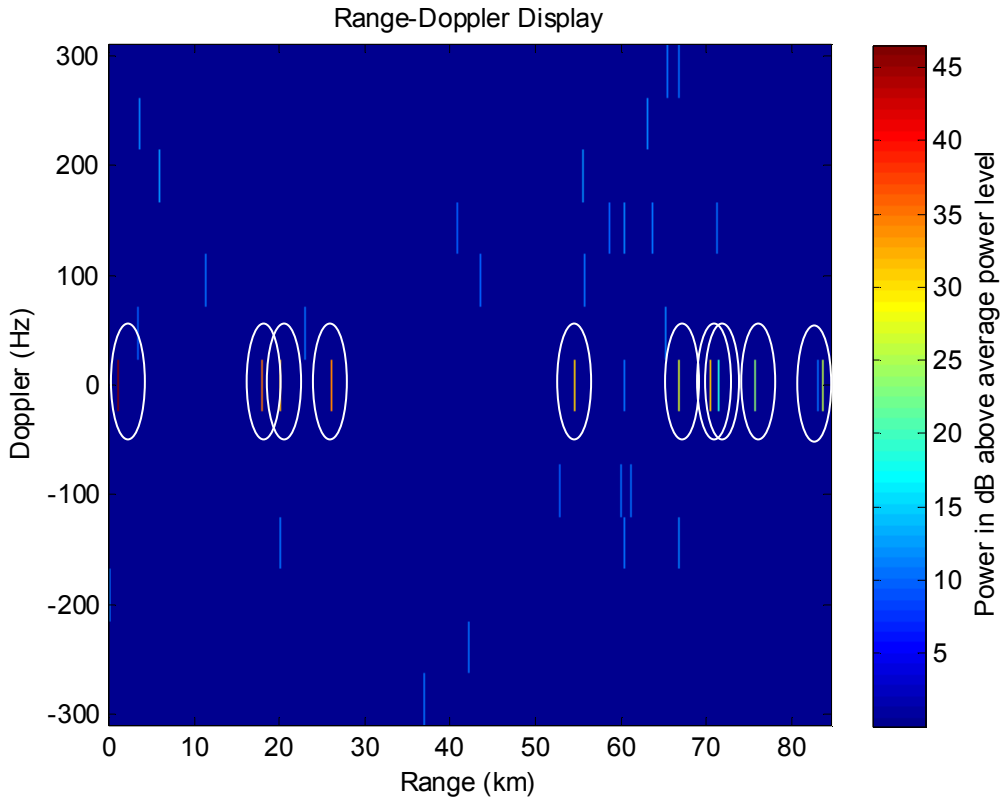

Figure 11 - ARD display for scenario with no targets and all 10 illuminators on. The 10 DSI detections are shown circled.

In the second scenario, a moving target has been introduced. The target has its initial position at Bristol Airport, and is travelling north at a speed of 180 m/s. Only one illuminator (located at Abergavenny) is transmitting, and the receiver is again located at the University of Bath. Figure 12 gives a representation of the scenario.

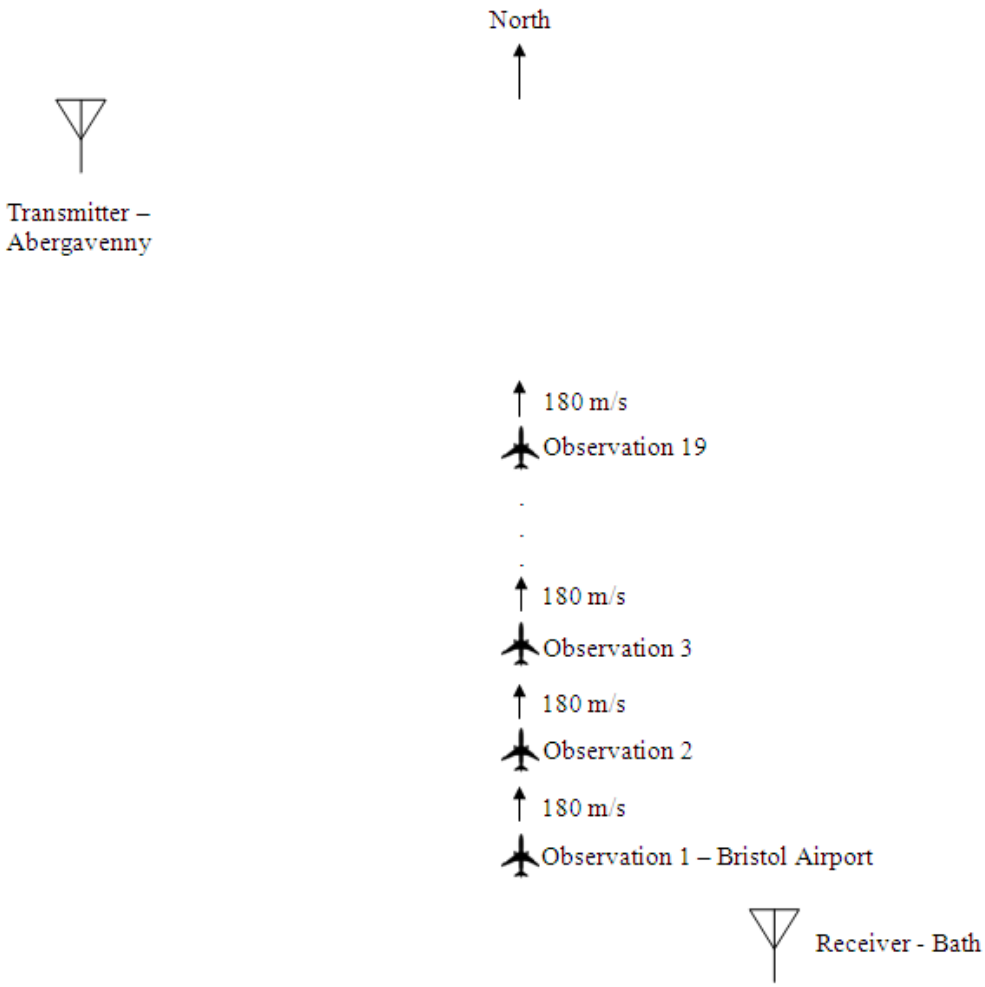

Figure 12 - Diagram showing second simulation scenario (not to scale)

In the second scenario, the transmitted radar signal was again modelled as a sequence of 32768 complex random numbers. There were three observations taken. Throughout the observations, the blue false detections due to the presence of noise fluctuate wildly in both number and position within the displays.

The first observation was taken one second after the target left its initial position. Figure 13 shows the ARD display produced during the first observation. A red detection corresponding to the DSI of the Abergavenny illuminator can be seen at a Doppler of zero and a range of about 71.8 km. A yellow detection, corresponding to the target return, can be seen at a range of about 81.2 km with non-zero Doppler. The non-zero Doppler arises from the fact that the velocity of the target, 180 m/s north, has resulted in a change in the distance from the Abergavenny transmitter to the target then to the receiver, $d_{TxTgtRx}$. During the 1 second interval between the first observation and the start of the target's trajectory, $d_{TxTgtRx}$ has decreased by 154 m. This corresponds to a Doppler shift of about -113 Hz which, when divided by the Doppler resolution (of about 47.7 Hz for the case of the Bath radar system) and rounded to the nearest integer, gives a Doppler cell value of m = -2. The yellow target detection can be seen in Figure 13 at a Doppler cell that includes the -100 Hz

marker, which corresponds (due to the Doppler cell resolution of 47.7 Hz) to the m value of -2.

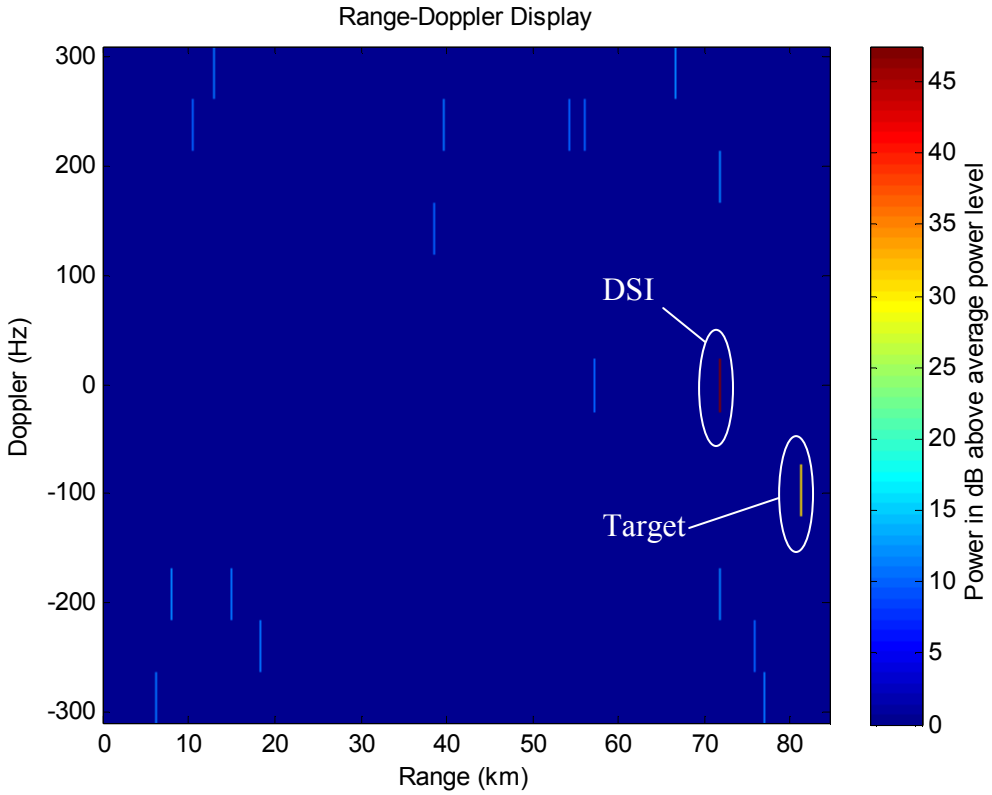

Figure 13 - ARD display for scenario with single target travelling north at 180 m/s and only one illuminator on, using simulated data, during first observation

Figure 14 shows the ARD display that was generated 17 seconds after the first observation. The target detection still has the same Doppler, but this time, its range can be clearly seen to have changed, to approximately 78.9 km.

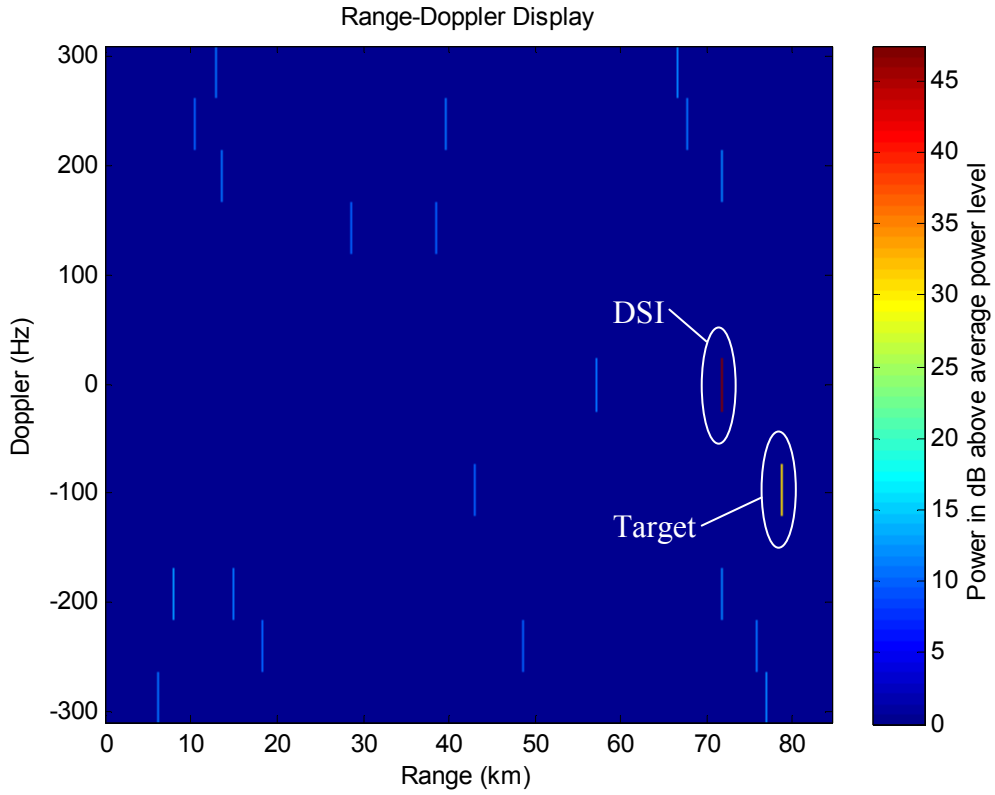

Figure 14 - ARD display for scenario with single target travelling north at 180 m/s and only one illuminator on, using simulated data, 17 seconds after first observation

Figure 15 shows the ARD display that was generated 31 seconds after the second observation. As expected, the Doppler and range of the red detection, corresponding to the DSI from the Abergavenny illuminator, have remained unchanged. The yellow target detection, however, has changed in both Doppler and range. The bistatic range has decreased by about 91 m, giving a Doppler shift of approximately -67 Hz. When divided by the Doppler resolution for this radar system and rounded to the nearest integer, a Doppler cell value m of -1 is obtained. This appears in the ARD as a detection in a Doppler cell at roughly -50 Hz. The range of the target detection has changed to about 75.5 km.

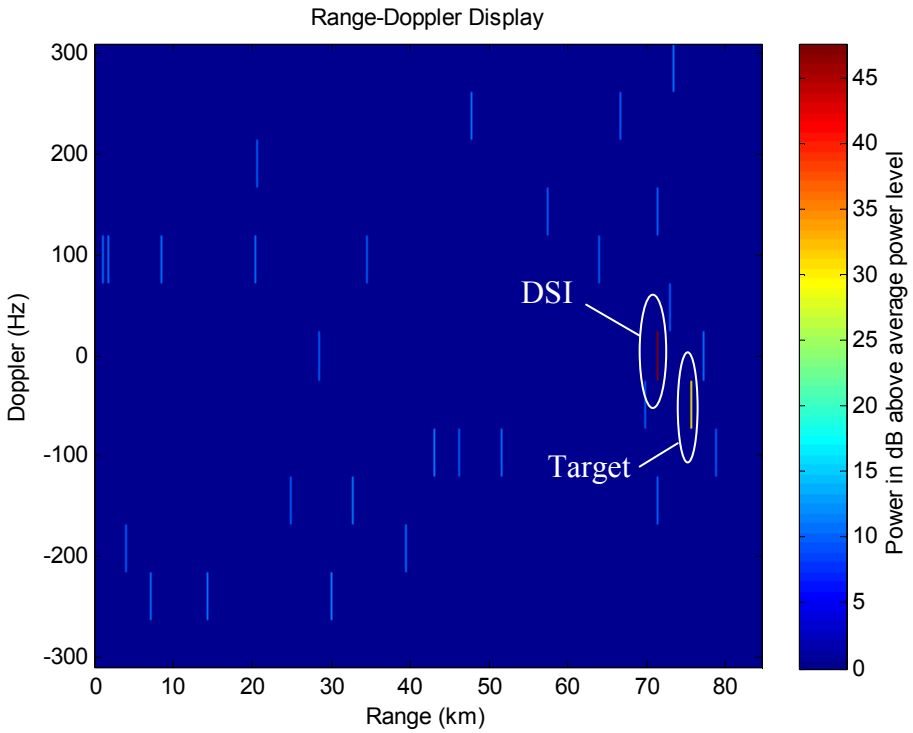

Figure 15 - ARD display for scenario with single target travelling north at 180 m/s and only one illuminator on, using simulated data, 31 seconds after second observation

2.7 Discussion

The discrepancy between the simulated and off-the-air autocorrelations indicate that the rudimentary model needs to be made more realistic. Although there are peaks in the simulated autocorrelation that occur with the same time delays as those in the off-the-air autocorrelation, their magnitudes differ. There are also a number of peaks in the simulated autocorrelation that are not present in the off-the-air autocorrelation. This suggests that the rudimentary model needs to account for losses suffered by the transmitted signals during propagation. In reality, transmitted signals are diffracted around obstacles and reflected from surfaces (multipath). Diffracted signals suffer losses as energy is diverted away from the direction of propagation. Reflected signals also experience a reduction in strength as the reflecting surface absorbs some of the energy of the incident ray. When a transmitted radar signal is reflected by terrain, the interaction results in a change to the polarisation of a certain proportion of the signal (depolarisation). Since the target receiver will respond only to signals of a particular polarisation, the depolarisation results in a loss to the signal entering the receiver. The diffraction, multipath and depolarisation losses all need to be modelled to accurately synthesise the received signals.

The simulated ARD displays show that the rudimentary model does not account for a large amount of DSI. There are far more signals entering the receiver due to diffraction and multipath than those produced by the rudimentary model. The addition of sophisticated propagation modelling is necessary to properly represent the degree of DSI present in the radar system environment.

Another limitation of the rudimentary model is that the Antenna Gain Unit takes the gain patterns of the transmitters and receiver to be direction independent and provides only a single gain value that represents the antenna look direction. The outputs of this Unit are used to calculate the power of the DSI, which in turn determines the characteristics of the radar signals simulated by the simulator. The antennas cannot always be assumed to be isotropic however. As we will see in Chapter 4, some receivers consist of a system of antennas, sometimes pointed in different directions, with a combined gain pattern that varies markedly with direction. The gain changes noticeably with the position of the antennas and the targets. More sophisticated modelling of the antenna gains is therefore required to achieve simulated radar signals that are more accurate and hence more realistic.

Similarly, the RCS Unit gives a representative value for the RCS of the target. The output of this Unit is used in the calculation of target returns. The RCS of a target is a measure of the energy scattered from the target in the direction of the receiver. In practice, when a target is illuminated, some of the transmitted energy is absorbed and the reflected energy is not distributed equally in all directions. A representative RCS value, such as that provided by the rudimentary model, is inadequate because the RCS of a target changes with the angle of incidence, the angle of view, and the frequency and polarisation of the radar signals. RCS is a matrix quantity rather than a single value. Hence the rudimentary model needs to be enhanced to include more advanced modelling of the target RCS in order to properly simulate radar signals.

3 Advanced Propagation

This chapter describes the development of the rudimentary model by the addition of more sophisticated propagation effects. As described in Chapter 2, the discrepancy between the real Bath autocorrelation and the simulation motivates the need to include contributions from 'hidden' transmitters through diffraction and reflections and also the effect of depolarisation. The enhancements made to the model to incorporate these factors, through the inclusion of new software modules, are discussed. The verification of the modules is described, and the effect of their refinements on DSI is explored.

3.1 Propagation Loss Unit

As mentioned in Chapter 2, the Propagation Loss Unit accounts for reductions to the signals as they travel over and above the spreading loss. In the rudimentary model, this Unit does not perform a function. The only loss that is modelled is spreading loss, which is accounted for by the Target Power Unit and the DSI Power Unit. At the next stage of development of the model, the Propagation Loss Unit is extended to include the effects of diffraction, multipath and depolarisation.

The Propagation Loss Unit is made up of a Terrain Map Generator, a Diffraction Loss Unit, a Multipath Loss Unit and a Depolarisation Loss Unit. Figure 16 shows a block diagram of the Propagation Loss Unit.

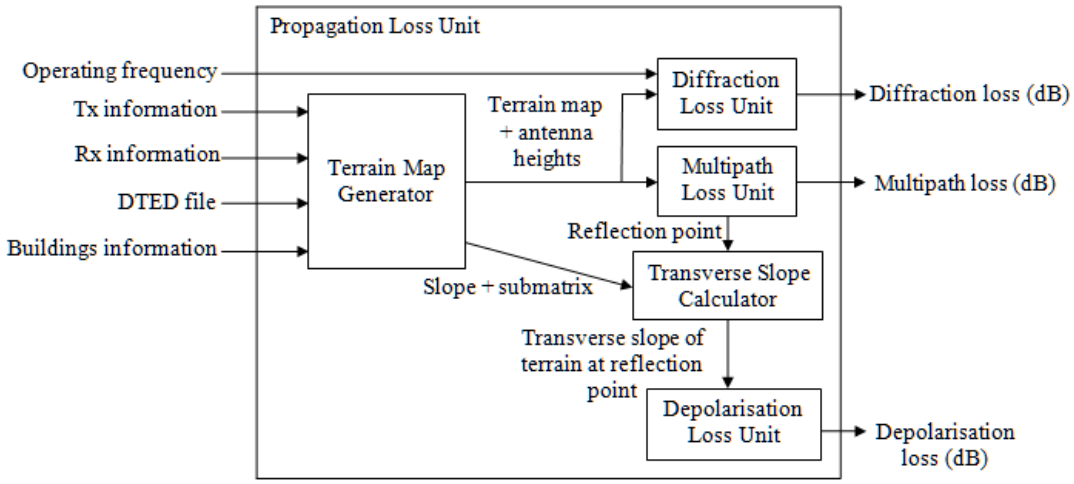

Figure 16 - Propagation Loss Unit block diagram

The inputs to the Propagation Loss Unit are the latitude and longitude coordinates of the transmitters and receiver and their heights above sea level (labelled as ‘Tx information’ and ‘Rx information’), a Detailed Terrain Elevation Data (DTED) file for the region containing the PBR system, information about any buildings in the region, and the operating frequency of the radar system.

The Terrain Map Generator processes the inputs to produce a terrain map and information about the antenna heights that is then fed into the Diffraction and Multipath Loss Units.

The Diffraction Loss Unit calculates the reduction (in decibels) of the transmitted signals caused by obstacles between the transmitters and receivers, the residual power being that due to diffraction around the obstacles. The Terrain Map Generator calculates the slope along the ground beneath the propagation path and also produces a submatrix from which transverse slopes can be calculated where needed. The slope and submatrix are sent to the Transverse Slope Calculator, which then calculates the transverse slope at reflection points provides by the Multipath Loss Unit. The Multipath Loss Unit calculates the points at which the signal is reflected for propagation by reflection.

The transverse slope of the terrain at each of the reflection points is determined and fed into the Depolarisation Loss Unit. This Unit computes the proportion of each transmitted signal that is lost because of changes in the signal polarisation through interaction with the terrain (i.e. depolarisation).

Each of the five components of the Propagation Loss Unit is described in more detail later in this chapter.

3.2 Terrain Map Generator

The Terrain Map Generator is responsible for converting information about the transmitters, receivers, buildings and surrounding topography of the PBR system into a form suitable for use by the Diffraction, Multipath and Depolarisation Loss Units. Figure 17 shows a block diagram of the Terrain Map Generator.

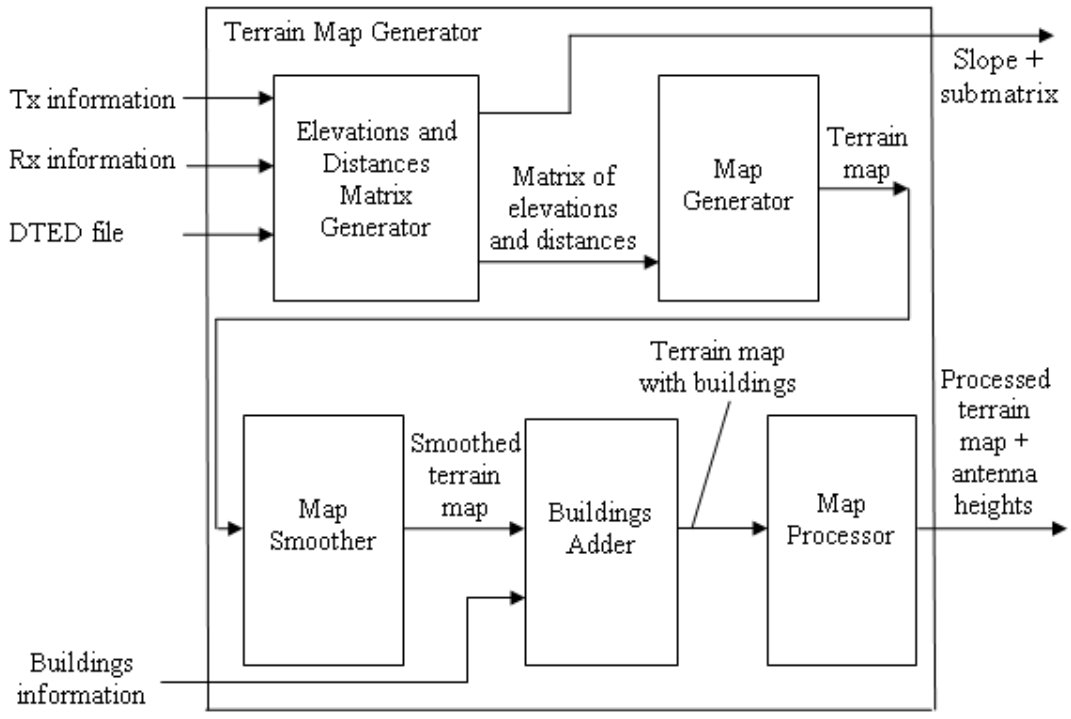

Figure 17 - Terrain Map Generator block diagram

The inputs to the Terrain Map Generator are the latitude and longitude coordinates and heights (in metres) above sea level of all the transmitters and receivers in the PBR system being simulated, a DTED file of the area covered by the system, and any information about buildings in the vicinity of the system. A DTED file contains a matrix of terrain elevations (in metres) above sea level at regular intervals of the area of interest.

For the application of the simulator, two scenarios were considered. The first scenario involved a receiver located at the University of Bath in the UK and 10 BBC DAB illuminators around the university. The latitude and longitude coordinates of the receiver and illuminators were obtained from information on the Web (the Wikipedia entry for the University of Bath [48]), and the 'mb21 UK Broadcast Transmission' website [49].) The heights of the receiver and illuminators were obtained from physical inspection at the University of Bath and from email correspondence with the BBC. The DTED file of the area covered by the radar system came from the Web (a website for the Shuttle Radar Tomography Mission detailed elevation models [50]). The locations and heights of the buildings in the vicinity of the radar system were gleaned from Google Earth and physical inspection at the University of Bath.

The second scenario involved a single illuminator at Mount Lofty in South Australia and receiver with a location to be determined by the simulator. The information about the illuminator came from the Web (the Wikipedia entry for Mount Lofty [51]). The DTED file for the area covered by the radar system was obtained from the SRTM website mentioned earlier.
The Terrain Map Generator first determines the coordinates in the matrix of elevations of each transmitter and receiver. For each transmitter and receiver pair that will be communicating, the Terrain Map Generator isolates a submatrix of the elevations matrix that is bounded by the minimum and maximum of the row numbers of the two antennas, and by the minimum and maximum of the column numbers of the pair. A straight line path between the transmitter and the receiver in this submatrix is then determined. The slope of the path and the submatrix are sent to the Transverse Slope Calculator. The path is divided into segments of equal length. At the ends of the segments, or waypoints, the elevation of the terrain is recorded, using interpolation within the submatrix if necessary. The elevations and their corresponding distances along the straight line path are stored in a matrix.

Given a set of land elevations above sea level and their corresponding distances along the earth's surface (a set of elevations), the Terrain Map Generator uses this information to generate a terrain map. The resulting boxlike sections of the terrain map are smoothed to form triangular segments using an algorithm that connects the midpoints of the sections. The Terrain Map Generator includes a feature for adding buildings. The inputs to this feature are the distance along the terrain where the building starts and ends along the horizontal, and the height of the building at the start and end points. The Terrain Map Generator determines the segment number of the terrain map where the building will be located. It is assumed that the length of the building fits within one segment of the terrain map. The building can then be incorporated into the terrain map using the aforementioned parameters.

Finally, the Terrain Map Generator processes the terrain map to prepare it for use by the other Units. The Generator adds the heights of the transmit and receive antennas, and passes this information, along with the terrain map, to the other Units.

3.3 Diffraction Loss Unit

3.3.1 Motivation

Diffraction is the apparent leakage of energy into regions that are inaccessible in the geometric optics limit. If a transmitter and receiver have no direct path, or no path by reflection, a signal can still pass from the transmitter to the receiver through diffraction. Some energy from the signal propagates into the shadow region behind an obstruction in the path of the signal. The diffraction process can be understood by using Huygen's principle [52].

As mentioned in Chapter 2, there is a lack of correspondence between the real Bath autocorrelation and the simulation. This is in part due to the presence of weaker illuminators other than those at Bath, Mendip and Wenvoe. There are in fact seven other DAB transmitters in the vicinity of the receiver. These transmitters are located at Abergavenny, Hannington, Membury, Naish Hill, Pur Down, Ridge Hill, and Stockland Hill. In the simplest model, these are assumed to be too weak or masked by ground topography, but this is not the case in reality. To study this, the simulator was expanded to incorporate a terrain map of the region containing these transmitters. Simulations were run with just the effects of diffraction due to topography taken into account.

The simulations showed that topography has no real effect except for the Pur Down transmitter, which caused a loss of about 4.5 dB. This is because the receiver and transmitters are all quite high up (the radar receiver is 20 m above the terrain). However, these calculations do not take into account the buildings that are in the vicinity of the receiver. Some of the buildings that stand between the receiver and transmitters also form diffractive screens. This can be seen in Figure 18, in which the circle shows the locality of the receiver and the arrows indicate the directions of the transmitters.

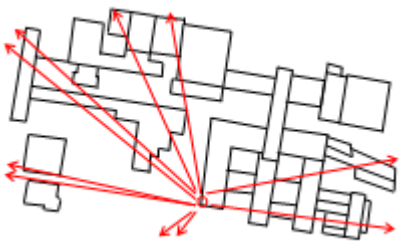

Figure 18 - Buildings in the vicinity of the receiver (shown circled)

For the Abergavenny transmitter, the diffraction screen has an effective height of about 20 m above the receiver at a distance of about 182.2 m from the

receiver. The diffraction screen for the Bath transmitter has a height of about 7.5 m above the receiver and is a distance of approximately 116.3 m from the receiver. Similarly, the Pur Down, Ridge Hill, St. Hilary and Wenvoe transmitters have diffraction screens of effective height about 20 m, 7.5 m, 7.5 m and 7.5 m, respectively, at distances of about 175.1 m, 88.9 m, 117.6 m and 115.6 m, respectively, away from the receiver.

Clearly, the diffractive effects of buildings of such heights in any PBR system will have a severe impact upon the DSI. The simulator thus needs to include a component that accounts for the diffractive effects of tall buildings and topographical features in the vicinity of the PBR system being simulated. The Diffraction Loss Unit was designed to perform this function.

3.3.2 Background Theory

Huygen's principle can be applied to diffraction over a screen as illustrated in Figure 19. Assume we have two antennas A and B. There is a screen between them that is orthogonal to the line joining the two antennas. It is of infinite extent in both x directions and the negative y direction. In the positive y direction, the screen has a finite height h. Z_A and Z_B are the distances of the screen from antenna A and B, respectively.

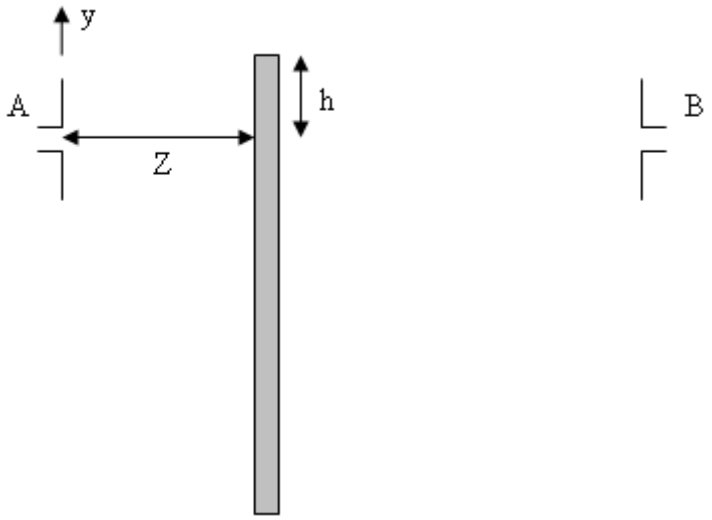

Figure 19 - Propagation obscured by a screen

Consider an electromagnetic field arising from a current distribution $\mathbf{J}_A$, another field arising from another current distribution $\mathbf{J}_B$, and a surface S that surrounds all sources. If S is a sphere of sufficiently large radius, the fields will behave in a wave-like fashion on this surface, that is, propagation will be in the radial direction. Loosely, the Lorentz reciprocity theorem states that the relationship between an oscillating current and the resulting field is unchanged if one interchanges the points where the current is placed and where the field is measured.

Now consider two antennas A and B. The electric field is zero inside the metal of the antennas, so the only contribution to the field comes from the vicinity of

the antenna feeds. A driven feed can be modelled as a cylindrical region across which there is a voltage drop and through which a current flows. From the Lorentz reciprocity theorem, it can be shown that the mutual impedance (the ratio of the voltage between either of two pairs of terminals to the current applied at the other pair of terminals when the circuit is open) of antenna A due to antenna B is the same as the mutual impedance of B due to A.

A surface S that stretches to infinity and separates antennas A and B is added. At the intersection of S with the line of sight between A and B, the phase is at a minimum. At points away from the point of intersection, the phase of the fields increase, but near the intersection, it is assumed that A and B are at a large enough distance from the screen for a plane wave approximation to be valid. At points close to A, the field of antenna B behaves as a plane wave. Assuming that A and B are close enough together for each to be in the radiation zone of the other, an expression for the mutual impedance can be derived.

If the surface S is now truncated to the screen in the scenario of Figure 19 and antenna A is assumed to be in the Fresnel zone of the screen, an expression for the mutual impedance with the screen present can be obtained.

The ratio of mutual impedance with the screen to that without the screen yields the ratio of the voltages at the receivers for the same driving current and scenario. Consequently, the square of the absolute value of the ratio will yield the ratio of powers at the receiver. The attenuation (or loss) L to the signal in decibels due to the screen is given by

$$L = 20\log_{10}\left(\frac{1}{\sqrt{\frac{1}{\pi}\left(\int_{\nu}^{\infty}\exp(-jY^2)dY\right)\left(\int_{\nu}^{\infty}\exp(-jY^2)dY\right)^*}}\right) \quad (10)$$

where $\nu = h\sqrt{\left(\frac{\beta}{2}\left(\frac{1}{Z_A}+\frac{1}{Z_B}\right)\right)}$, $Y = y\sqrt{\left(\frac{\beta}{2Z_A}+\frac{\beta}{2Z_B}\right)}$, $\beta = \frac{2\pi}{\lambda}$ for the wavelength λ at the operating frequency (220 MHz for DAB-based radar) [53] and * denotes the complex conjugate. See Appendix A for the derivation of the expression for the attenuation expression.

For values of v less than 0, the simulator multiplies the v by -1 then proceeds with the calculations as for values of v greater than or equal to 0.

Propagation of transmitted radar signals over complex terrain, such as hilly ground, can be approximated by the use of an effective screen. In Bullington's equivalent knife edge approximate model, the hilly terrain is substituted by a single "equivalent" knife edge at the point of intersection of the horizontal ray from the transmit and receive antennas, that at worst touches the peaks of the hills, as shown in Figure 20. Bullington studied the cases of two or more knife-edge obstacles between the transmitter and receiver. In these studies, graphical integration suggested that the approach gave an error that was no worse than 2 or 3 decibels [55]. However, Bullington's method has a major limitation if there are important obstacles along the radio path that are ignored because the

intersecting line from the transmitter to the receiver passes above the peak of the obstacles. In this case there can be significant errors [56].

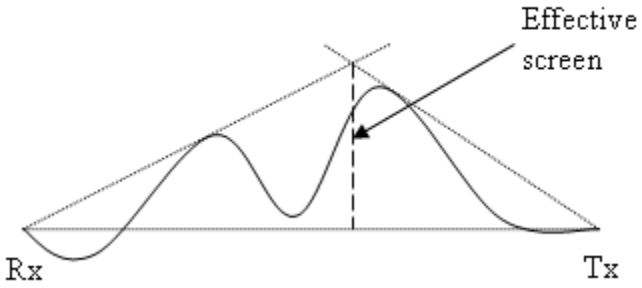

Figure 20 - Propagation over hilly ground

3.3.3 Operation

The Diffraction Loss Unit takes in a processed terrain map from the Terrain Map Generator and first adds the heights of the transmitter and receiver to the map. To perform distance calculations, the Unit converts the elevation and distance values in the terrain map to Cartesian coordinates with the origin centred on the transmit antenna. The y-coordinate of the receiver, and the y-coordinate of all elevations that are not located at the origin, all need to be corrected by a factor to account for the curvature of the earth. The correction factor *y* is given by

$$y = \frac{-x^2}{2R_e} \qquad (11)$$

where x is the distance from the origin along the terrain (for x less than or equal to 50 km) and R_e is the radius of the earth. This correction factor is added by the Unit to the y-coordinate of all points with an x-coordinate other than that of the origin in the terrain map.

The Unit uses Bullington's equivalent knife edge approximate model to calculate the attenuation to the radar signals by topographical diffraction. The location of the diffractive screen due to the topography is determined by finding the angle between the transmit antenna and each of the elevation points in the terrain map. The maximum of these angles is stored. The process is repeated for the receive antenna to find the maximum receiver angle.

A line is extended from the transmit antenna at the maximum transmitter angle, and a line is extended from the receive antenna at the maximum receiver angle. The point of intersection of the two lines is then the top of the diffractive screen. A line is drawn to connect the top of the transmitter with the top of the receiver. The vertical distance between this baseline and the point of intersection is the height h of the screen. In the case of a line-of-sight path between transmitter and receiver, diffraction can still effect the loss. The screen will now be below line of sight and the value of h will be negative. The effect, however, rapidly diminishes with respect to height below the line of sight.

Using the terrain map, the operating frequency, the maximum transmitter and receiver angles and h, the parameter ν for the Fresnel integrals in equation (10) can be calculated. The Diffraction Loss Unit then determines the additional attenuation to the signal in decibels, using equation (10). Figure 21 shows a block diagram of the Diffraction Loss Unit.

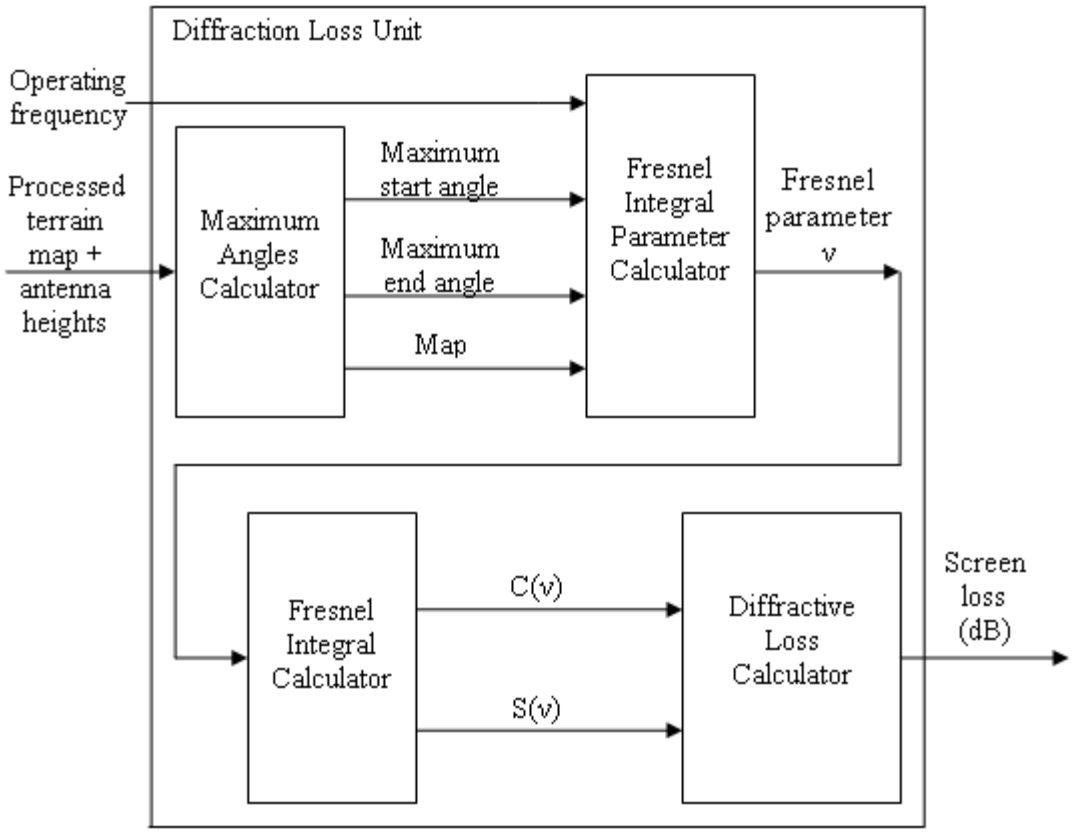

Figure 21 - Diffraction Loss Unit block diagram

3.3.4 Verification

The Diffraction Loss Unit was tested using a comparison with some of the results of a study performed by Ong and Constantinou. In their paper [57], Ong and Constantinou describe how they applied an asymptotic path-integral technique to radiowave propagation over an infinitely wide, perfectly conducting rectangular plateau for a ground-based transmitter and receiver. The total attenuation function was resolved into two components: that due to the fields travelling over the plateau and that due to the fields interacting with the top of the plateau. These components were determined quantitatively in the study. To test the Diffraction Loss Unit, the experimental results for only the non-interacting field were used for comparison.

In their study, Ong and Constantinou used an aluminium plateau that was situated on an aluminium ground plane at a frequency of 9.6 GHz. The infinite-width plateau was modelled by a box whose width was approximately 30 λ, and its depth was 4 λ in the direction of propagation. The transmitting antenna used was a ground-based λ/4 monopole and the receiving antenna was an X-

band rectangular waveguide positioned at ground level. The two antennas were situated at a distance of 30 λ from the front and back vertical faces of the plateau respectively. A set of measurements was taken by varying the height of the plateau from 0 to 15 λ. Figure 22 shows the geometry of the experimental setup.

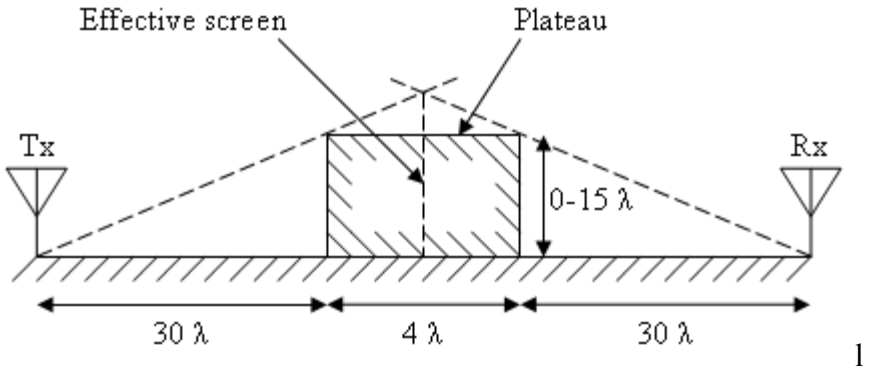

Figure 22 - Geometry for infinite-width plateau model

Figure 23 shows the normalised attenuation against the plateau height for the total and individual component fields. The solid line shows the total field, the dashed line gives the non-interacting field, and the dotted line indicates the interacting field, all as predicted by theory. The total field found by experimentation is marked as °. As mentioned earlier, the test for the Diffraction Loss Unit is concerned only with measurements for the non-interacting field, marked as Δ.

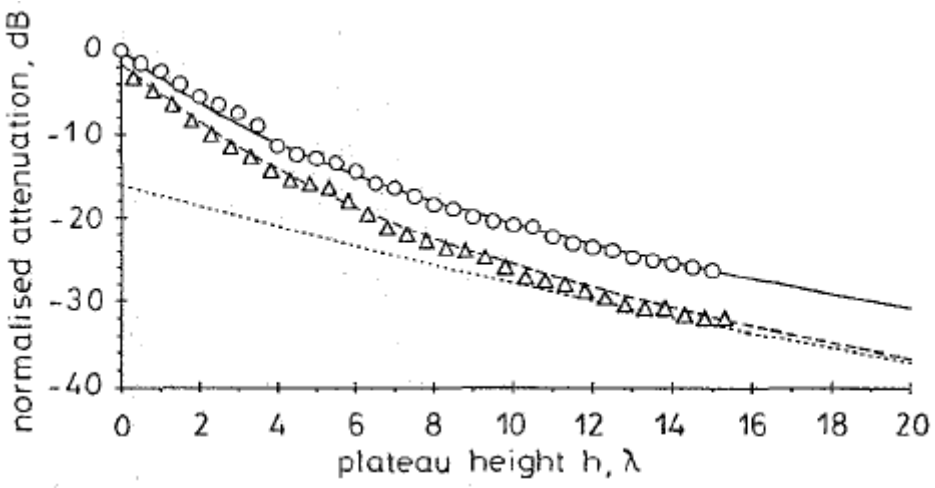

Figure 23 - Numerical and experimental results for the normalised attenuation function against plateau height for total and individual component fields [57]. The Diffraction Loss Unit test is concerned only with the experimental results for the non-interacting field (marked as Δ)

To test the Diffraction Loss Unit, a scenario similar to that used in the Ong and Constantinou study was run through the Unit. A terrain map of a plateau with the same dimensions and spacing from the transmitter and receiver as that used in the study was input to the Unit. The height of the plateau was varied from 0 to 15 λ, and the heights of the ground-based transmitter and receiver were assumed to be 0. For each plateau height, the attenuation due to the effective

diffractive screen was computed in decibels by the Unit. Figure 24 shows the plot of attenuation against plateau height.

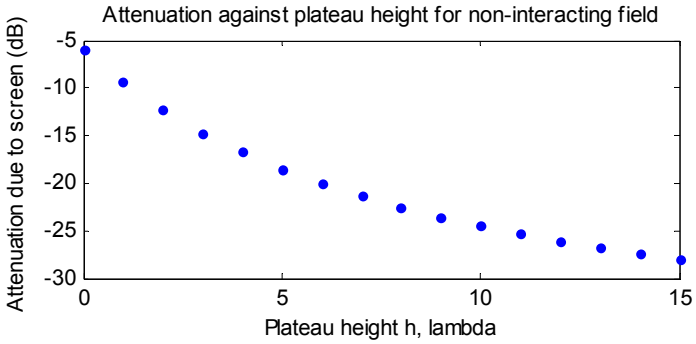

Figure 24 - Plot of attenuation against plateau height for the non-interacting field obtained during testing of Diffraction Loss Unit

There is agreement to within about 4 dB between the plot of attenuation versus plateau height for the non-interacting field produced by the Ong and Constantinou study and that produced by the Diffraction Loss Unit. This error is of the order to be expected from the Bullington approach and indicates that the Diffraction Loss Unit is functioning correctly.

3.4 Multipath Loss Unit

3.4.1 Background Theory

Multipath is the propagation phenomenon that results in radio signals reaching the receiving antenna by two or more paths. For a given transmitter and receiver, in addition to the direct signal between the two antennas in addition to signals, there are usually propagation paths caused by reflections from the ground and objects lying in the region between the receiver and transmitter. The Multipath Loss Unit of the simulator models the effects of these reflections.

The French mathematician Fermat (1601-1665) postulated that, no matter to what kind of reflection or refraction a ray is subjected, it travels from one point to another in such a way as to make the time taken a minimum [58]. The Multipath Loss Unit uses this principle to determine the paths taken by the non-direct signals, that is, the signals reflected by terrain and objects (such as buildings) between the illuminator and receiver. Fermat's principle is used to find reflection points on the ground and objects between the illuminator and the receiver, the point being that which makes the total distance minimum.

3.4.2 Operation

The Multipath Loss Unit takes in a processed terrain map from the Terrain Map Generator. The Unit converts the elevation and distance values in the map to Cartesian coordinates. The elevation values are corrected to take into account the curvature of the earth.

To determine the reflected paths, the total path length of the terrain map is first calculated. The total path length is divided into a number of segments that is dictated by a user-specified number of points to be searched. For each segment, there are a required number of reflection points to be analysed. The coordinates of these points are determined along with their corresponding path lengths.

Once a set of reflection points and their corresponding path lengths has been obtained, the Multipath Loss Unit finds the stationary points (maxima or minima) among them. Stationary points that lie outside of the terrain map are removed. Similarly, stationary points with corresponding paths that are invalid (that is, the paths appear to travel through the terrain) are discarded. Spurious stationary points are eliminated by testing whether the angle made by the incident ray with the segment of the terrain map that contains the stationary point is equal to the angle made with the same segment made by the reflected ray. The remaining set of values are stationary points with corresponding paths that represent the paths of reflected signals.

Figure 25 shows a block diagram of the Multipath Loss Unit's operation.

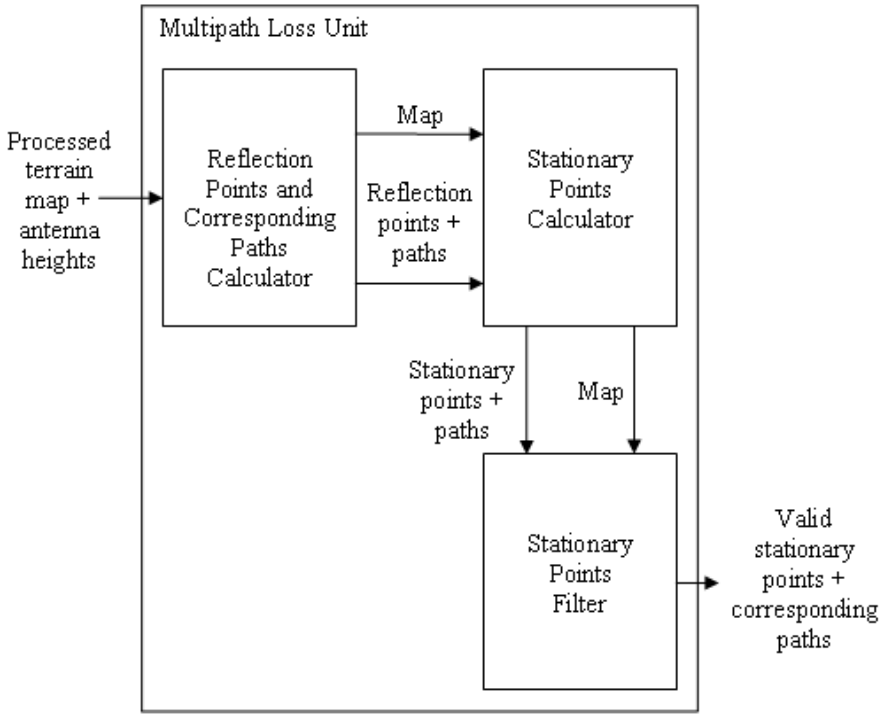

Figure 25 - Multipath Loss Unit block diagram

3.4.3 Verification

The Multipath Loss Unit was tested using the case of an illuminator and receiver separated by a uniformly sloping section of terrain. The illuminator was located 5 m above ground at a point with a terrain elevation of 50 m above a reference height. Over a distance of 500 m, the terrain sloped downwards to a point with elevation of 0 m above the reference and where the receiver was located (also 5 m above the ground). Figure 26 shows the test scenario.

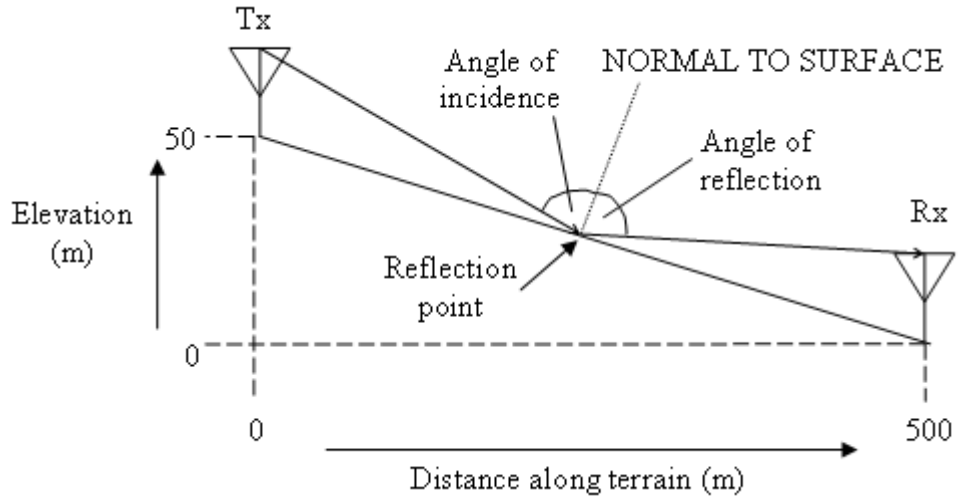

Figure 26 - Test scenario for Multipath Loss Unit verification

In the Multipath Loss Unit, the reflection point is calculated by Fermat's principle which finds the shortest reflected path between the illuminator and receiver. A measure of its effectiveness is how well it predicts the known result that the angle of incidence should equal that of reflection. It does this to within 0.005 degrees for the example given.

In accordance with Fermat's principle, the Multipath Loss Unit selects the stationary points with corresponding paths that are minima. For a given stationary point, the distance r (in m) between the transmitter and the stationary point along the reflected ray is computed. The normalised electric field amplitude is then calculated using

$$E = R\frac{1}{r}e^{-j\beta r} \qquad (12)$$

where R is the reflection coefficient (assumed to be -1 for the frequencies used in passive radar), $\beta = \frac{2\pi f}{c}$, f is the operating frequency in Hz and c is the speed of light in m/s. The power of the electric field is obtained by taking the square of the absolute value of E, and this quantity is converted to decibels. The result is the attenuation or loss, in decibels, to the DSI power due to multipath.

3.5 Depolarisation Loss Unit

3.5.1 Background Theory

When a transmitted radar signal is reflected by terrain, the interaction results in a change to the polarisation of a certain proportion of the signal. If the original transmitted signal was vertically polarised, some of the signal would become horizontally polarised because of the reflection, and the signal arriving at the receiver could be significantly different in polarisation to that which was originally transmitted. In this case, depolarisation describes the proportion of

vertically polarised signal that has become horizontally polarised and to which the target receiver will respond (DAB transmissions are vertically polarised and targets are normally detected using horizontal polarisation).

For an electric field $\mathbf{E}^i$ incident upon a flat surface with unit normal **n**, the reflected field $\mathbf{E}^r$ is given by

$$\mathbf{E}^r = R_V[2\mathbf{n}(\mathbf{n}\cdot\mathbf{E}^i) - \mathbf{E}^i] \qquad (13)$$

where the reflection coefficient can be approximated as $R_V = -1$ at the VHF/UHF frequencies typically used in passive radar. The approximate value of the reflection coefficient was obtained as follows.

Consider an electromagnetic wave that is incident upon the ground ($\varepsilon_r = 10$ and $\sigma = 0.01$) at an angle φ from the normal. The reflection coefficient R_V is given by

$$R_V = \frac{\cos\varphi\eta_r^{-2} - \sqrt{\eta_r^{-2} - \sin^2\varphi}}{\cos\varphi\eta_r^{-2} + \sqrt{\eta_r^{-2} - \sin^2\varphi}} \qquad (14)$$

where

$$\eta_r = \frac{\varepsilon_r^{-1/2}}{\sqrt{1 - \frac{j\sigma}{\omega\varepsilon}}} = \frac{\varepsilon_r^{-1/2}}{\sqrt{1 - \frac{j}{0.0556f}}} \qquad (15)$$

for f in megahertz.

At the UHF/VHF frequencies usually used in passive radar (220 MHz for DAB-based radar), $\eta_r << 1$ and as grazing incidence is approached (φ tends to 90°), the reflection coefficient

$$R_V \approx \frac{-\sqrt{\eta_r^{-2} - 1}}{\sqrt{\eta_r^{-2} - 1}} \approx -1. \qquad (16)$$

Assume the electric field is in the y-direction, so

$$\mathbf{E}^i = E^i\hat{\mathbf{y}} \qquad (17)$$

For a totally flat surface, the unit normal n is in the y-direction, so n = (0,1,0).

For a flat surface tilted in the x-direction at an angle α to the x-axis, n = (sin α, cos α,0).

Since α is small, sin $\alpha \approx \alpha$ and cos $\alpha \approx 1$, so $\mathbf{n} \approx (\alpha,1,0)$. Thus $\mathbf{n}.\mathbf{E}^i \approx (\alpha,1,0).(0,E^i,0) = E^i$.

So

$$\mathbf{E}^r \approx R_V[2(\alpha,1,0)E^i - E^i\hat{\mathbf{y}}] \qquad (18)$$

and the horizontal component is then $E^r_h \approx R_V 2\alpha E^i$.

Since power is proportional to the square of the electric field, the power in the horizontal component of the reflected electric field is given by

$$P_h \approx (R_V 2\alpha) 2 P_v \qquad (19)$$

where P_v is the power in the vertical component of the incident electric field. For a transverse terrain slope of 0.05 (typical of terrain around the radar at Bath), this gives a cross polarisation loss of approximately -20 dB. This is typical of cross polarisation losses experienced at Bath.

3.5.2 Operation

For each illuminator, at the reflection point determined by the Multipath Loss Unit, the transverse slope of the terrain is calculated and fed into the Depolarisation Loss Unit.

The Depolarisation Loss Unit calculates the power in the horizontal component of a vertically polarised electric field reflected from a sloping surface, given the incident electric field, the vertical polarisation reflection coefficient, and the transverse slope of the surface.

The Unit first calculates the angle in radians made by the slope with the horizontal:

$$\alpha = \text{arc tan(slope)} \qquad (20)$$

The magnitude of the loss in translation to horizontal component is then determined:

$$P_{r_h} = (R_V 2\alpha)^2 P_{i_v} \qquad (21)$$

Finally, the Unit converts the result to decibels:

$$P_{r_h} = 10 \log_{10}(P_{r_h}) \qquad (22)$$

3.6 Effect of refinements on DSI

Once the Propagation Loss Unit was incorporated into the simulator, the DSI power was calculated with the diffractive, multipath, depolarisation and signal processing noise losses taken into account. Also included in this simulation were the seven weaker illuminators located at Abergavenny, Hannington, Membury, Naish Hill, Pur Down, Ridge Hill and Stockland Hill. Figure 27 shows the autocorrelation of the Synthesised Signal.

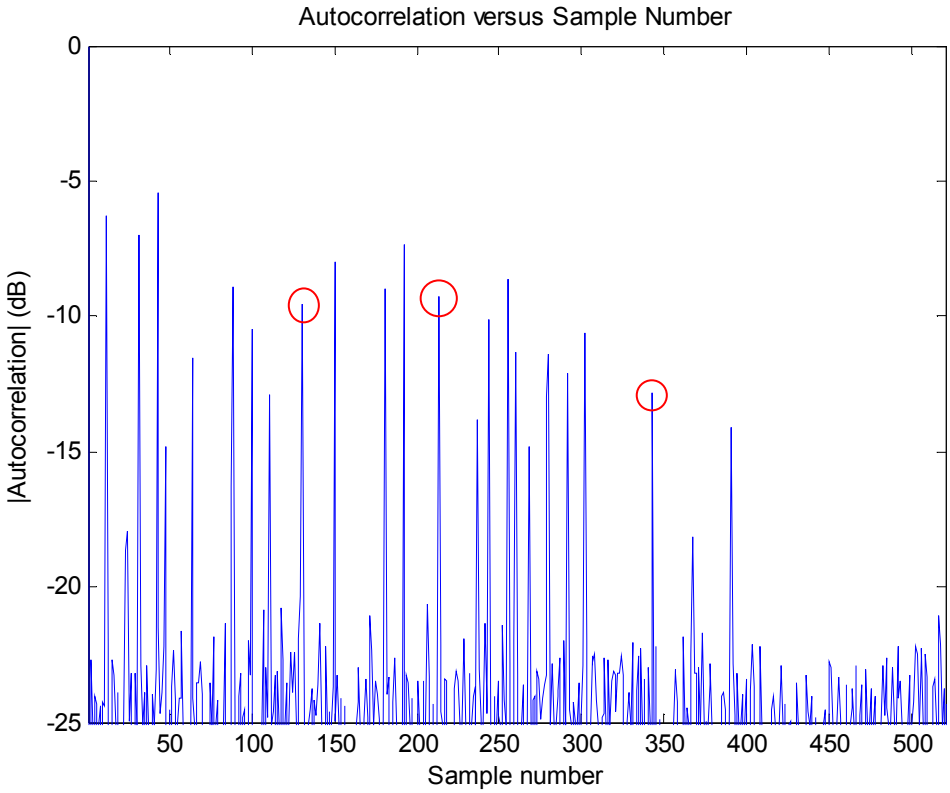

Figure 27 - Autocorrelation of Synthesised Signal

As with the autocorrelation of the Synthesised Signal produced by the rudimentary model, the cross-correlations of the three major illuminators can be seen and are shown circled. The peaks show the total signal correlated with itself (the signal at the origin), the Bath and Mendip signals' cross-correlation (at a delay of 131 time units), the Mendip and Wenvoe signals' cross-correlation (213 time units' delay) and the Bath and Wenvoe signals' cross-correlation (343 time units' delay). However, there are also additional cross-correlations corresponding to the seven other illuminators.

Figure 28 gives the autocorrelation of the Off-the-Air Signal, reproduced from Chapter 2 for comparison. The cross-correlations of the three main illuminators are shown circled.

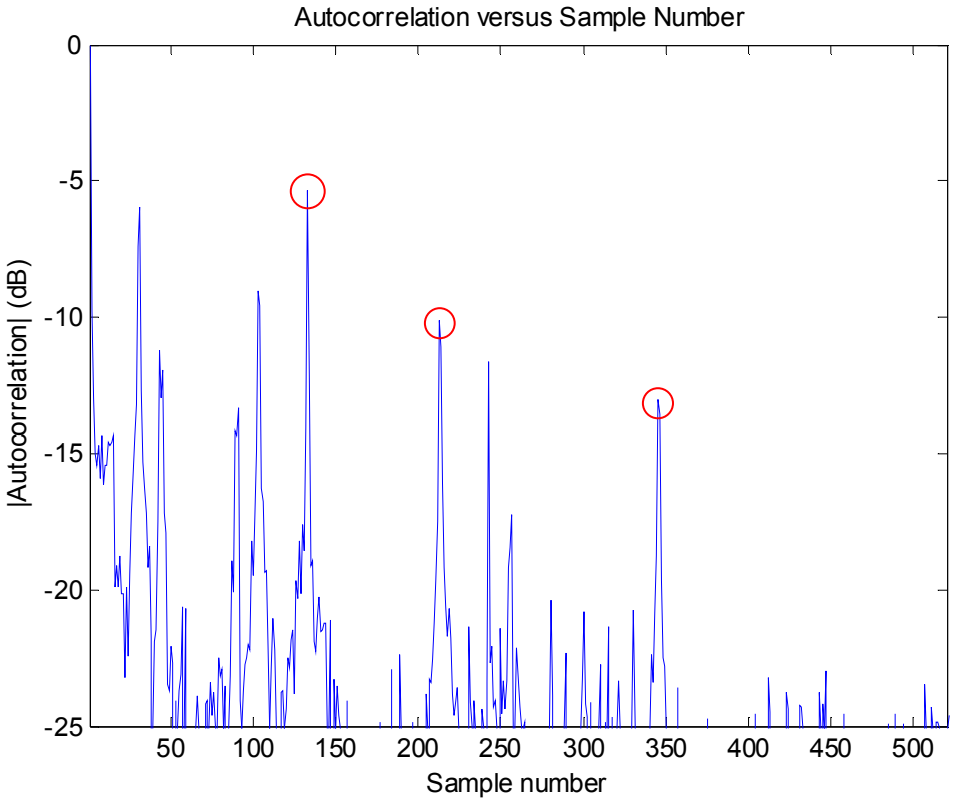

Figure 28 - Autocorrelation of Off-the-Air Signal

Viewing the autocorrelation of the Synthesised Signal in relation to that of the Off-the-Air Signal, one will note that the cross-correlations of the latter can be found in the former. The peaks in the case of the Synthesised Signal are generally higher than those of the Off-the-Air Signal however. It would appear that the refinements made to the rudimentary model to include the weaker illuminators and propagation and signal processing noise reductions are still not quite sufficient to produce an autocorrelation that matches that of the Off-the-Air Signal exactly. Such a model is obviously difficult to achieve in practice. The peaks in the autocorrelation of the Synthesised Signal occur at the same sample numbers as those of the Off-the-Air Signal, but they differ in magnitude by several decibels. It is clear that a further explanation needs to be found for the discrepancy in magnitude. One possible explanation lies in the complexity of the environment around the receiver location. The university campus around the receiver might be too complex for the approximations used in the Bullington method. Such an environment, however, is not a normal choice for a radar and so for operational use, the simplifications might not to be such a great problem.

4 Radar Cross-section Modelling

In the rudimentary model, the RCS Unit gave a representative value for this quantity. Similarly, the Antenna Gain Unit took the gain pattern of the transmitters and receiver to be direction independent and provided a gain value that is the antenna gain in the look direction. The outputs of these two Units are used in the calculation of target returns and the power of the DSI. More sophisticated modelling of the target RCS and receive antenna gains is required to achieve simulated radar signals that are more accurate and hence more realistic. Computer software called the Numerical Electromagnetics Code (NEC) was used to perform this modelling. This chapter describes the NEC modelling, and discusses its implications for radar modelling in general.

4.1 Explanation of the Problem

The RCS of a target is a measure of its detectability by a radar. The gain of an antenna relates its intensity in a given direction to the intensity that would be produced by a hypothetical ideal antenna that radiates isotropically and has no losses.

One approach to reducing the DSI problem (described in Chapter 2) is to operate the target orientated antenna (the receiver) in cross-polarisation to the transmitter. In a specified plane containing the reference polarisation ellipse, the polarisation orthogonal to the reference polarisation is called the cross-polarisation. The reference polarisation is called the co-polarisation [59]. In the Bath PBR scenario, the original broadcasts were vertically polarised, and the target array was operated in cross-polarisation to these (that is, the target array was operated in horizontal polarisation). The target array thus picked up far less DSI than it would have done if it had been operated in co-polarisation. Unfortunately, using cross-polarisation causes a reduction in the RCS of targets. Most targets produce strong cross-polarisation however, so this approach does not greatly reduce target returns [60].

To develop and test DSI reduction methods such as using cross-polarisation, the simulator needs to incorporate more advanced modelling of the target RCS and antenna gains than is used in the rudimentary model. As mentioned at the beginning of this chapter, the RCS and Antenna Gain Units of the rudimentary model used only representative values for these quantities. The next level of modelling involves the addition to the simulator of RCS values corresponding to a 360-degree sweep in the azimuthal plane for a given target, and of the transmitter and receiver gain patterns. This more sophisticated modelling allows the simulator to produce more realistic simulated radar signals. The more accurate target RCS and antenna gain modelling also enables us to determine whether, and to what extent, the reduction in target RCS due to cross-polarisation is compensated for by the reduction in DSI.

NEC is a computer code for analysing the electromagnetic response of antennas and other arbitrary metal structures consisting of wires and surfaces in free space or over a ground plane. The analysis involves the numerical solution

of integral equations for induced currents. This avoids many of the simplifying assumptions required by other solution methods. NEC is thus an accurate tool for electromagnetic analysis and modelling [62].

NEC was used to model the RCS of a small executive jet and to model the gain patterns of the receive antennas in the PBR system.

4.2 Target RCS Modelling

The RCS, denoted by σ, of a target is an indication of the size of the target and the ability of the target to reflect radar energy. σ has units of m². The RCS is a measure of the energy scattered from the target in the direction of the receiver. A larger RCS indicates that the target is more detectable. If absolutely all of the incident radar energy on the target were to be reflected equally in all directions, then the radar cross section would be equal to the cross sectional area of the target as seen by the transmitter. In practice, some of the energy is absorbed and the reflected energy is not distributed equally in all directions. The RCS is therefore difficult to estimate and is usually determined by measurement or simulation.

The RCS of a target depends on a number of different factors. These include the material of which the target is made, the physical geometry and exterior features of the target, the size of the target relative to the frequency of the transmitter, and the incident and reflected angles of the radar signals. Bistatic cross sections are more complex than monostatic cross sections because σ for the bistatic case is a function of aspect angle and bistatic angle [2].

The RCS of a target changes with the angle of incidence, the angle of view, and the frequency and polarisation of the radar signals. In practice, RCS is a matrix quantity, with the rows of the matrix being referenced to the viewing angle (0 to 359 degrees, in 1-degree increments, anticlockwise from the target's direction of travel), and the columns being referenced to the illumination angle (also 0 to 359 degrees, in 1-degree increments, anticlockwise from the target's direction of travel). It should be noted that the cross section also depends on the elevation angles, but these will vary over a much smaller range. The RCS patterns generated for illustration purposes, however, were produced for a representative value.

As mentioned previously, an application of the simulator is to develop and test DSI reduction methods such as using cross-polarisation. For this application, both co- and cross-polarised target cross sections need to be considered in order to evaluate the radar system.

4.2.1 Modelling of Small Executive Jet

Small executive jets are typical aircraft at airports such as Bristol Airport in the UK. A small executive jet was modelled with a mesh cylinder for the body and simple flat meshes for the wings and tailplane.

The dimensions of the aircraft were taken as follows:

Length = 21.06 m
Wingspan = 17.85 m
Tail height = 1.25 m
Fuselage height = 2.0 m
Wing area = 62.29 m^2

From these dimensions, the cylinder for the body was taken to have a radius of 1 m and a length of 21.06 m.

The operating frequency for DAB was taken to be f = 220 MHz. The speed of light c = 3e8 m/s. The wavelength lambda = c/f = 1.363m. The gaps in the cylinder mesh were less than lambda/4 in length. The ends of the cylinder, the wings and the tailplane had gaps of length less than lambda/8.

The cylinder was modelled as an octagonal prism, with its ends as circular discs. The wings were modelled as two horizontal rectangles and the tailplane as two smaller horizontal rectangles and one vertical rectangle.

A MATLAB program was written to generate the aircraft mesh and write it to a text file, which was then converted to an NEC file.

Figure 29 shows the aircraft mesh as seen in NEC.

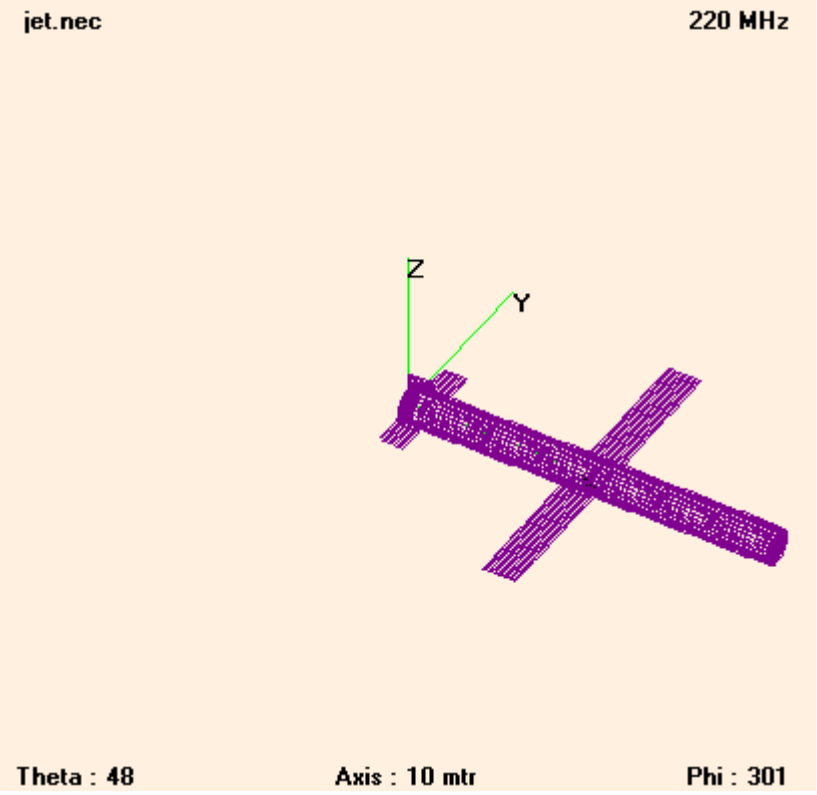

Figure 29 - Mesh for small executive jet

4.2.2 Simulation of RCS of Small Executive Jet

The RCS pattern of the jet mesh was simulated in NEC for various elevation angles of incidence and angles of view. Figure 30 shows these angles relative to the positions of the target, transmitter and receiver. It was assumed that the line joining the transmitter and receiver is horizontal, and that the target is the same distance from the transmitter and the receiver. Then

Angle of incidence = Angle of view = arctan(Height/L) (23)

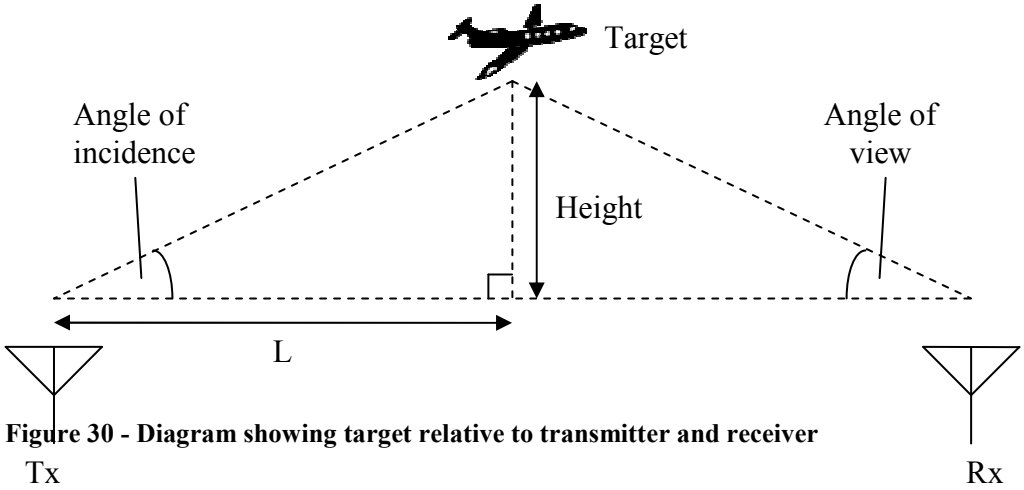

Figure 30 - Diagram showing target relative to transmitter and receiver

For height = 8 km and L = 25 km, the angle of incidence and angle of view are about 18 degrees. This angle was used in the NEC simulations that are described next.

To verify that the RCS patterns of the small executive jet have the correct magnitude, the maximum RCS values for end-on and side-on illumination were compared with the maximum monostatic backscatter values of a cylinder with the same dimensions as the body of the jet. The cylinder is essentially the jet without its wings and tailplane. The body length is 21.06 m, which is greater than ten times the wavelength (10*1.363 m =13.63 m), so the Rayleigh scattering regime may be used.

In the case of specular scattering with wavelength λ, the maximum monostatic RCS is given by

$$\sigma = 4\pi \frac{A_{effective}^2}{\lambda^2} \qquad (24)$$

from [63].

For a flat surface, $A_{effective} = A_{physical}$. The ends of a cylinder have $A_{physical} = \pi a^2$, where a is the radius of the cylinder. For a radius a of 1m, $A_{physical} = \pi$ m^2, so $A_{effective} = \pi$ m^2. Substituting this with $\lambda = 1.363$ m into (24) gives $\sigma = 66.7$ m^2. Converting to decibels gives

$$\sigma = 10 \log_{10}(66.7) = 18.2 \text{ dB} \qquad (25)$$

The RCS pattern obtained with nose-on illumination in vertical polarisation of the jet has a maximum backscatter value of about 15 dB. For tail-on illumination in vertical polarisation of the plane, the maximum backscatter value is approximately 13 dB. There is good agreement between the maximum RCS of the aircraft for end-on illumination and the theoretical maximum RCS of a cylinder with the same dimensions as the aircraft.

For a singly curved surface (of a cylinder), the maximum monostatic RCS is given by

$$\sigma = \frac{2\pi a}{\lambda} l^2 \qquad (26)$$

where a is the radius and l is the length of the cylinder [63].

With a length of 21.06 m, the maximum expected RCS is 33.1 dB. The RCS pattern obtained with side-on illumination in vertical polarisation of the jet has a maximum backscatter value of about 30 dB. This is close to the theoretical value.

The aircraft mesh was illuminated from various angles and the resulting RCS pattern was viewed at an elevation angle of 18 degrees in the azimuthal plane in both vertical and horizontal polarisation.

Figure 31 shows the radar cross section pattern for nose-on illumination (phi = 0 degrees) in vertical polarisation, relative to the Cartesian coordinate axes. Note that the RCS pattern is shown relative to the aircraft.

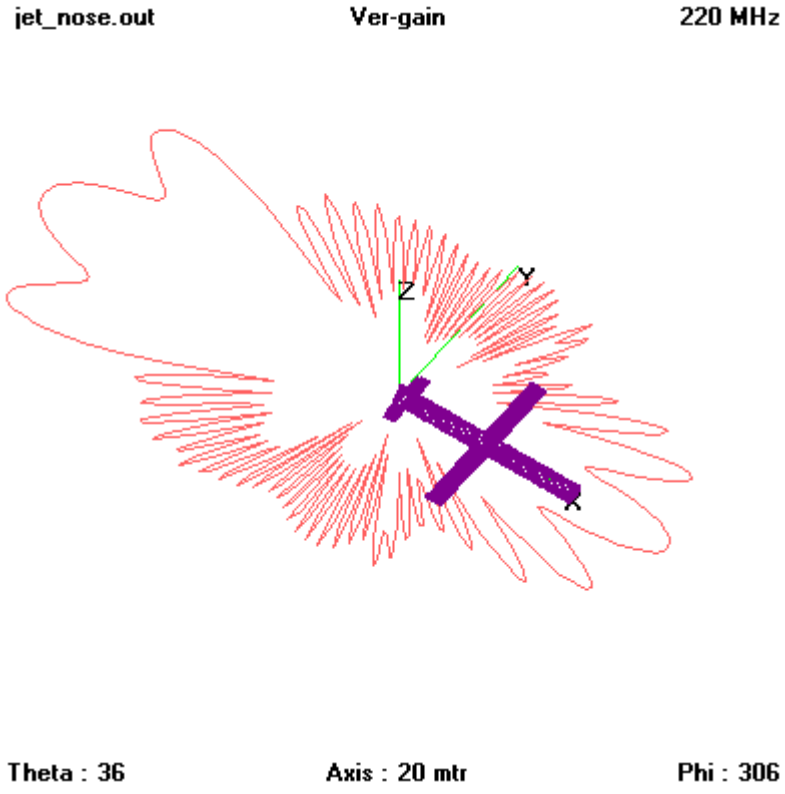

Figure 31 - Radar cross section pattern for nose-on illumination (phi = 0 degrees) in vertical polarisation, relative to coordinate axes (not to scale)

The illumination angle was changed to side-on (phi = 90 degrees). Figure 32 shows the RCS pattern in vertical polarisation relative to the aircraft.

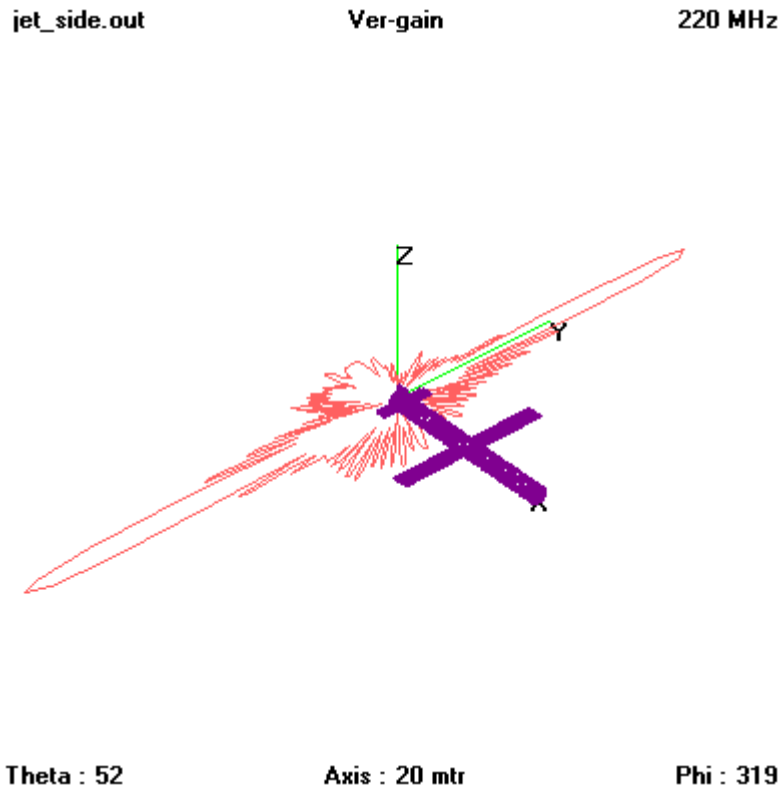

Figure 32 - Radar cross section pattern for side-on illumination (phi = 90 degrees) in vertical polarisation, relative to coordinate axes (not to scale)

Figure 33 shows the RCS pattern for nose-on illumination in vertical polarisation. As the illuminator was operated in vertical polarisation, this pattern is in co-polarisation relative to that of the illuminator. As expected, the RCS pattern is maximum in the direction of forward transmission (phi = 180 degrees). The RCS pattern is symmetric about the plane's axis of symmetry (phi = 0 to 180 degrees).

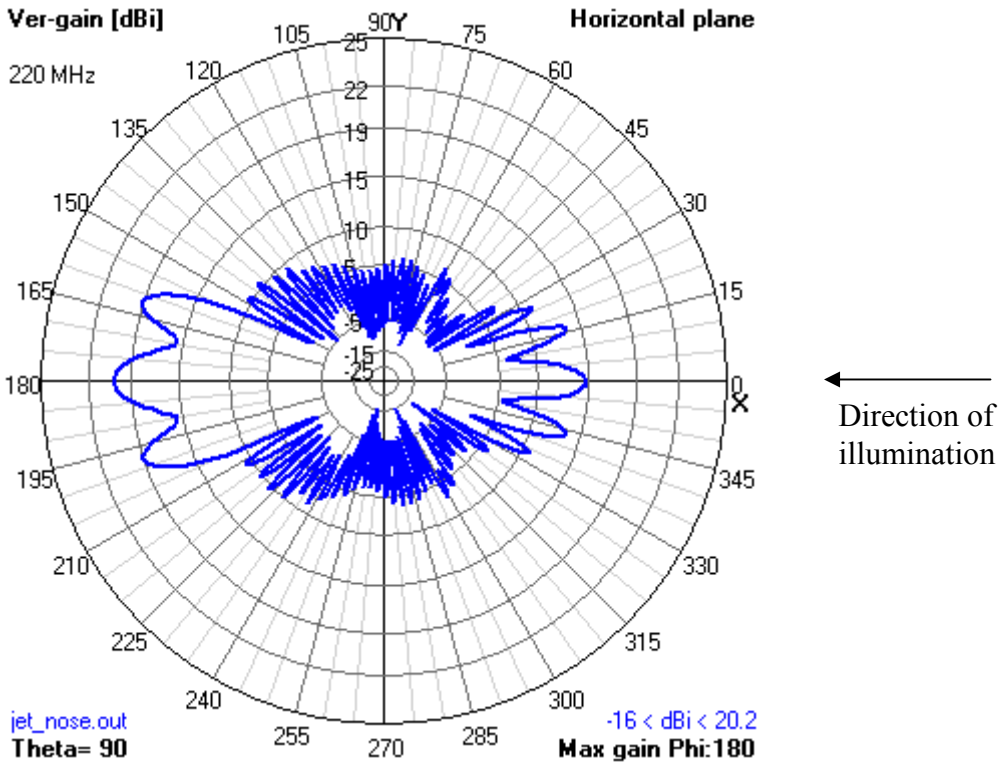

Figure 33 - Radar cross section pattern for nose-on illumination (phi = 0 degrees) in vertical polarisation

Figure 34 shows the RCS pattern for side-on illumination in vertical polarisation. As the illuminator was operated in vertical polarisation, this pattern is in co-polarisation relative to that of the illuminator. As expected, the RCS pattern is maximum in the direction of forward transmission (phi = 270 degrees). The RCS pattern is not symmetric since the aircraft is not symmetric when viewed from the side.

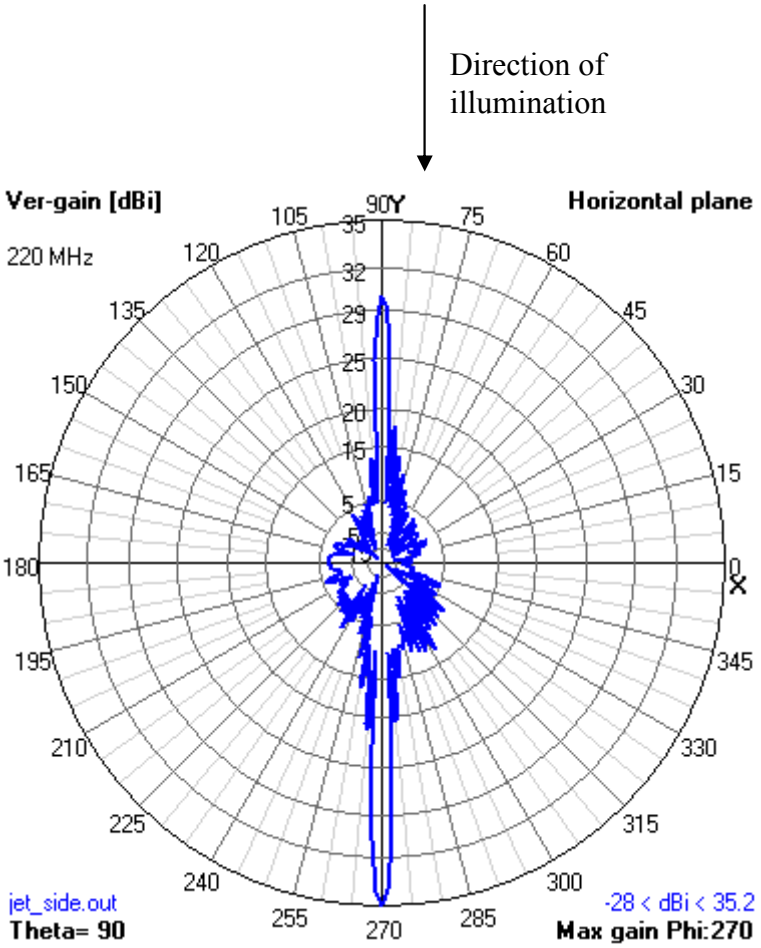

Figure 34 - Radar cross section pattern for side-on illumination (phi = 90 degrees) in vertical polarisation

The illumination angle was changed to tail-on (phi =180 degrees). Figure 35 shows the RCS pattern for end-on illumination in vertical polarisation. As expected, the RCS pattern is maximum in the direction of forward transmission (phi = 0 degrees). The RCS pattern is symmetric about the aircraft's axis of symmetry (phi = 0 to 180 degrees).

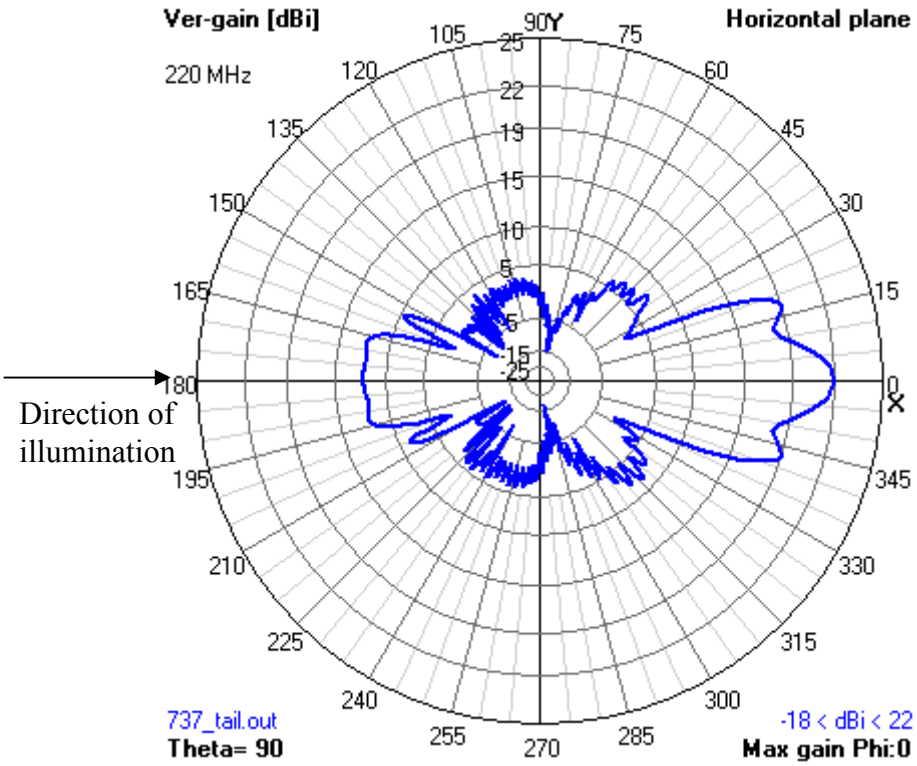

Figure 35 - Radar cross section pattern for tail-on illumination (phi = 180 degrees) in vertical polarisation

The illumination angle was changed to phi = 45 degrees). Figure 36 shows the RCS pattern for 45-degree illumination in vertical polarisation. As expected, the RCS pattern is maximum in the direction of forward transmission (phi = 225 degrees). The RCS pattern is not symmetric since the aircraft is not symmetric when viewed from an angle of 45 degrees from its nose.

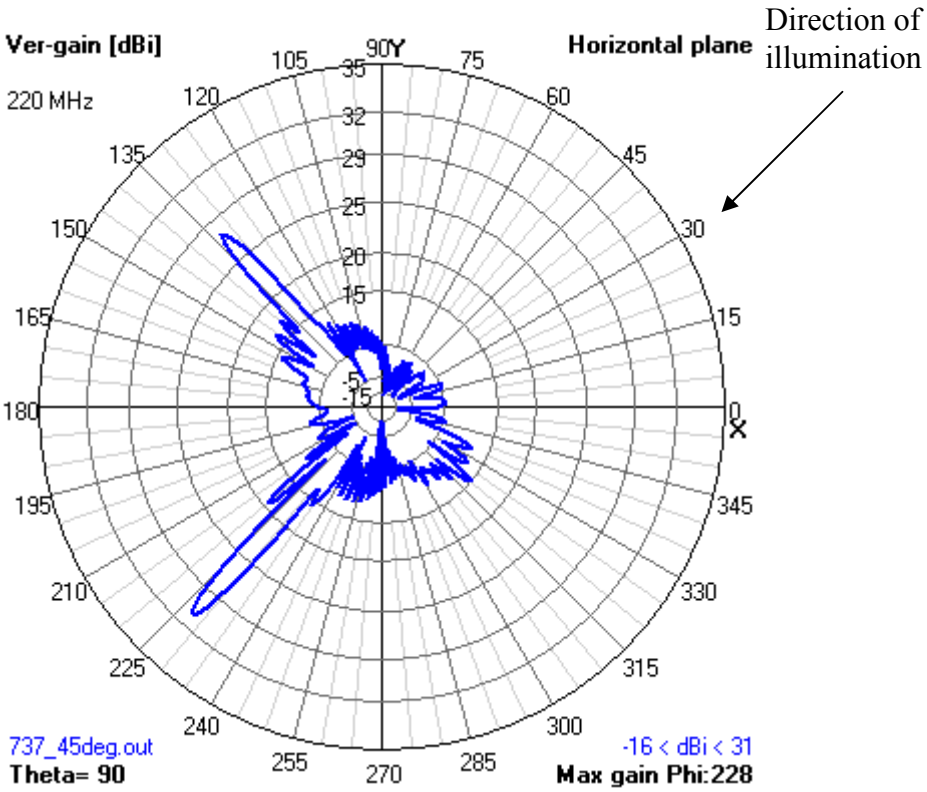

Figure 36 - Radar cross section pattern for 45-degree illumination in vertical polarisation

Figure 37 shows the RCS pattern for nose-on illumination in horizontal polarisation. As the illuminator was operated in vertical polarisation, this pattern is in cross-polarisation relative to that of the illuminator.

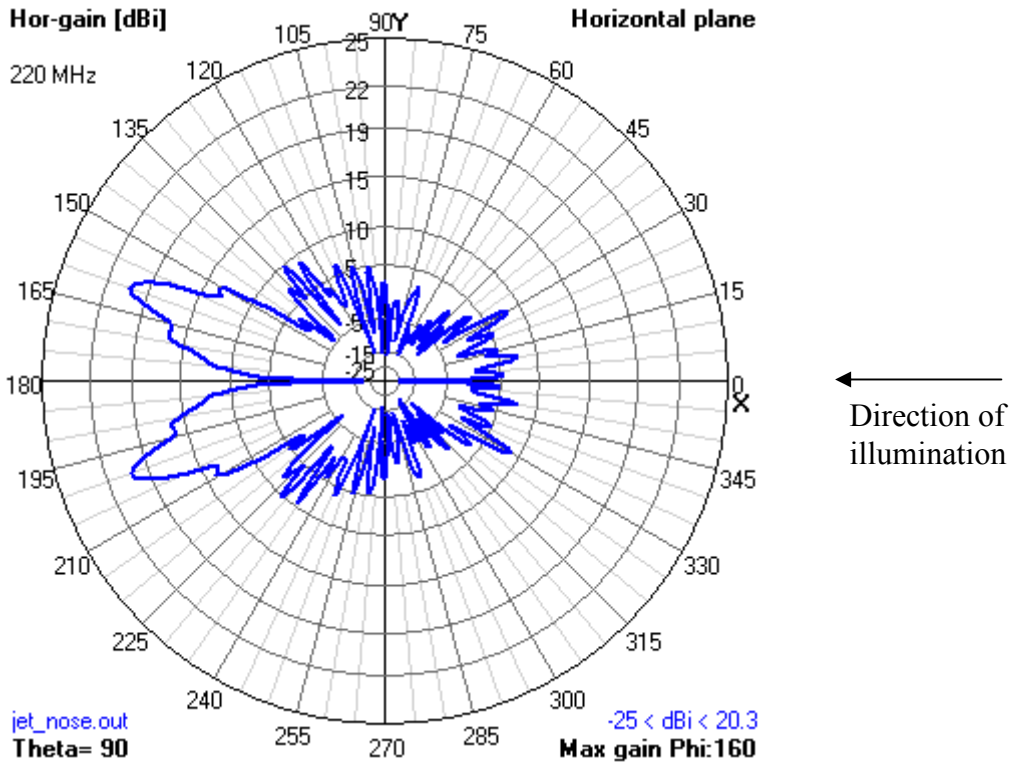

Figure 37 - Radar cross section pattern for nose-on illumination (phi = 0 degrees) in horizontal polarisation

Figure 38 shows the RCS pattern for side-on illumination in horizontal polarisation. As the illuminator was operated in vertical polarisation, this pattern is in cross-polarisation relative to that of the illuminator.

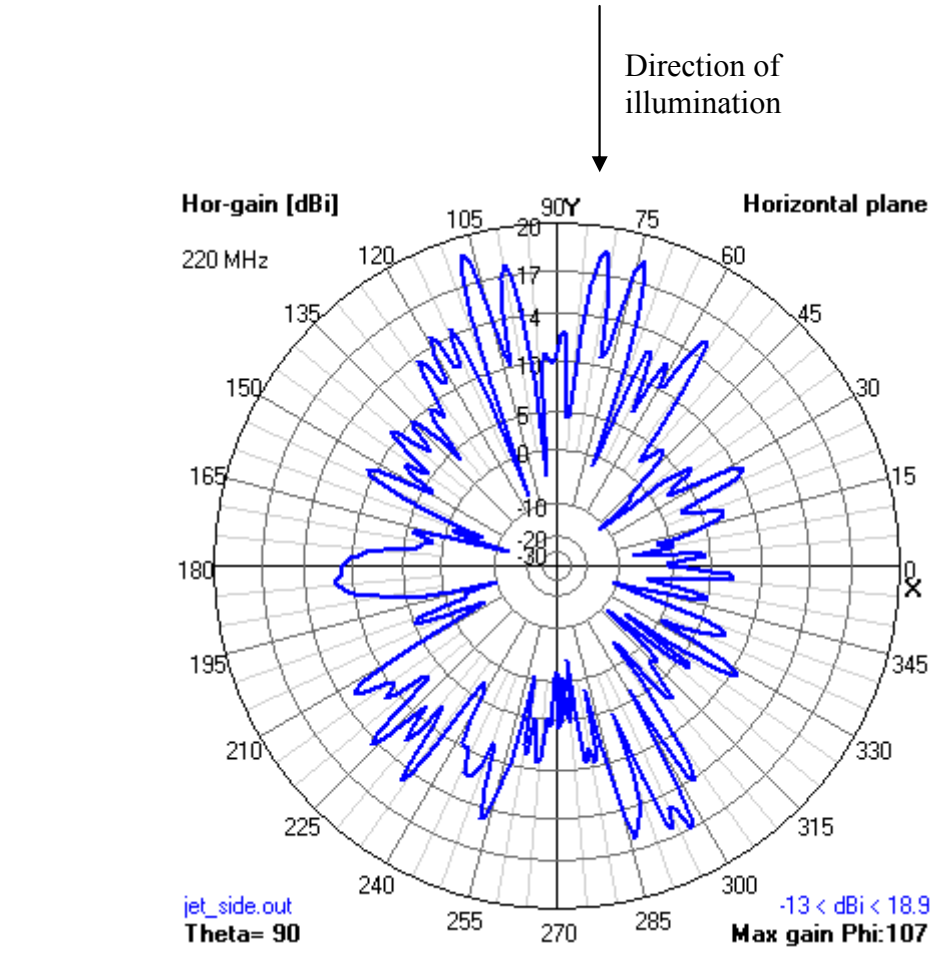

Figure 38 - Radar cross section pattern for side-on illumination (phi = 90 degrees) in horizontal polarisation

Figure 39 shows the RCS pattern for tail-on illumination in horizontal polarisation.

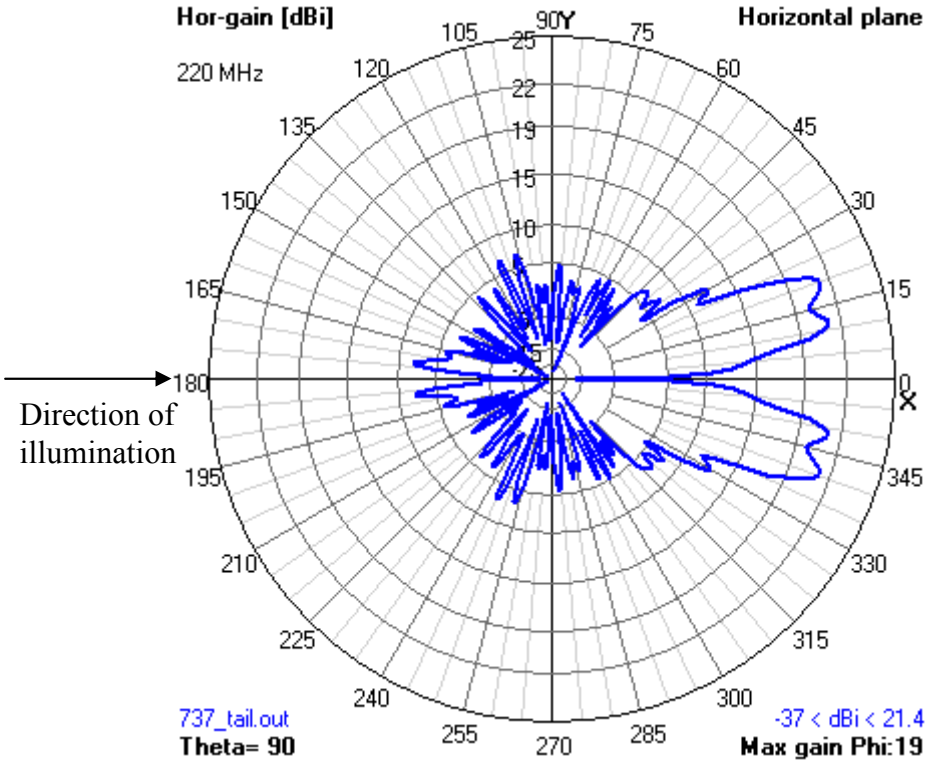

Figure 39 - Radar cross section pattern for tail-on illumination (phi = 180 degrees) in horizontal polarisation

Figure 40 shows the RCS pattern for 45-degree illumination in horizontal polarisation.

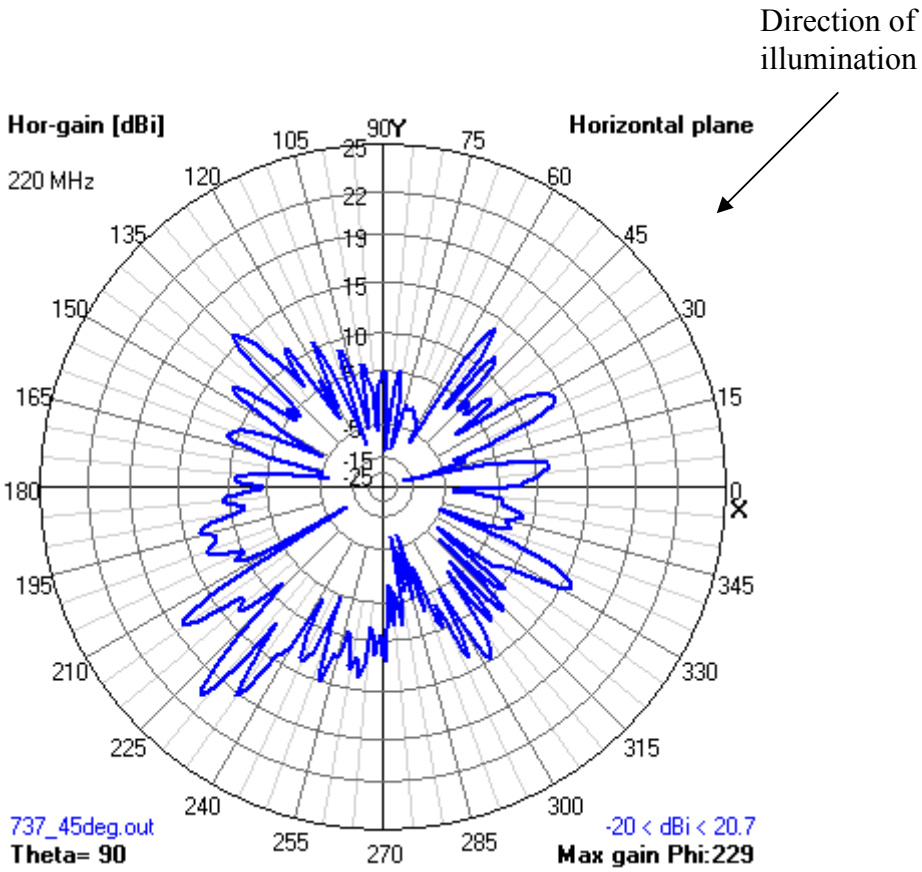

Figure 40 - Radar cross section pattern for 45-degree illumination in horizontal polarisation

NEC simulations were run for elevation angles of 0 and 10 degrees, and illumination angles in 1-degree increments from 0 to 359 degrees anticlockwise from the target's direction of travel. For each elevation angle, the RCS pattern data was saved in a file containing a 360×360 matrix with the rows corresponding to the RCS value for every one degree in azimuth (0 to 359 degrees) and the columns corresponding to the RCS for every one degree in illumination angle (0 to 359 degrees) for illumination in horizontal polarisation. A similar file was produced for illumination in vertical polarisation.

Appendix B gives representative matrices for the elevation angles of 0 and 10 degrees in horizontal and vertical polarisation.

A MATLAB program was written to use the positions and heights of the illuminator, receiver and target to calculate the illuminator incident angle and the receiver viewing angle (that is, the elevation angle). Another MATLAB program was written to read the data file for the calculated elevation angle and polarisation, using nearest neighbour interpolation to select the elevation angle and its corresponding data file. Given the receiver position, the target position and the target's direction of travel (the angle anticlockwise from 0 degrees or 'East'), the first program calculates the illumination direction and the receiver's

viewing direction relative to the target's direction of travel. The illumination direction and viewing direction are each converted to a value between 0 to 359 degrees relative to the target direction, and the program uses the two values to search for and return the corresponding RCS value in the appropriate data file. Interpolation between the rows of the matrix of RCS values, corresponding to interpolation within the circle of the azimuthal viewing plane, is used where necessary.

The RCS Unit is constructed out of the aforementioned MATLAB programs. Depending on the elevation (in degrees above the horizontal) of the target and the polarisation (horizontal or vertical) of the electric field incident upon the target, an appropriate file containing the RCS pattern of the target is chosen. The target's direction of travel is determined using the current and previous position of the target. This gives the angle that the target makes anticlockwise from 0 degrees or 'East'. The Unit then calculates the illumination direction (in degrees anticlockwise from the direction of target travel) and the viewing direction (in degrees anticlockwise from the direction of target travel). The Unit then looks up the RCS 'gain' corresponding to the illumination and viewing directions, interpolating within viewing angles if necessary.

The output of the unit is σ in units of square metres, and this is fed into the bistatic radar equation of the Target Power Unit.

4.3 Antenna Gain Modelling

4.3.1 Transmitter Gain Pattern

The gain patterns of the transmitters are assumed to be isotropic in azimuth.

4.3.2 Receiver Gain Pattern

The receiver system consists of three separate Yagi antennas, each pointed in the direction of the major illuminators (one for Bath, one for Mendip and one for Wenvoe). The system also has an array of two four-element Yagi-Uda antennas in broadside that is pointed towards the area of expected targets [60]. While the rudimentary model assumed the receiver gain pattern to be a single representative scalar value, in reality, the gain varies with the position of the antennas and the targets.

The far-field gain pattern of the receiver system was simulated using NEC. A four-element Yagi-Uda antenna was constructed. Standard design guidelines were applied for a boom length of 0.8 m and a wavelength λ of approximately 1.36 m for an operating frequency of 220 MHz in the case of the Bath PBR system. The driven element length was set at 0.47λ, the reflector element length 0.482λ, the first director element length 0.428λ and the second director length element 0.424λ. The elements were spaced 0.2λ apart [64]. The geometry of the antenna is shown in Figure 41.

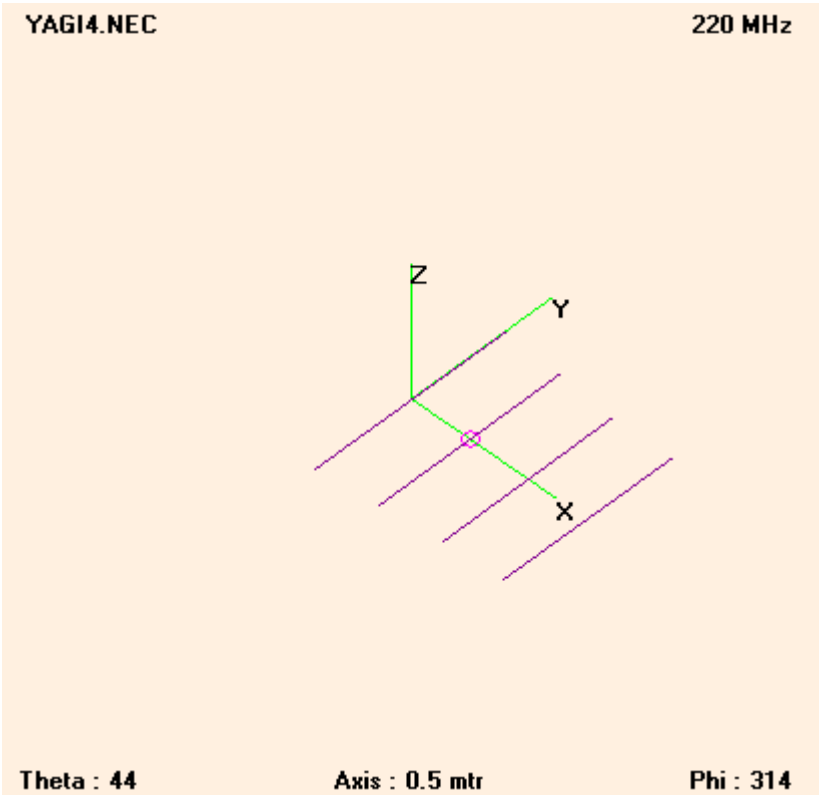

Figure 41 - Geometry of Yagi-Uda antenna

The far-field gain pattern was simulated and plotted in the azimuthal direction. The pattern is shown in Figure 42.

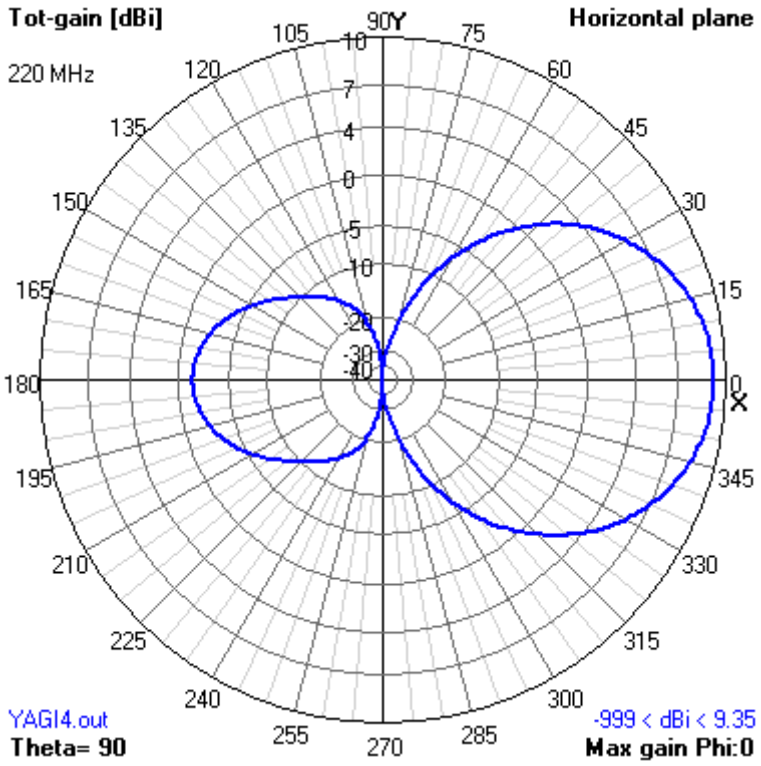

Figure 42 - Far-field gain pattern of Yagi-Uda antenna

The gain pattern data was saved in a file with the gain in decibels listed for every one degree in azimuth. A MATLAB program was written to read the data file. Given the boresight direction of the receiver array and the target direction, both in degrees (0 to 359) east of North, the program searches for and returns the corresponding gain value in the data file. Interpolation is used where necessary.

The process was repeated for the receiver array pointing towards the region of expected targets. Two four-element Yagi-Uda antennas were constructed according to the same design as that of the antennas pointing towards the illuminators. The two Yagi-Uda antennas were placed in broadside and spaced λ/2 m apart. The geometry of the target-pointing array is shown in Figure 43.

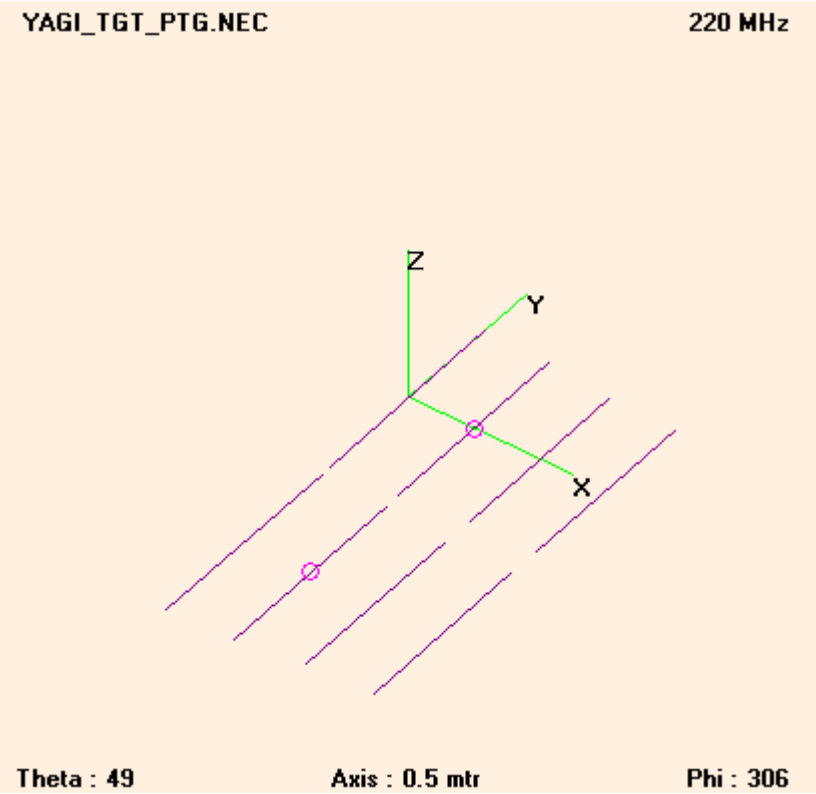

Figure 43 - Geometry of target-pointing array

NEC was used to simulate the far-field gain pattern, which was plotted in the azimuthal direction. The pattern is shown in Figure 44.

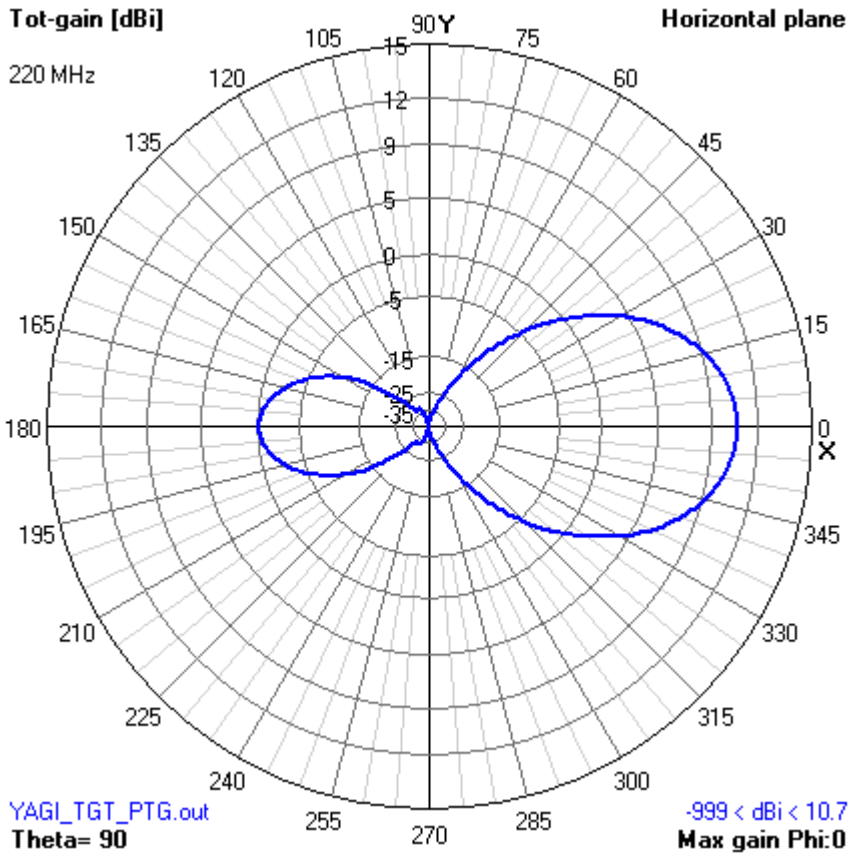

Figure 44 - Far-field gain pattern of receiver array pointing towards area of expected targets

As for the receiver array pointing towards illuminators, the gain pattern data for the receiver array pointing towards area of expected targets was saved in a file with the gain in decibels listed for every one degree in azimuth. The same MATLAB program used to read the data file for the illuminator-orientated receiver can be deployed for the target-orientated array data file.

The Antenna Gain Unit is built on the aforementioned MATLAB program. The Unit takes in a receiver position (latitude and longitude coordinates), the position (latitude and longitude coordinates) of an object, a file containing the gain pattern of the receiver, depending on whether the object is an illuminator or a target, and a reference position towards which the receiver boresight is directed. If the object is an illuminator, the reference position is that of an illuminator. For the Bath PBR system, the illuminator would be one of three illuminators (at Bath, Mendip or Wenvoe). If the object is a target, the reference position is that of the area of expected targets. In the case of the Bath PBR system, the area of expected targets is Bristol Airport. The program calculates the angle between the receiver boresight and the object direction, looks up the gain value (in dBi, or decibels relative to isotropic) in the antenna gain pattern, and returns the receiver gain (as a floating point number) in the direction of the object.

For each illuminator of the radar system, the Antenna Gain Unit uses the file containing the gain pattern of the illuminator-orientated receiver to calculate the receiver gain G_R towards the illuminator. The gain is used to calculate the DSI due to the illuminator in question, using G_R in the Friis equation of the

DSI Power Unit. Similarly, for a target, the Antenna Gain Unit consults a target-orientated receiver gain pattern file to find the gain of the receiver in the direction of the target. The gain is then fed into the bistatic radar equation of the Target Power Unit.

4.4 Implications for Radar Modelling

Having a realistic model of the target RCS enables us to experiment with DSI mitigation methods, such as that using cross-polarisation. This chapter has described the modelling of RCS in the azimuthal plane to within an accuracy of one degree for the illumination direction for two different elevations (0 and 10 degrees above the horizontal), with the illumination in horizontal and vertical polarisation. Previously, the rudimentary model of the RCS had merely provided a basic representative value that did not take into account polarisation. The added ability to calculate the target RCS in both co- and cross-polarisation now allows us to observe the effect of operating the receiver in cross-polarisation to that of the illuminators .

It is possible for the RCS to be decreased by the use of cross-polarisation during the cross correlation process and we must therefore ensure that any reduction in target RCS is more than compensated for by the reduction in DSI. This issue is discussed in more detail in the next chapter (Chapter 5), in which all of the modelling elements described so far are brought together to form a model of the DSI and target return signals arriving at the radar receiver. The signal-to-noise ratio at the receiver is considered to evaluate the effectiveness of DSI reduction methods on the radar system.

Since the gain of the receiver varies with the position of the illuminators and the target, the NEC modelling of the receiver described in the current chapter has similarly enhanced the functionality of the rudimentary model. The rudimentary model assumed the receiver gain pattern to be a single representative scalar value for the receiver look direction. The gain patterns produced by the NEC modelling in this chapter vary markedly with direction for both the illuminator-orientated and target-orientated receiver. As the receiver gain is used to calculate the DSI, the sophistication introduced by the NEC receiver gain modelling has made the DSI modelling more realistic. The benefits can be seen in Chapter 5, where the simulator is used to experiment with different radar configurations to improve the DSI problem.

5 Some Applications of the Simulator

The software modules described in the preceding chapters together to form a complete radar simulator that can model both target returns arriving at the radar receiver and DSI (the output of the antenna). In this chapter we demonstrate the capability of this simulator by using it to investigate several realistic scenarios and also to look at some DSI mitigation strategies.

5.1 Simulation of Several Realistic Scenarios

The refined PBR system model, with its individual modules verified separately and incorporated into a functioning whole, are here tested as a complete entity. To determine its effectiveness, a number of realistic scenarios were played through the simulator. Firstly, flight paths of aircraft were input to the simulator to see whether the simulator could produce ARDs corresponding to a typical flight trajectory.

In the first flight scenario, an aircraft flies parallel to the line joining the Bath illuminator and the radar receiver at the University of Bath. In the research preceding the current project, a series of observations of a similar scenario involving a medium passenger jet was taken. It was found that as the aircraft neared the perpendicular bisector of the line joining the illuminator at Bath and the receiver, there was a decrease in both its Doppler and range. Once the aircraft had crossed the bisector, its Doppler became negative while its range increased [60]. As is to be expected, the accumulated observations form a parabolic path on the ARD display (which is terminated by the obstruction caused by a building), as shown in Figure 45.

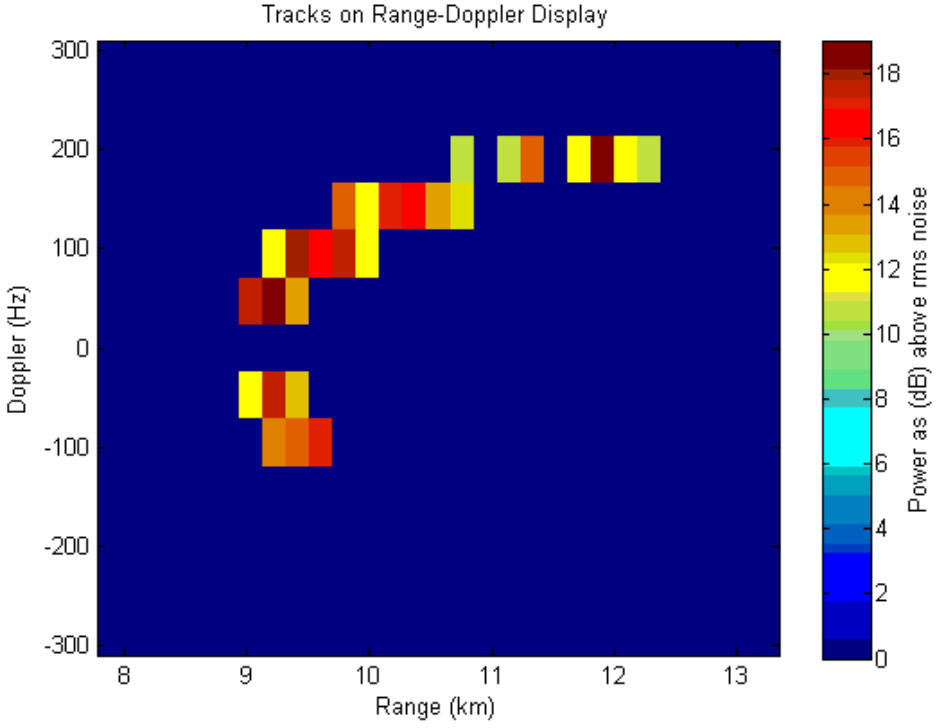

Figure 45 - Accumulated observations of aircraft crossing boresight in prior research project

In the simulated scenario, a small executive jet travels parallel to the line joining the Bath illuminator and the receiver at a speed of 150 m/s and at a constant altitude of 1000 m. The observations were taken at 1-second intervals. As expected, the resulting ARD display of Figure 46 shows a parabolic trajectory with the Doppler changing from positive to zero to negative.

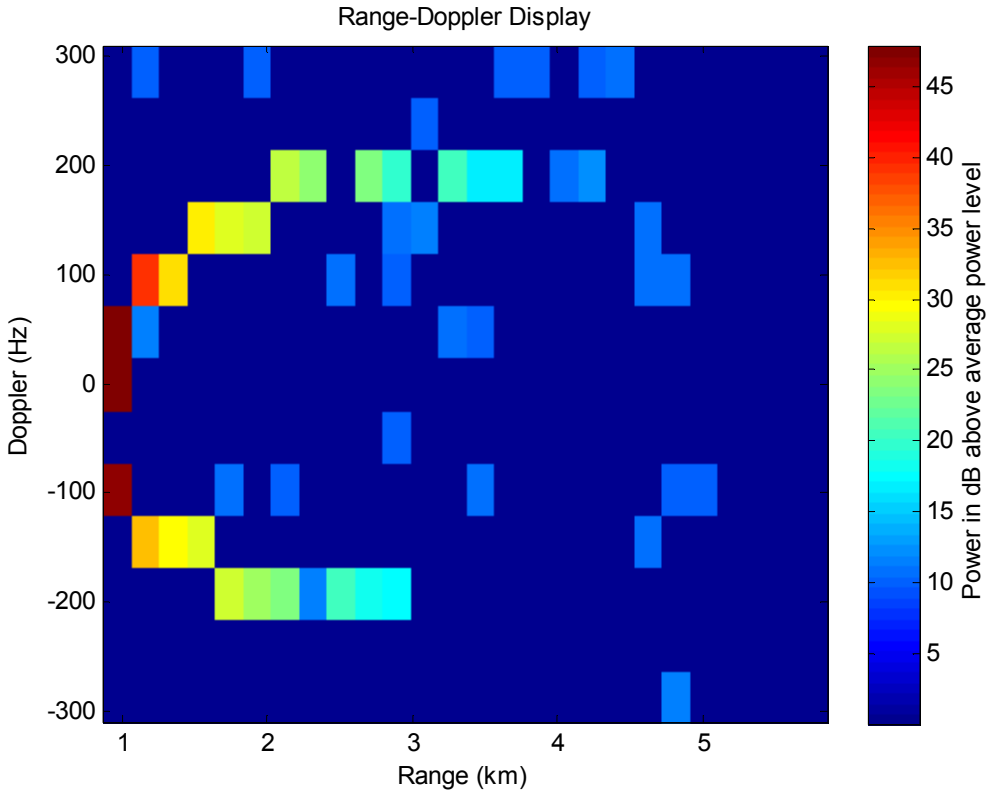

Figure 46 - Simulated observations of aircraft crossing boresight

The parabolic trajectory of the simulated observations is less clear than that of the actual observations for several reasons. It should be noted, however, that the target in the simulated observations has a smaller RCS than the target in the actual observations. The target is a medium passenger jet and would therefore have an RCS of about 5 dB more than that of a small executive jet (based on rescaling according to size), resulting in a greater signal strength in the ARD display. The NEC modelling of targets is extremely resource intensive and the modelling of an executive jet is all that can be achieved with current resources (see Chapter 4). Using simple rescaling, however, there is broad agreement between simulated and observed results. The additional detections at low power levels are due to noise in the radar system.

A second scenario involves a small passenger jet that is flying anticlockwise in a circle of radius 10 km around Bristol Airport at a height of 1000 m. The RCS for this case was generated by adding 5dB to that of a small executive jet. Figure 47 shows the resulting ARD display.

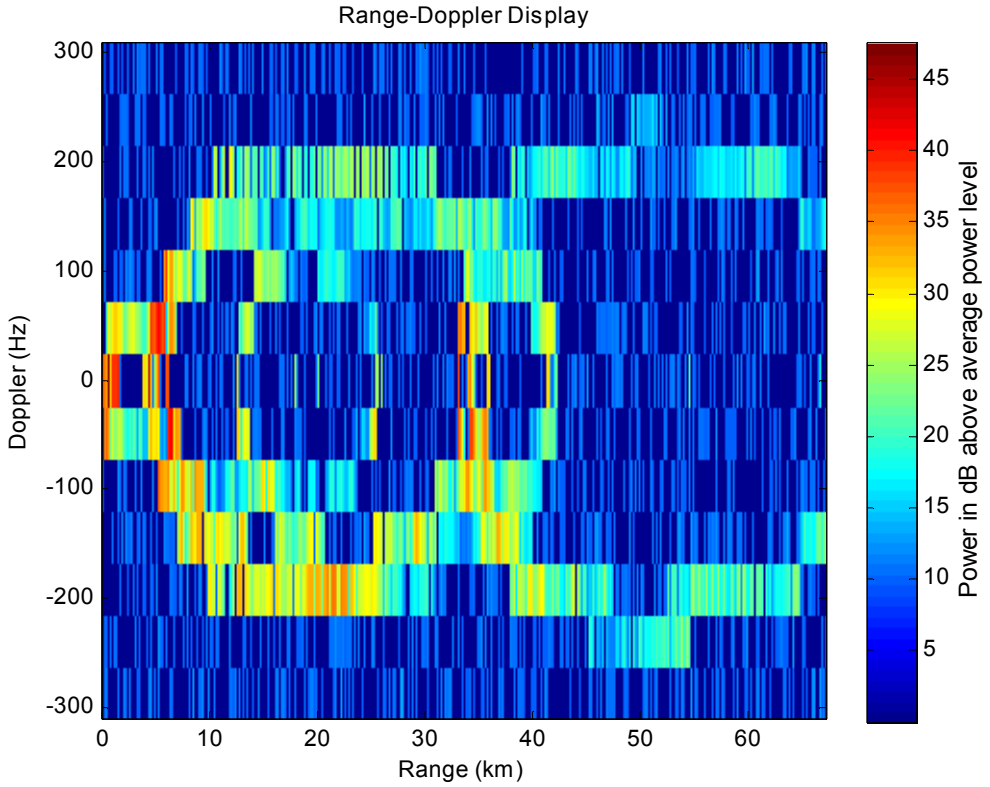

Figure 47 - Simulated observations of aircraft circling Bristol Airport

It will be noted that the tracks shown in the ARD display follow a curved path that is mostly symmetric about the zero Doppler line. The multiplicity of tracks is due to the presence of multiple illuminators. For each track, as the aircraft flies in a circle, its changing bistatic range is reflected in the changing Doppler, crossing from positive to zero to negative when the plane has moved from a path of increasing change in bistatic range to one of decreasing change in bistatic range. When the plane completes its circuit around Bristol Airport, its range is obviously restored to its starting value. The results are to be expected and confirm that the simulator is working well for such scenarios.

5.2 Application of Modelling to DSI Mitigation

As mentioned earlier, DSI is a major problem in all passive radar systems because it causes a large reduction in the dynamic range that is available for target detection. In cases of very strong DSI, the target returns are completely swamped by the DSI and hence hidden. This often happens when digital receivers are used due to the limited sampling that is available. DAB networks are particularly problematic because there are often a large number of illuminators present that are transmitting virtually identical signals on the same frequency (a single frequency network). Such a system exists in the UK. For a PBR system to function correctly, the strength of the DSI in the target channel must be decreased until both the target and the DSI are within DR of the target channel receiver [60].

A particularly important application of the simulator is the investigation of methods for reducing DSI. For example, the receiver could be sited in a dip in

the terrain to 'hide' from DSI. This technique of shielding by topography is first investigated for a radar located near Bath. The simulator was used to test DSI at various locations around Bath and the maximum DSI (maximum over the various illuminators) estimated from the simulation results. This process then allowed the determination of the radar location that gives the lowest DSI. This analysis was then repeated for a radar in the Adelaide region (a single illuminator system).

5.2.1 Investigating DSI around Bath

There are 10 illuminators transmitting in the Bath scenario, each contributing its own DSI. A program was written to draw a map of the maximum DSI over the region of possible radar receiver positions, the operation of which is described below.

With the exception of the illuminator at Bath, each illuminator was modelled as being omnidirectional. The Bath illuminator, however, has a highly directional antenna pattern and this must be taken into account in the simulations (a pattern was derived from data available on the Web [65]). For a suitable region around Bath, a matrix of receiver locations (in terms of latitude and longitude coordinates) was defined. On the assumption of direct propagation, the DSI power of each illuminator at each of these locations was calculated and stored in a matrix. The direct propagation, however, can be obscured by the ground topography and digital terrain maps are used to find this obscuration (the topography over the region of interest is shown in Figure 48).

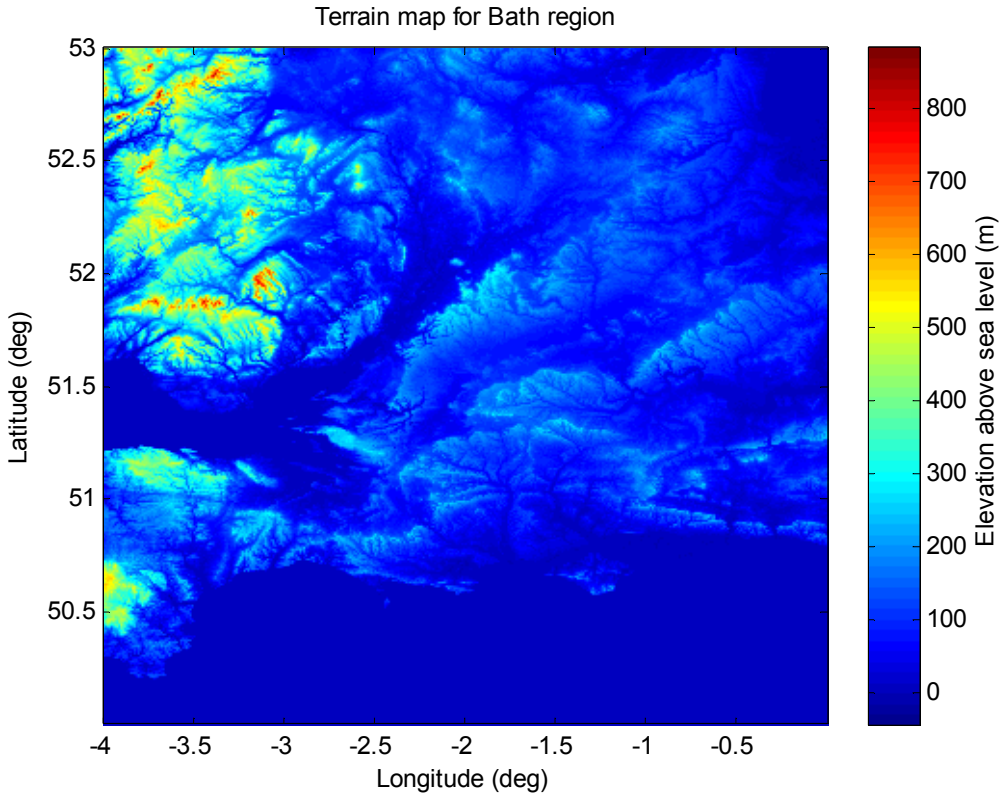

Figure 48 - The terrain map for the Bath region

For DSI sources that are obscured by topography, there is still some power that arrives by the mechanism of diffraction and this power is calculated by the Propagation Loss Unit. For obscured illuminators, the power in the DSI power matrix was then replaced by the diffracted power. From the power matrices for the individual illuminators, the total DSI at each point of the test region can then be obtained.

Figure 49 and Figure 50 show the individual distributions of DSI power for Bath and Mendip transmitters respectively. The receiver is located about 201 m above sea level, so this was the height at which the DSI power values were calculated. Figure 51 shows the distribution of DSI power from Mendip as calculated by a full propagation simulator of the parabolic equation (PE) variety [66]. The similarity with the results of the simple diffraction calculations of the current approach shows that the simpler approach is adequate for the purposes of the radar simulator. This is important as full propagation simulations are far too slow for a practical radar simulator. The complexity of the PE algorithms is several orders of magnitude greater than that of the method used by the simulator being described in this thesis. The effective screen approach of the Diffraction Loss Unit only gives a first order estimation (giving an error that is no worse than 2 or 3 decibels [55]), but this is judged to be sufficient for the current application.

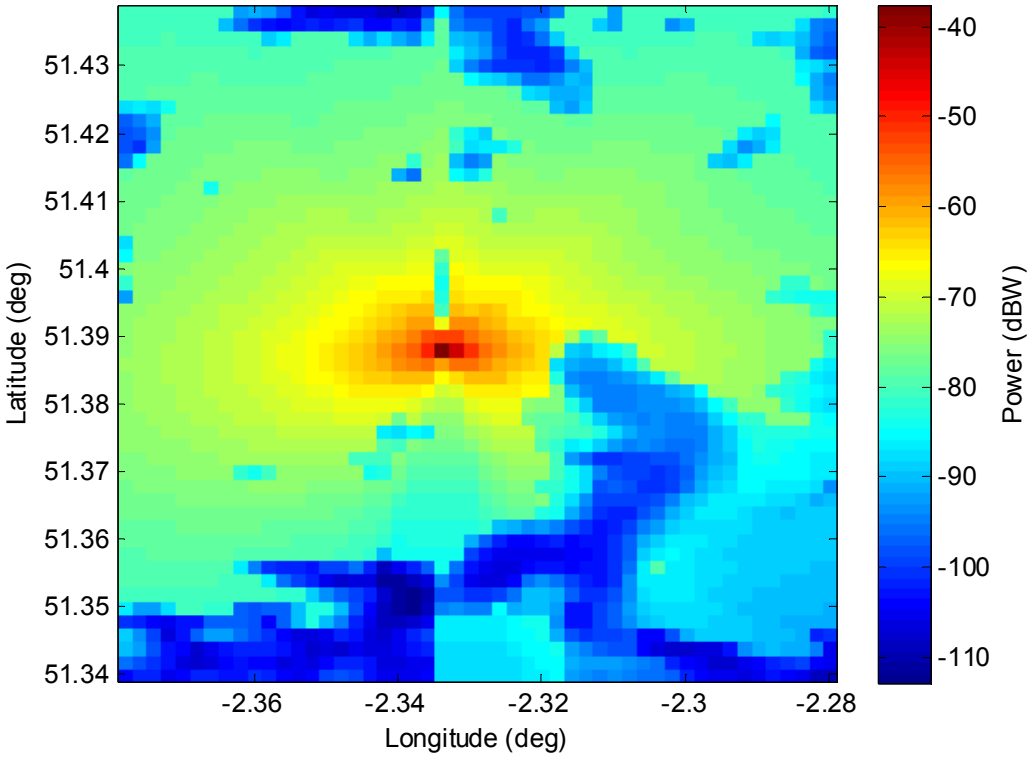

Figure 49 - Map of illumination from Bath, at a height of 201 m above sea level

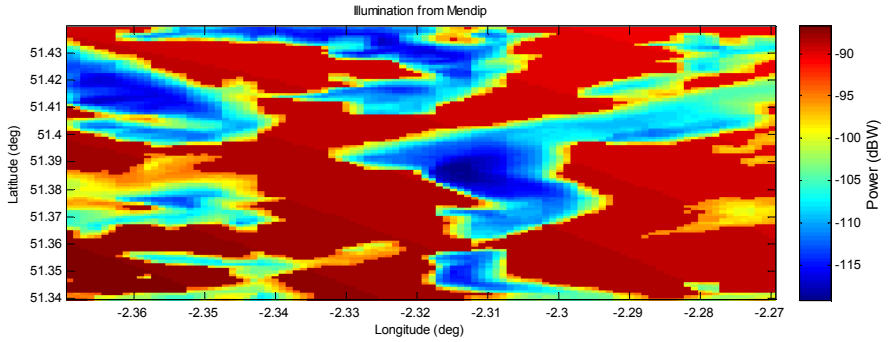

Figure 50 - Map of illumination from Mendip, at a height of 201 m above sea level

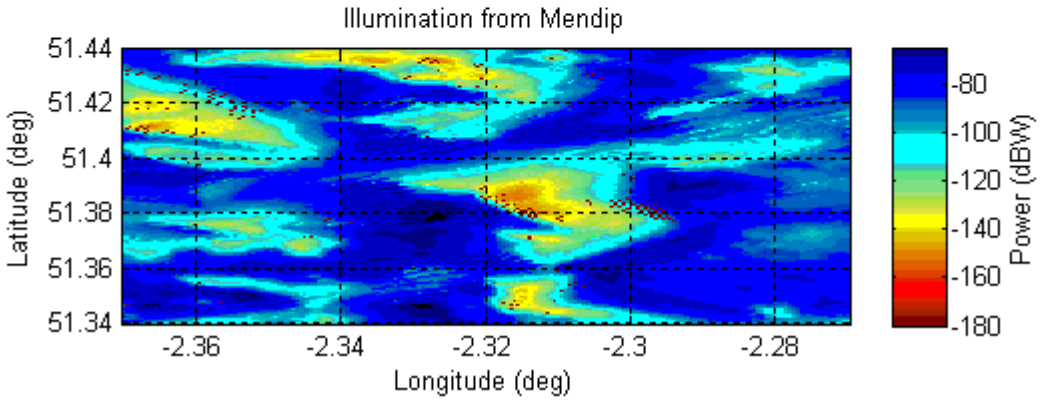

Figure 51 - Map showing illumination from Mendip at a height of about 201 m above sea level calculated by a PE simulator [66]

Figure 52 and Figure 53 show the distribution of DSI power from Naish Hill and Wenvoe, respectively.

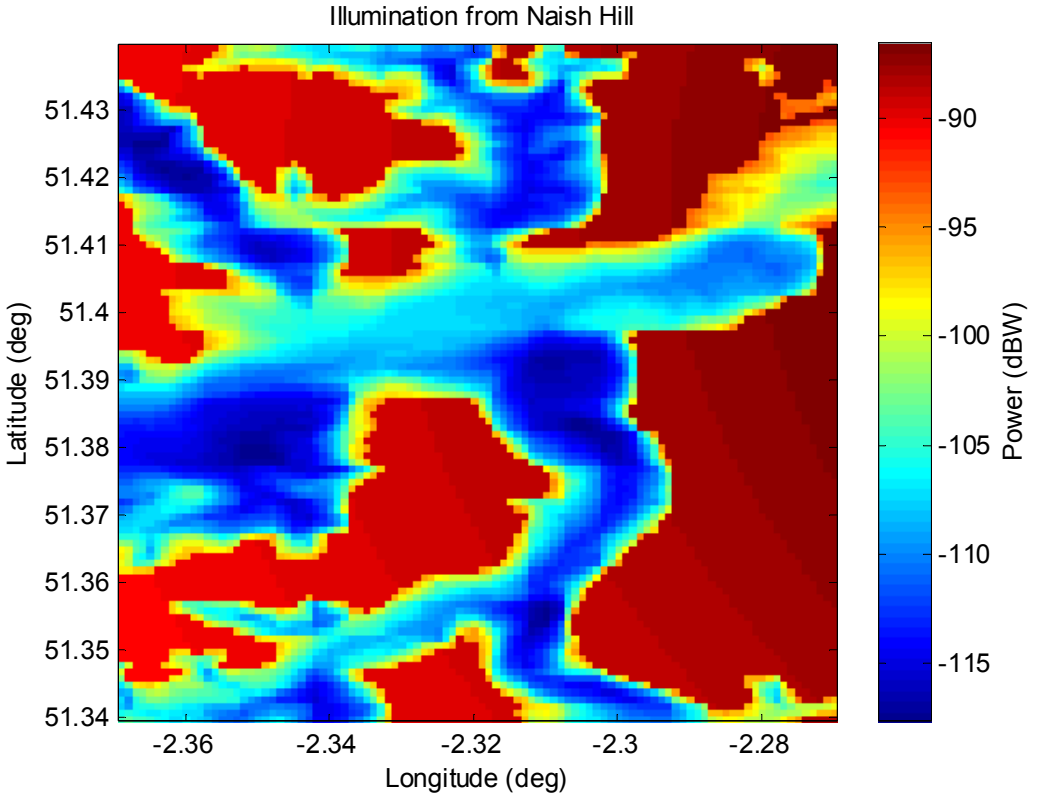

Figure 52 - Map of illumination from Naish Hill, at a height of 201 m above sea level

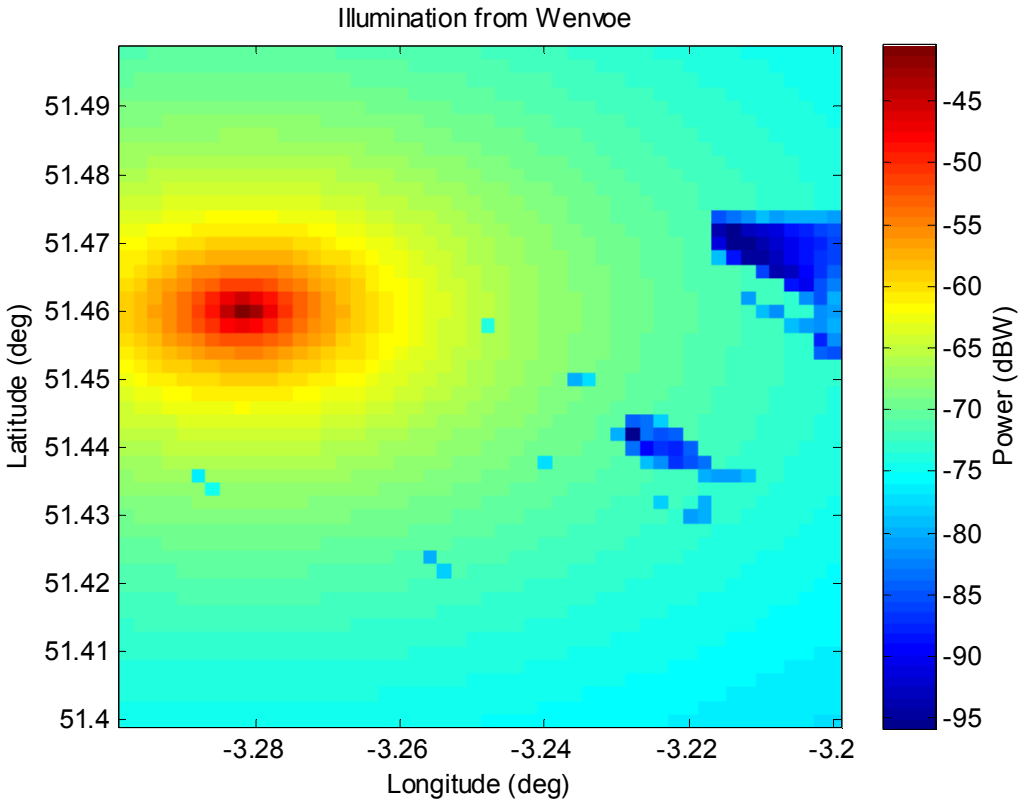

Figure 53 - Map of illumination from Wenvoe, at a height of 201 m above sea level

To see how the radiated signal power varies with height, a map of the distribution of DSI power from Wenvoe was simulated for a receiver height of first 250 m and then 300 m above sea level. Figure 54 and Figure 55 show the maps. The signal power decreases with increasing distance from the transmitter, but at greater heights, there are fewer obstructions to the propagation of the signals.

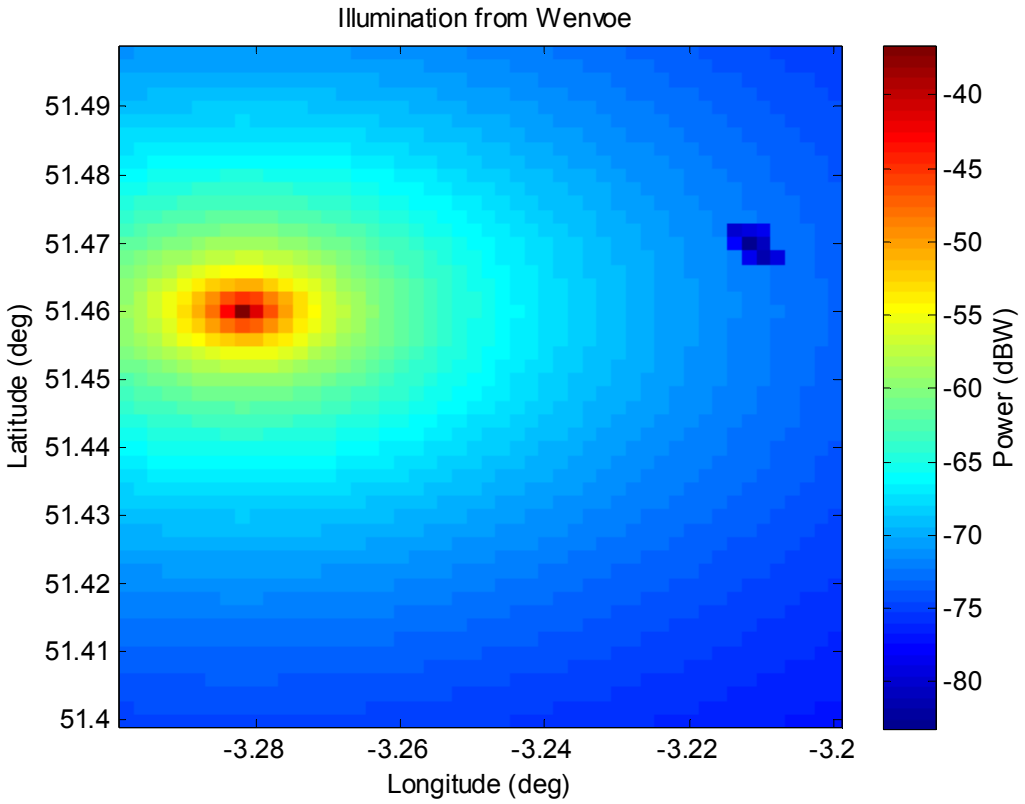

Figure 54 - Map of illumination from Wenvoe at a height of 250 m above sea level

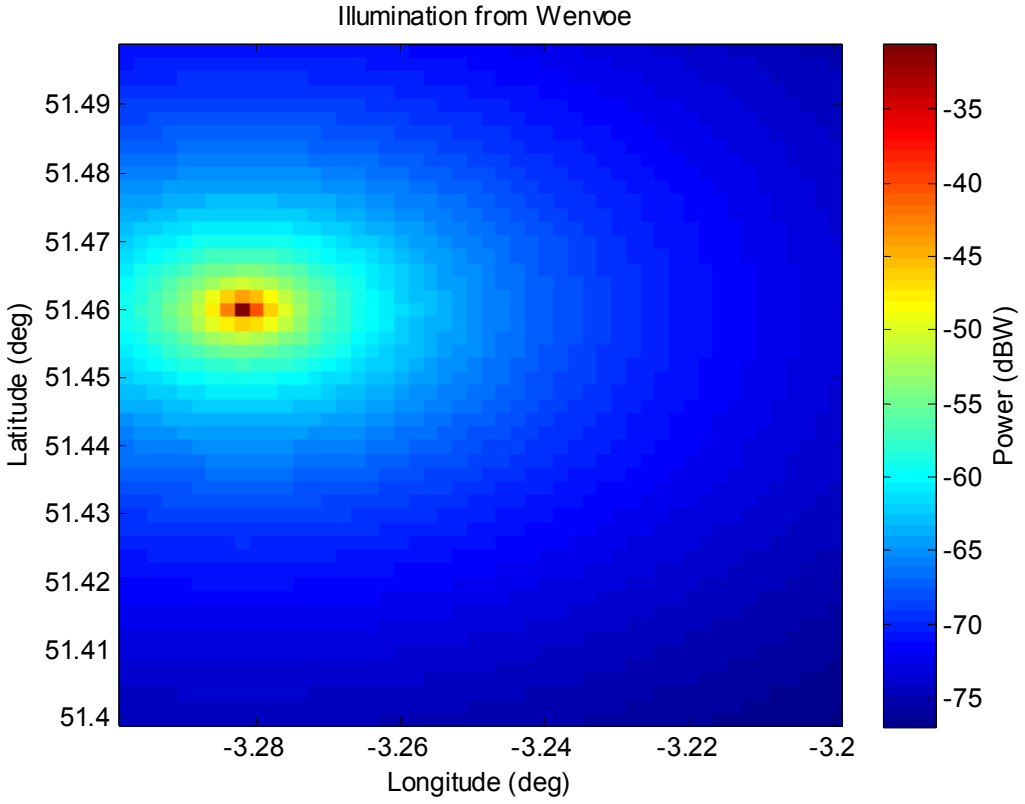

Figure 55 - Map of illumination from Wenvoe at a height of 300 m above sea level

Figure 56 shows a map of total DSI power across a region with an area of about 12 km by 12 km, centred on the University of Bath at (51.378944°N, 2.327967°W).

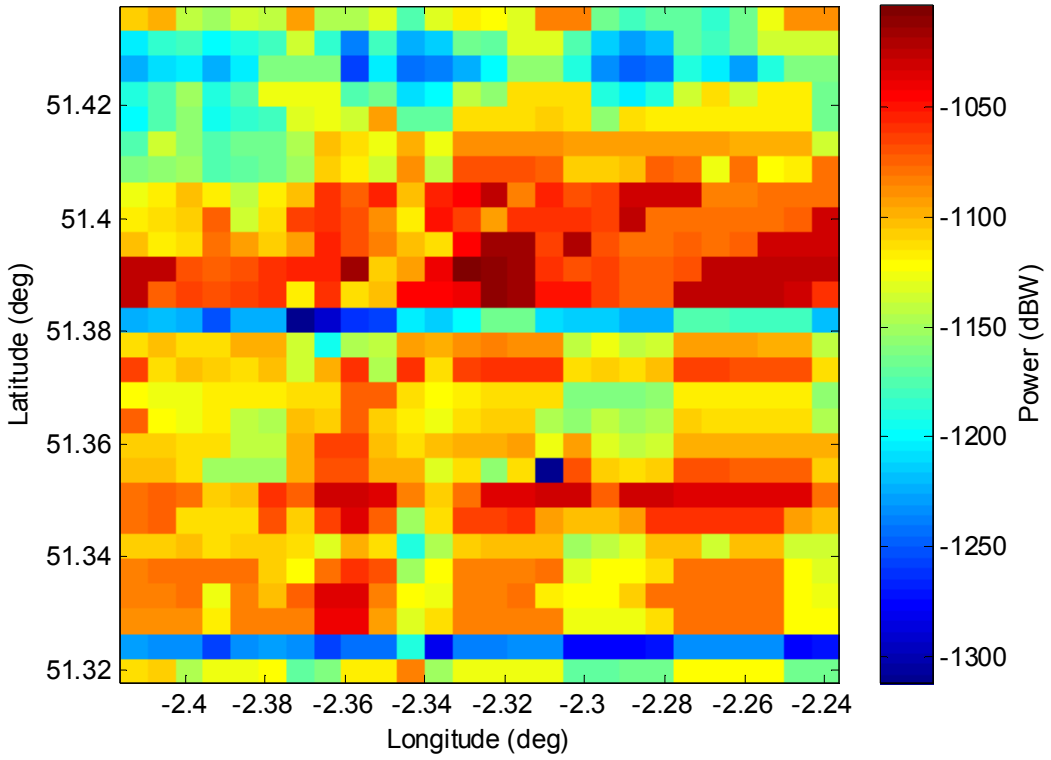

Figure 56 - Map of total DSI power across region centred on the University of Bath at (51.378944°N, 2.327967°W)

The distribution of DSI for all the individual illuminators, can then be used to find a map of total DSI power over the region of interest (this is shown in Figure 56). From the map of total power, it can be seen that there is a low DSI point at (51.356°N, 2.31°W). If a radar receiver is stationed at a position with low DSI, we need to know whether the radar is able to see targets (a low DSI point is not necessarily a good radar location). Aircraft travelling at low altitudes may be invisible to the receiver at a low DSI site if there are obstructions, such as a hill, in the line of sight between the target and the receiver. A target visibility unit has been developed for the simulator and addresses the question of whether the radar can see the desired targets from a particular low DSI location. For a given target height, the visibility unit calculates the positions for which there is direct line of sight to the target (hence making it detectable).

Figure 57 gives an example of a target visibility map for the low DSI site (51.356°N, 2.31°W) in which there are regions where the target is not visible. The receiver height was 20 m above the ground. The red area indicates the region in which targets are visible from the site, while the blue area indicates where targets are not visible from the site.

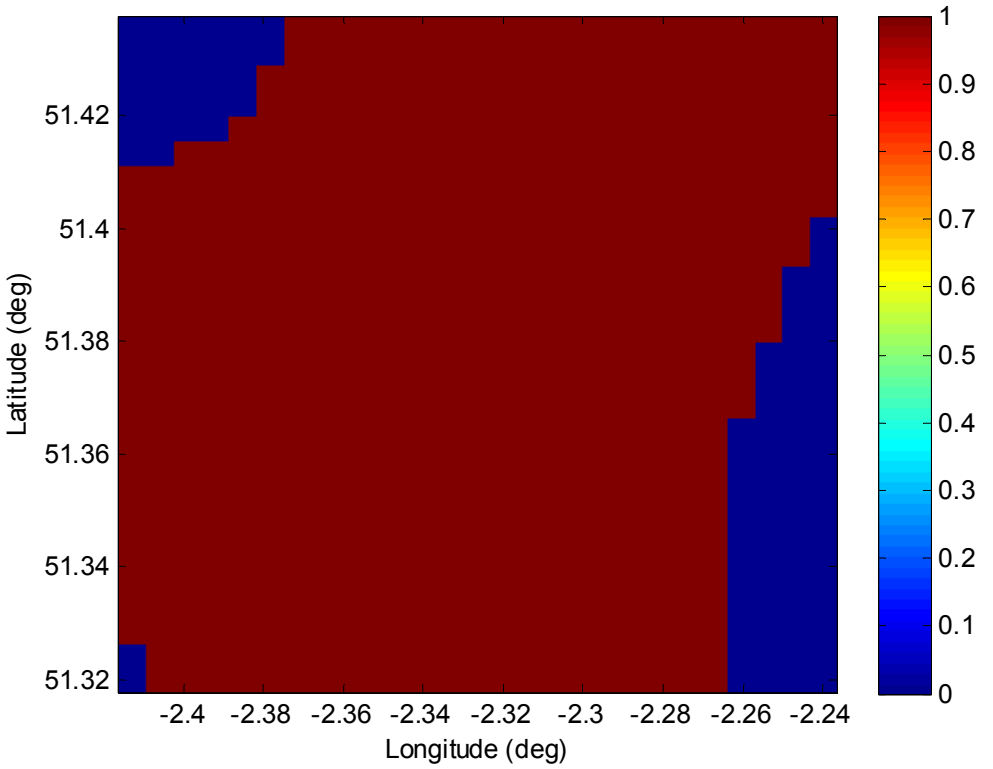

Figure 57 - Map of target visibility around low DSI site at (51.356˚N, 2.31˚W)

The receiver height was changed first to 30 m then to 40 m above the ground. Figure 58 and Figure 59 show the resulting target visibility maps. As expected, the visibility of the target increases with height.

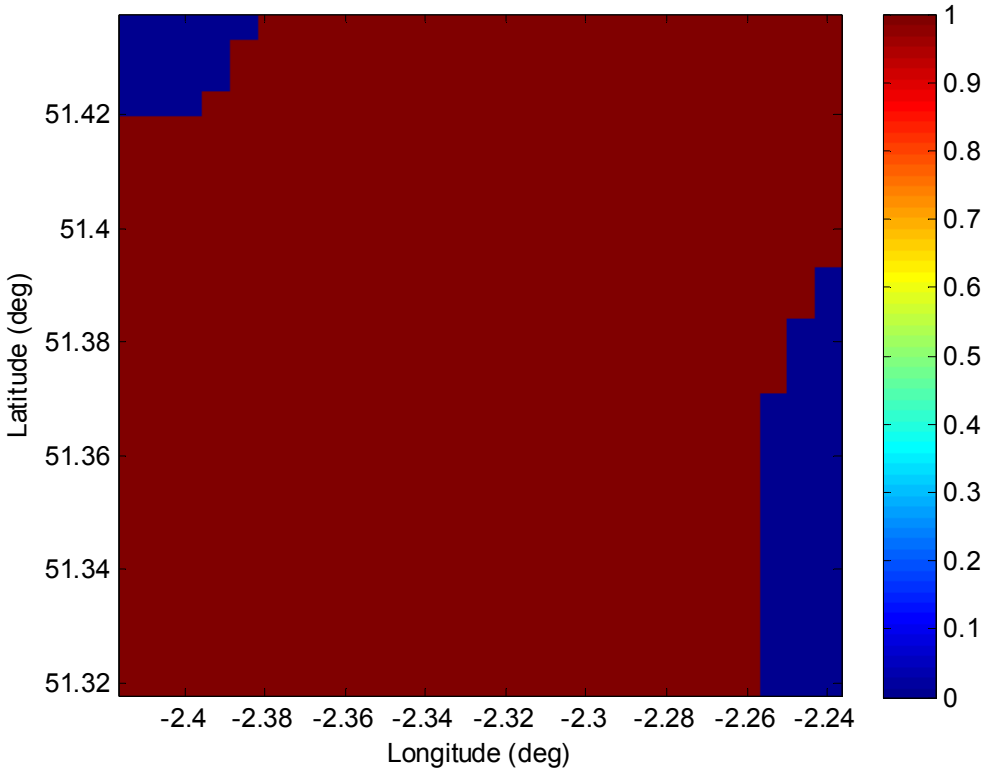

Figure 58 - Map of target visibility around low DSI site at (51.356˚N, 2.31˚W) with receiver 30 m above ground

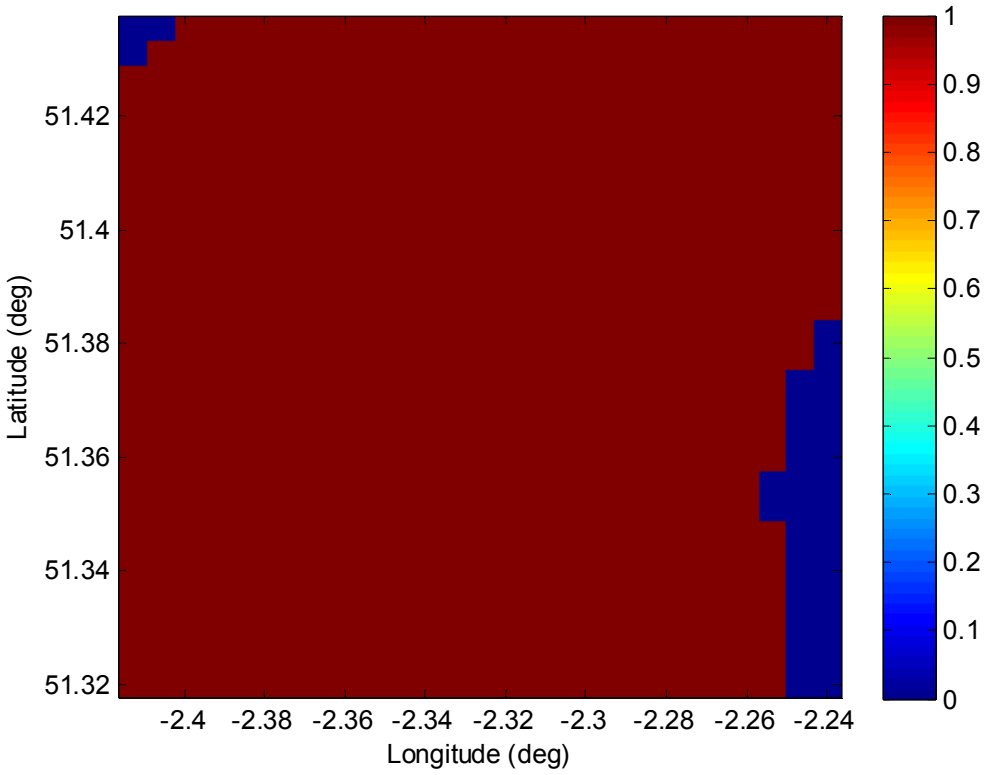

Figure 59 - Map of target visibility around low DSI site at (51.356°N, 2.31°W) with receiver 40 m above ground

5.2.2 Investigating DSI around Adelaide

The simulator has also been used to investigate DSI in the Adelaide area of South Australia. Once again, the ground topography was obtained from digital terrain maps and the resulting topography for the Adelaide area is shown in Figure 60.

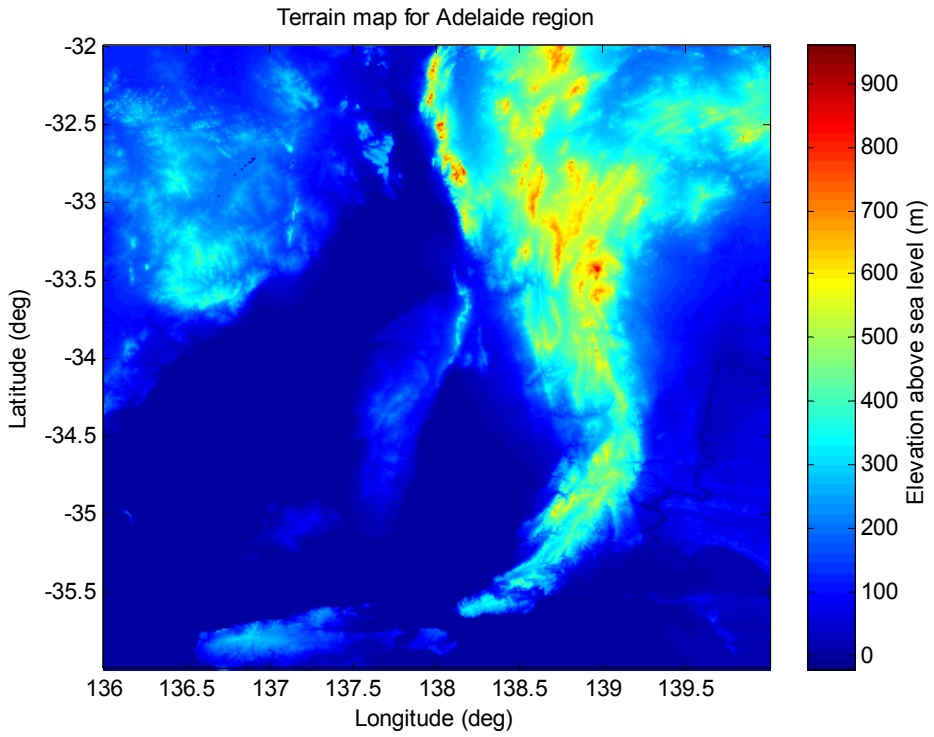

Figure 60 - Terrain map for the Adelaide region

For the Adelaide area, the main illuminator is located at Mount Lofty with the following specifications.

Location:	(34.9825°S, 138.706667°E)
Site height:	727 m
Antenna height:	121 m
ERP:	50 kW, omnidirectional
Operating frequency:	206.352 MHz

A map showing the maximum DSI for the area was calculated by the simulator and is shown in Figure 61.

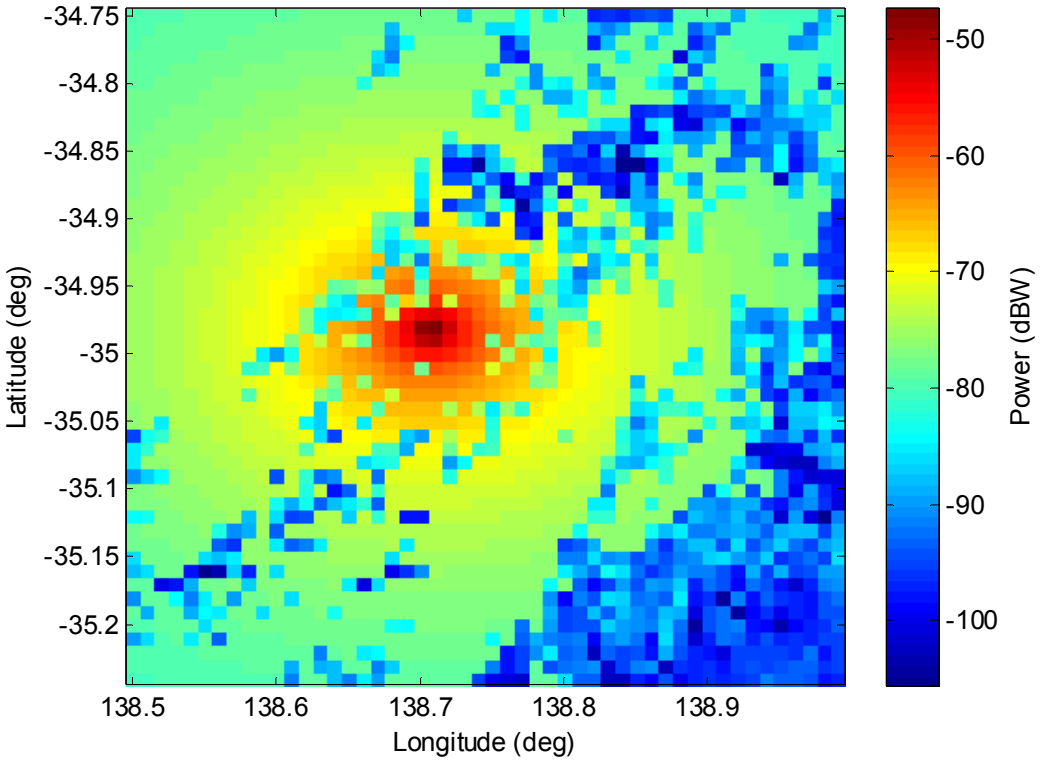

Figure 61 - First map showing maximum DSI around Mt Lofty illuminator at (34.9825°S, 138.706667°E)

A low DSI spot at (35.07°S, 138.85°E), is located in the Adelaide foothills. The visibility for a target, flying at an altitude of 1000 m is shown in Figure 62. Once again, the red area indicates the region in which targets are visible from the low DSI site, while the blue area indicates the area where targets are not visible from the low DSI site.

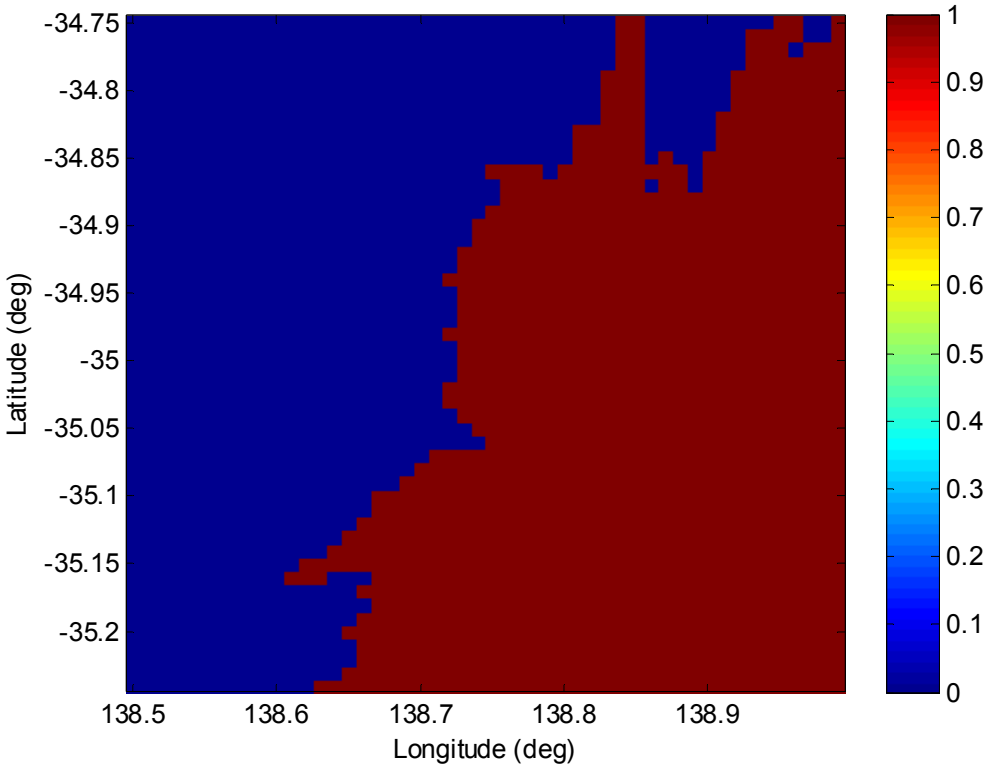

Figure 62 - Map of target visibility around low DSI site at (35.07°S, 138.85°E)

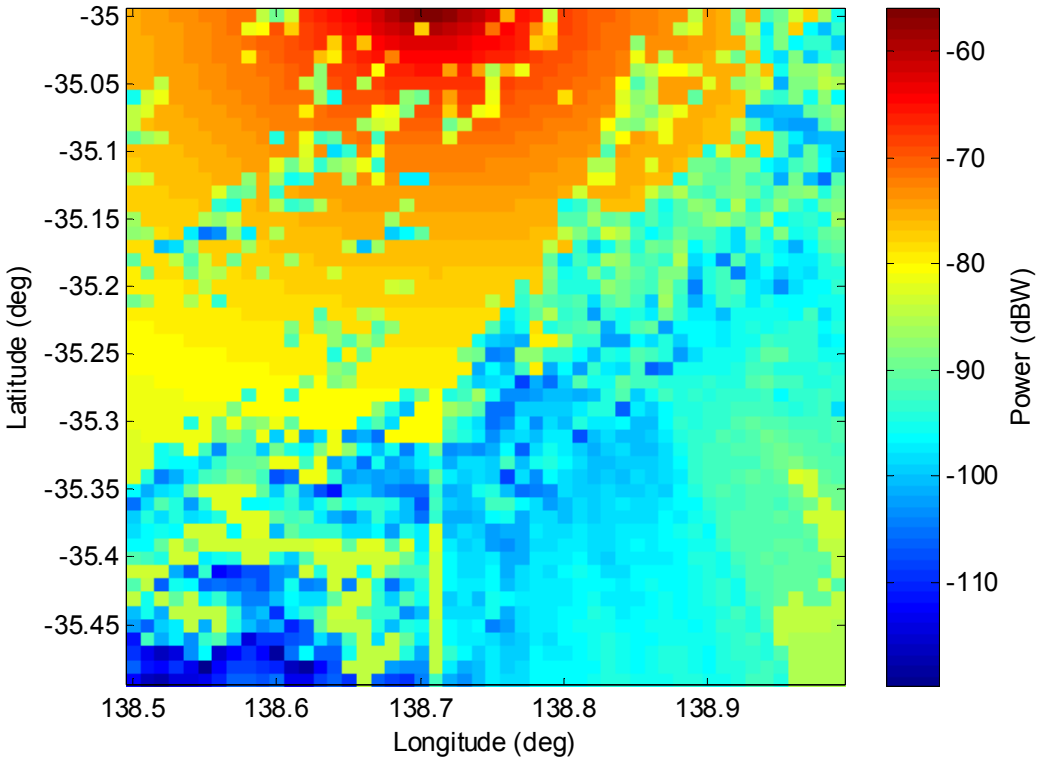

Figure 63 - Second map of maximum DSI around Mt Lofty illuminator

Figure 63 shows the distribution of DSI further to the south of the illuminator. A low DSI spot at (35.5°S, 138.5°E), south of the Adelaide CBD, was identified. As before, the target visibility at an altitude of 1000 m was

calculated. The results are given in Figure 64. The red area indicates the region in which targets are visible from the low DSI site, while the blue area indicates where targets are not visible from the site.

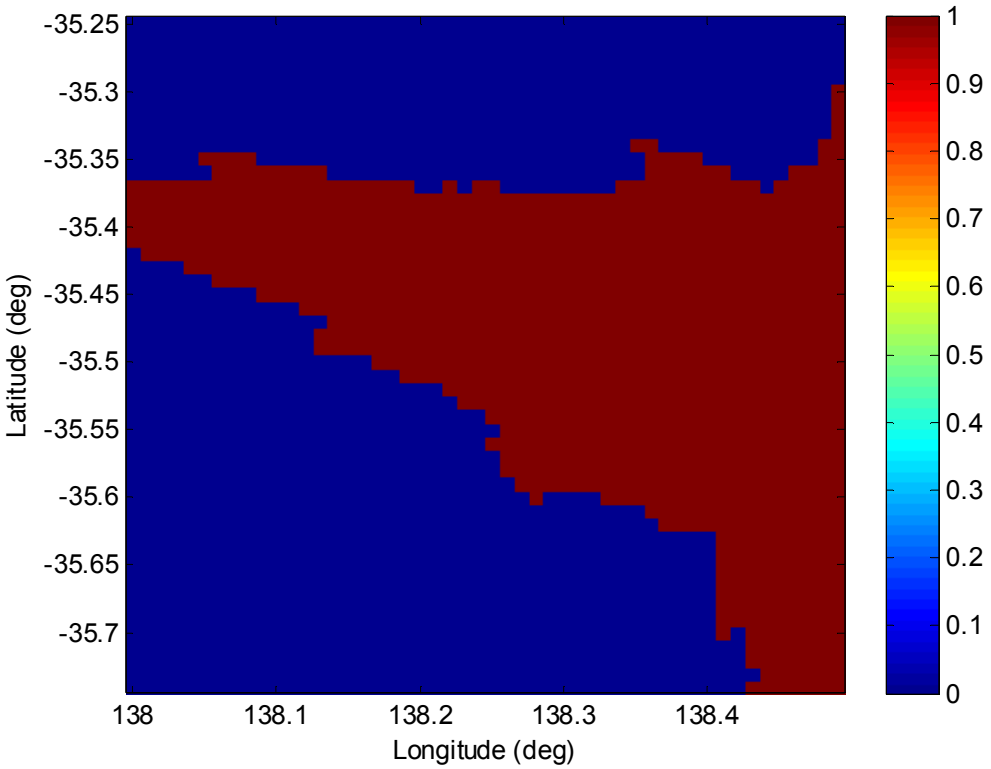

Figure 64 - Map of target visibility around low DSI site at (35.5°S, 138.5°E)

It can be seen that additional coverage is provided by the new site. But it is important to note that each site only has partial coverage. It is possible, however, that a network of passive radar receivers could be stationed at suitable low DSI sites and together provide overlapping areas of target visibility could then be combined to supply a more comprehensive coverage.

5.3 Discussion

The success of the simulator has been demonstrated by the simulation of realistic scenarios. The correspondence between the simulated and actual aircraft trajectories shows that the simulator is working satisfactorily.

Having a reliable model of a PBR system means that the model can be applied in many different areas of PBR systems engineering. This chapter has explored only one application of the model, namely, the testing of the DSI mitigation technique of hiding from DSI using surrounding natural terrain formations. The model has been used to predict locations in which the receiver will suffer from less DSI, but where targets flying at 900-1000 m above sea level will still be visible. Knowledge of these desirable receiver locations can be used in the design of a PBR system, particularly for decisions concerning the siting of receivers.

The target visibility maps produced by the model have highlighted the possibility of using a network of receivers to extend the coverage of the radar system. This is only one indication of the versatility of the model. The fast and efficient simulator allows radar engineers to investigate and optimise a large number of parameters, producing realistic and accurate results in a short time period so that many different simulations can be run without needing to resort to costly experiments on actual radar systems.

6 Conclusion and Future Work

6.1 Summary

This thesis has described a project to develop a modelling and simulation environment for a general PBR system. The project began with a rudimentary model, described in Chapter 2, that was verified by comparison of the autocorrelation of a synthesised radar signal produced by the simulator with that of an off-the-air DAB signal.

The rudimentary model was made more realistic by the addition of more sophisticated propagation effects, namely, diffraction, multipath and depolarisation. The propagation effects were incorporated into the simulator as software modules which were individually tested using proven physical optics principles, as described in Chapter 3.

Further enhancements to the model were made with the development of its RCS and Antenna Gain Units in Chapter 4. These Units initially provided only representative scalar values that were direction-independent. NEC modelling was used to increase the sophistication and hence accuracy of these Units.

The model was then used to simulate a number of realistic scenarios involving typical aircraft flight paths around the University of Bath in the UK, described in Chapter 5. The output of the simulator was found to agree with data collected at this location.

Finally, the model was applied to the testing of a DSI mitigation technique, namely, shielding by topography, using the Bath region as a test case. The success of the simulation results suggests that the technique can be used in the Adelaide area of South Australia. One outcome of the simulations is the idea that a network of passive radar receivers can be situated at low DSI spots to provide combined coverage of the Adelaide area.

6.2 Extensions

A suggested extension to the project is to build on the ARD Display Generator to develop a target tracker that uses the simulator. The tracks indicating the range and Doppler of the target can be used as the basis for a more sophisticated tracker.

The NEC modelling of the small executive jet could be made more accurate. For example, the wings of the aircraft could be swept back instead of being positioned perpendicularly to the body. The aircraft nose could be tapered instead of being cylindrical, and the tailfins could be more realistically modelled rather than being shaped as flat rectangular plates. Additional aircraft models such as a medium passenger jet and a helicopter could be added.

The RCS modelling could be extended beyond lookup tables that provide RCS as a function of incident angle. Galloway [67] describes how Roke Manor

Research developed an RCS physical optics based prediction code with shooting bouncing ray multiple scattering and physical theory of diffraction edge scattering facilities for the simulation of radar systems. He points out that lookup tables always have a limitation on angle resolution. This presents a problem when targets are electrically large, as their scintillation rate will not be modelled accurately. Galloway puts forward a network application interface (API) that gives RCS signature data as a function of aspect to the resolution of the numerical representation of the aspect description in the request message. This has the advantage of requiring significantly less memory than that which would be needed to store a lookup table of a similar resolution. In addition, the prediction resource required to produce the data for the lookup table is much less. A possible direction for future work on the current project could therefore be the incorporation of RCS prediction code, negating the need for resource-intensive lookup tables.

In a similar vein, the antenna modelling could be taken to a higher level of sophistication beyond lookup tables. Prediction code could be developed to increase the resolution of the modelling while decreasing the memory and data production resource required.

The simulator was used to test the DSI mitigation technique of shielding received signals from DSI by topography. Another extension to the project could be to deploy the simulator for testing other DSI reduction techniques such as azimuthal null formation in the direction of illuminators using a phased array of antennas. This technique can also null out desired target returns. A way of reducing DSI is to then further isolate the illuminators by detecting targets in horizontal polarization, cross to that of the illuminators [68].

The simulator is not limited to DAB based radars, and can be modified to use other illumination signals such as digital video broadcast (DVB) signals.

Appendix A – Derivation of Loss Due to a Screen

Huygen's principle can be applied to diffraction over a screen as illustrated in Figure A. Assume we have two antennas A and B. There is a screen between them that is orthogonal to the line joining the two antennas. It is of infinite extent in both x directions and the negative y direction. In the positive y direction, the screen has a finite height h. Z_A and Z_B are the distances of the screen from antenna A and B, respectively.

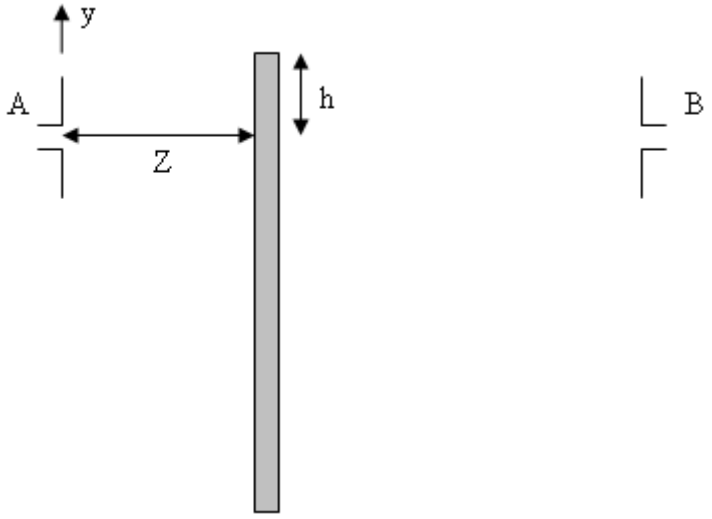

Figure A - Propagation obscured by a screen

Without the screen present, the mutual impedance between antennas A and B is given by

$$Z_{AB} = \frac{j\omega\mu}{4\pi D} h_{eff}^{A} . h_{eff}^{B} \exp(-j\beta D) \qquad (27)$$

where ω is the angular frequency, μ is the permeability of the medium, $\mathbf{h}^{\mathbf{A}}_{\mathbf{eff}}$ and $\mathbf{h}^{\mathbf{B}}_{\mathbf{eff}}$ are the effective length of antennas A and B, respectively, D = Z_A + Z_B, and $\beta = \frac{2\pi}{\lambda}$ for the wavelength λ at the operating frequency (220 MHz for DAB-based radar) [53].

With the screen present, the mutual impedance between antennas A and B is given by

$$Z_{AB} = \frac{j\omega\mu\sqrt{j}}{4\pi D\sqrt{\pi}} h_{eff}^{A} . h_{eff}^{B} \exp(-j\beta D) \int_{\upsilon}^{\infty} \exp(-jY^2) dY \qquad (28)$$

where $\nu = h\sqrt{\left(\frac{\beta}{2}(\frac{1}{Z_A} + \frac{1}{Z_B})\right)}$ and $Y = y\sqrt{\left(\frac{\beta}{2Z_A} + \frac{\beta}{2Z_B}\right)}$.

Taking the ratio of the mutual impedance with the screen to that without the screen gives

$$\frac{Z_{AB\_screen}}{Z_{AB\_no\_screen}} = \frac{\sqrt{j}}{\sqrt{\pi}} \int_{\upsilon}^{\infty} \exp(-jY^2) dY \quad (29)$$

The ratio of these impedances yields the ratio of the voltages at the receivers for the same driving current and scenario. Consequently, the square of the absolute value of the ratio will yield the ratio of powers at the receiver. Consequently, the attenuation (or loss) L to the signal in decibels due to the screen is given by

$$L = 20\log_{10}\left(\frac{1}{\sqrt{\frac{1}{\pi}\left(\int_{\nu}^{\infty} \exp(-jY^2) dY\right)\left(\int_{\nu}^{\infty} \exp(-jY^2) dY\right)^*}}\right) \quad (10)$$

where * denotes the complex conjugate. The integral can be evaluated using Fresnel integrals via

$$\begin{aligned} &\int_{\nu}^{\infty} \exp(-jt^2) dt = \int_{\upsilon}^{\infty} \cos(t^2) dt - j\int_{\upsilon}^{\infty} \sin(t^2) dt \\ &= \int_0^{\infty} \cos(t^2) dt - \int_0^{\upsilon} \cos(t^2) dt - j\left[\int_0^{\infty} \sin(t^2) dt - \int_0^{\upsilon} \sin(t^2) dt\right] \\ &= C(\infty) - C(\upsilon) - j[S(\infty) - S(\upsilon)] \end{aligned} \quad (30)$$

where $C(x) = \int_0^x \cos(t^2) dt$ and $S(x) = \int_0^x \sin(t^2) dt$ are the Fresnel integrals.

Now

$$C(\infty) = S(\infty) = \sqrt{\frac{\pi}{8}}, \quad (31)$$

so

$$\int_{\upsilon}^{\infty} \exp(-jt^2) dt = \sqrt{\frac{\pi}{8}} - C(\upsilon) - j\sqrt{\frac{\pi}{8}} + jS(\upsilon) \quad (32)$$

Some authors, such as Abramowitz and Stegun [54], define C(x) and S(x) using $\frac{\pi}{2}t^2$ as the argument. Then

$$C(y) = \int_0^y \cos\left(\frac{\pi}{2}t^2\right) dt = 0.5 + f(y)\sin\left(\frac{\pi}{2}y^2\right) - g(y)\cos\left(\frac{\pi}{2}y^2\right) \quad (33)$$

and

$$S(y) = \int_0^y \sin\left(\frac{\pi}{2}t^2\right) dt = 0.5 - f(y)\cos\left(\frac{\pi}{2}y^2\right) - g(y)\sin\left(\frac{\pi}{2}y^2\right) \quad (34)$$

where

$$f(z) = \frac{1 + 0.926z}{2 + 1.792z + 3.104z^2} + \varepsilon(z) \quad (35)$$

and

$$g(z) = \frac{1}{2 + 4.142z + 3.492z^2 + 6.670z^3} + \varepsilon(z) \quad (36)$$

(for $0 \le z \le \infty$ with $|\varepsilon(z)| \le 2 \times 10^{-3}$) are rational approximations [54].

The Fresnel integrals C(v) and S(v) in equation (32) can then be obtained from the above approximations using a change of variables via

$$C(x) = \int_{t=0}^{t=x} \cos(t^2)dt = \sqrt{\frac{\pi}{2}} \int_{u=0}^{u=\sqrt{\frac{2}{\pi}x}} \cos(\frac{\pi}{2}u^2)du \quad (37)$$

and

$$S(x) = \int_{t=0}^{t=x} \sin(t^2)dt = \sqrt{\frac{\pi}{2}} \int_{u=0}^{u=\sqrt{\frac{2}{\pi}x}} \sin(\frac{\pi}{2}u^2)du \quad (38)$$

Appendix B – RCS Matrices from NEC Simulations

The following tables contain representative matrices of the RCS values used in the simulator. The rows correspond to the RCS value (in decibels) for every 45 degrees in azimuth, labelled in the tables as 'AZIMUTH' (0 to 180 degrees) and the columns corresponding to the RCS for every 90 degrees in illumination angle, labelled in the tables as 'ILLUM' (1 to 360 degrees).

Elevation angle = 0 degrees, vertical polarisation:

		AZIMUTH			
I		**45°**	**90°**	**135°**	**180°**
L	**90°**	0.72	33.22	3.76	-14.17
L	**180°**	2.66	-1.42	-1.6	22.16
U	**270°**	10.13	40.81	7.58	-20.96
M	**360°**	8.33	3.81	14.87	33.51

Elevation angle = 0 degrees, horizontal polarisation:

		AZIMUTH			
I		**45°**	**90°**	**135°**	**180°**
L	**90°**	-17.69	-3.92	-8.7	-5.08
L	**180°**	-29.84	-28.54	-24.08	-26.24
U	**270°**	-18.34	-3.78	-7.84	-4.11
M	**360°**	-27.61	-21.44	-24.99	-16.43

Elevation angle = 10 degrees, vertical polarisation:

		AZIMUTH			
I		**45°**	**90°**	**135°**	**180°**
L	**90°**	-2.71	32.01	3.98	1.93
L	**180°**	5.28	-0.1	-2.05	14.34
U	**270°**	4.33	39.03	0.01	1.86
M	**360°**	9.9	-0.18	13.18	25.23

Elevation angle = 10 degrees, horizontal polarisation:

		AZIMUTH			
I		**45°**	**90°**	**135°**	**180°**
L	**90°**	-0.94	5.58	-13.91	3.7
L	**180°**	2.56	6.18	-7.02	-27.17
U	**270°**	9.36	-0.14	1.93	3.88
M	**360°**	4.96	-12.96	-6.82	-26.42

Appendix C – Matlab Code Listing

A.1 Propagation Loss Unit

```
% propag_loss_unit.m

% Propagation Loss Unit
% This Unit calculates the propagation loss in decibels to the
transmitted
% signals due to diffraction, multipath and depolarisation

function
[diff_loss,diff_td,mult_loss,mult_td,depol_loss,spn_loss] =
propag_loss_unit(origin,k,freq,Tx_info,Rx_info,d_TxRx,elevs_fil
e,bldgs_info,c)

% Generate a terrain map
[terrain_map,Start_height,End_height,slope]
 =
terr_map_gen(origin,Tx_info,Rx_info,d_TxRx,elevs_file,bldgs_inf
o);

% Calculate loss in decibels due to diffraction
[diff_loss,diff_td] =
diff_loss_unit(freq,terrain_map,Start_height,End_height,c);

% Calculate loss in decibels due to multipath
[mult_loss,refl_pt_x,mult_td]=
mult_loss_unit(terrain_map,freq,c);

depol_loss = zeros(1,length(refl_pt_x));

if refl_pt_x > 0
    for i = 1:length(refl_pt_x)
        % Calculate transverse slope of terrain at reflection
point(s)
        trans_slope =
calc_trans_slope(submatrix,slope,refl_pt_x(i));

        % Calculate loss in decibels due to depolarisation
        depol_loss(i) = depol_loss_unit(trans_slope);
    end
end

% Processing noise reduction factor (dB)
spn_loss = 20;
```

A.2 Terrain Map Generator

```
% terr_map_gen.m

% Terrain Map Generator
% This Unit generates a terrain map, given:
% - latitude and longitude coordinates and heights of
transmitters
% - latitude and longitude coordinates and heights of receivers
% - Detailed Terrain Elevation Data (DTED) file
% - information about buildings
```

```
function [terrain_map,Start_height,End_height,slope]
 =
terr_map_gen(origin,Tx_info,Rx_info,d_TxRx,elevs_file,bldgs_inf
o)

% Generate a set of elevations with their corresponding
distances along
% the terrain
[submatrix,elev_dists,Rx_col_max,slope]
 = gen_elev_dists(origin,Tx_info,Rx_info,d_TxRx,elevs_file);
% Generate a terrain map
num_bldgs = bldgs_info(1,1,1);
num_bits = 20;

% Definition of 'terrain_map':
% A terrain map is made up of arbitrary length segments with
the option
% of discontinuity in elevation
% Bit 1: Previous elevation point
% Bit 2: Next elevation point
% Bit 3: Distance along terrain
terrain_map =
generate_terrain_map(elev_dists,num_bldgs,num_bits);

% Smooth the terrain map
terrain_map = smooth_map(elev_dists,terrain_map);

% Add buildings to the terrain map
if num_bldgs >= 1
    for i = 1:num_bldgs
        i;
        start_dist(i) = bldgs_info(i,2);
        end_dist(i) = bldgs_info(i,3);
        start_height(i) = bldgs_info(i,4);
        end_height(i) = bldgs_info(i,5);
        terrain_map =
add_bldg(i,terrain_map,num_bldgs,start_dist(i),end_dist(i),star
t_height(i),end_height(i));
    end
end

% Add heights (in m) of start antenna and end antenna
if Rx_col_max == 0
    Start_height = Rx_info(4);
    End_height = Tx_info(4);
else % Rx_col_max = 1
    Start_height = Tx_info(4);
    End_height = Rx_info(4);
end


% gen_elev_dists.m

% Generates a set of elevations with their corresponding
distances along
% the terrain

function [submatrix,elev_dists,Rx_col_max,slope]
 = gen_elev_dists(origin,Tx,Rx,d_TxRx,elevs_file)
```

```
% Definition of elev_dists:
% Bit 1: Elevation (in m above sea level)
% Bit 2: Distance along terrain (in m)

elevations=imread(elevs_file);

% Determine coordinates of endpoints
long_step = 0.000833333333333;  % longitudinal pixel size -
corresponds to
% 3 arc seconds = 3/3600 of a degree
lat_step = -0.000833333333333;  % latitudinal pixel size

% Coordinates of receiver
elev_Rx = ceil([(Rx(1)-origin(1))/lat_step (Rx(2)-
origin(2))/long_step]);
% Elevation of receiver
elevations(elev_Rx(1),elev_Rx(2));

% Coordinates of transmitters
elev_Tx = ceil([(Tx(1)-origin(1))/lat_step (Tx(2)-
origin(2))/long_step]);
% Elevation of transmitters
elevations(elev_Tx(1),elev_Tx(2));

% Determine which coordinates are larger
max_row = elev_Rx(1);
Rx_row_max = 1;     % flag that indicates receiver row is
maximum
min_row = elev_Tx(1);
if elev_Tx(1) > max_row
    % Transmitter row is maximum
    max_row = elev_Tx(1);
    Rx_row_max = 0;
    min_row = elev_Rx(1);
end

max_col = elev_Rx(2);
Rx_col_max = 1;     % flag that indicates receiver column is
maximum
min_col = elev_Tx(2);
if elev_Tx(2) > max_col
    % Transmitter column is maximum
    max_col = elev_Tx(2);
    Rx_col_max = 0;
    min_col = elev_Rx(2);
end

% Determine which cells to include
clear submatrix;
submatrix=elevations(min_row:max_row,min_col:max_col);
n_rows = length(submatrix(:,1));   % number of rows
n_cols = length(submatrix(1,:));   % number of columns

% Construct a set of elevations and their corresponding
distances along
% the path from source to destination
if numel(submatrix) == 1
    % Construct elev_dists matrix
    elev_dists(1,1) = submatrix;
    elev_dists(1,2) = d_TxRx;
    slope = 0;
else
```

```
    post_spacing = d_TxRx/sqrt((n_rows-1)^2+(n_cols-1)^2); % in
m
    step_size = post_spacing/5; % in m
    slope = (n_rows-1)/(n_cols-1);

    rows = 1:n_rows;
    cols = 1:n_cols;

    c_limit = (n_cols-2)*post_spacing/step_size;
    r_limit = (n_rows-2)*post_spacing/step_size;

    % Test whether path starts in row 1
    if Rx_col_max == Rx_row_max
        % Traverse submatrix from top left to bottom right
        % Traverse half of first submatrix element
        for i = 1:ceil((post_spacing/step_size)/2)
            elev(i) = submatrix(1,1);
        end
        elev_len = length(elev);
        % Traverse intermediate submatrix elements
        for i = 1:c_limit
            c(i) = 1+i*step_size/post_spacing;
            % To avoid interp2 returning 0 from overrunning the
last element
            if c(i) > n_cols
                c(i) = n_cols;
            end
            if slope == Inf
                r(i) = c(i);
            else
                r(i) = slope*c(i);
            end
            % To avoid interp2 returning 0 from an incomplete
element
            if r(i) < 1
                r(i) = 1;
            end
            % To avoid interp2 returning 0 from overrunning the
last element
            if r(i) > n_rows
                r(i) = n_rows;
            end
            % Perform interpolation
            rows = double(rows);
            cols = double(cols);
            submatrix = double(submatrix);
            c(i) = double(c(i));
            r(i) = double(r(i));
            if n_rows == 1
                elev(elev_len+i) =
interp1(cols,submatrix,c(i));
            else
                if n_cols == 1
                    elev(elev_len+i) =
interp1(rows,submatrix,r(i));
                else
                    % Perform two-dimensional interpolation
within submatrix if necessary
                    elev(elev_len+i) =
interp2(cols,rows,submatrix,c(i),r(i));
                end
            end
        end
```

```
        elev_len = length(elev);
        % Traverse half of final submatrix element
        for i = 1:ceil((post_spacing/step_size)/2)
            elev(elev_len+i) = submatrix(n_rows,n_cols);
        end
    else
        % Traverse submatrix from bottom left to top right
        % Traverse half of first submatrix element
        for i = 1:ceil((post_spacing/step_size)/2)
            elev(i) = submatrix(n_rows,1);
        end
        elev_len = length(elev);
        % Traverse intermediate submatrix elements
        for i = 1:c_limit
            c(i) = 1+i*step_size/post_spacing;
            % To avoid interp2 returning 0 from overrunning the
last element
            if c(i) > n_cols
                c(i) = n_cols;
            end
            if slope == Inf
                r(i) = n_rows-c(i);
            else
                r(i) = n_rows-slope*c(i);
            end
            % To avoid interp2 returning 0 from overrunning the
last element
            if r(i) > n_rows
                r(i) = n_rows;
            end
            % To avoid interp2 returning 0 from an incomplete
element
            if r(i) < 1
                r(i) = 1;
            end
            % Perform interpolation
            rows = double(rows);
            cols = double(cols);
            submatrix = double(submatrix);
            c(i) = double(c(i));
            r(i) = double(r(i));
            if n_rows == 1
                elev(elev_len+i) =
interp1(cols,submatrix,c(i));
            else
                if n_cols == 1
                    elev(elev_len+i) =
interp1(rows,submatrix,r(i));
                else
                    % Perform two-dimensional interpolation
within submatrix if necessary
                    elev(elev_len+i) =
interp2(cols,rows,submatrix,c(i),r(i));
                end
            end
        end
        elev_len = length(elev);
        % Traverse half of final submatrix element
        for i = 1:ceil((post_spacing/step_size)/2)
            elev(elev_len+i) = submatrix(1,n_cols);
        end
    end
```

```
    % Calculate distance between waypoints
    x = step_size;
    y = slope*x;
    if slope == Inf
        waypt_spacg = step_size;
    else
        waypt_spacg = sqrt(x^2+y^2);
    end

    % Construct elev_dists matrix
    elev_len = length(elev);
    elev_dists = double(zeros(length(elev),2));
    elev_dists(1,1) = elev(1);
    elev_dists(1,2) = waypt_spacg/2;
    for i = 2:length(elev)-1
        elev_dists(i,1) = elev(i);
        elev_dists(i,2) = elev_dists(i-1,2)+waypt_spacg;
    end
    elev_dists(length(elev),1) = elev(length(elev));
    elev_dists(length(elev),2) = elev_dists(length(elev)-
1,2)+waypt_spacg/2;
end


% generate_terrain_map.m

% Generates a matrix called map using the matrix 'elev_dists',
including a
% number ('num_bldgs') of buildings and with each row using a
number
% ('num_bits') of bits to store data

function [map] =
generate_terrain_map(elev_dists,num_bldgs,num_bits)

% Definition of 'map':
%   A terrain map is made up of arbitrary length segments with
the option
%   of discontinuity in elevation
%   Bit 1: Previous elevation point
%   Bit 2: Next elevation point
%   Bit 3: Distance along terrain
%
% Definition of 'elev_dists':
%   Matrix of land elevations and distances along terrain
%   Bit 1: Land elevation above sea level (in m)
%   Bit 2: Distance along terrain (in m)

map = zeros(length(elev_dists(:,1))+2+num_bldgs*2,num_bits);
% Process starting point (location of transmit antenna)
map(1,1) = elev_dists(1,1);
map(1,2) = elev_dists(1,1);
map(1,3) = 0;
if length(elev_dists(:,1)) > 1
    % Process contents of 'elev_dists'
    for i = 1:length(elev_dists(:,1))
        map(i+1,1) = elev_dists(i,1);
        map(i+1,2) = elev_dists(i,1);
        map(i+1,3) = elev_dists(i,2);
    end
end
i = length(elev_dists(:,1));
```

```
% Process ending point (location of receive antenna)
map(i+2,1) = elev_dists(i,1);
map(i+2,2) = elev_dists(i,1);
map(i+2,3) = elev_dists(i,2);


% smooth_map.m

% Smooths the matrix 'map' by connecting the midpoints of the
way-points in
% the matrix 'elev_dists'

function [map] = smooth_map(elev_dists,map)

% Definition of 'map':
%   A terrain map is made up of arbitrary length segments with
the option
%   of discontinuity in elevation
%   Bit 1: Previous elevation point
%   Bit 2: Next elevation point
%   Bit 3: Distance along terrain

% Definition of 'elev_dists':
%   Matrix of land elevations and distances along terrain
%   Bit 1: Land elevation above sea level (in m)
%   Bit 2: Distance along terrain (in m)

% Process starting point (location of transmit antenna)
midpoint = elev_dists(1,2)/2;
map(2,3) = midpoint;

if length(elev_dists(:,1)) == 1
    % Assign midpoint
    map(2,1) = elev_dists(1,1);
    map(2,2) = map(2,1);
    % Assign ending point
    map(3,1) = elev_dists(1,1);
    map(3,2) = map(3,1);
    map(3,3) = elev_dists(1,2);
end

% Find the midpoint of each block
for i = 2:length(elev_dists(:,1))
    midpoint = (elev_dists(i,2)-elev_dists(i-
1,2))/2+elev_dists(i-1,2);
    % Store the midpoint
    map(i+1,3) = midpoint;
end
% Process ending point (location of receive antenna)
map(i+2,3) = elev_dists(i,2);


% add_bldg.m

% Adds a building to the matrix 'map'

% Building parameters:
%   start_dist:   distance along terrain where building starts
%   end_dist:     distance along terrain where building ends
%   start_height: height of building at starting distance
%   end_height:   height of building at ending distance
```

```
function [map] =
add_bldg(index,map,num_bldgs,start_dist,end_dist,start_height,e
nd_height)

% Determine which segment of map building lies in
i = 1;
while i < length(map(:,1))+1
    if start_dist <= map(i,3)
        seg = i-1;  % segment of map that building lies in
        i = length(map(:,1))+1; % Break out of while loop
    else
        i = i+1;    % Continue searching
    end
end

% Make room in 'map' for the starting and ending points of the
building
for i = length(map(:,1))-2:-1:seg+1
    map(i+2,:) = map(i,:);
end

% Calculate adjustment factors
angle = atan((map(seg+1,1)-map(seg,1))/(map(seg+1,3)-
map(seg,3)));
land_start_height = (start_dist-
map(seg,3))*tan(angle)+map(seg,1);
land_end_height = (end_dist-map(seg,3))*tan(angle)+map(seg,1);

% Add building to 'map'
map(seg+1,1) = land_start_height;
map(seg+1,2) = land_start_height+start_height;
map(seg+1,3) = start_dist;

map(seg+2,1) = land_end_height+end_height;
map(seg+2,2) = land_end_height;
map(seg+2,3) = end_dist;

% Remove segments of 'map' that are now covered by building
i = seg+3;
del_cntr = i;   % end segment (delete counter)
% Find where segments to be removed end
while i <= length(map(:,1))-(num_bldgs-index)*2
    if map(i,3) < end_dist
        del_cntr = del_cntr+1;
    end
    i = i+1; % Continue searching
end

if del_cntr > seg+3
    for i = seg+3:length(map(:,1))-2
        map(i,:) = map(i+2,:);
    end
end

% Copy over elements to a new map
for i = 1:length(map(:,1))-(num_bldgs-index)*2-2
    new_map(i,:) = map(i,:);
end
clear map;
map = new_map;
```

A.3 Diffraction Loss Unit

```
% diff_loss_unit.m

% Diffraction Loss Unit
% This Unit calculates the propagation loss in decibels to the
transmitted
% signals due to diffraction

function [diff_loss,diff_td] =
diff_loss_unit(freq,terrain_map,Start_height,End_height,c)

% Definition of 'freq':
% Operating frequency in Hz

% Definition of 'terrain_map':
% A terrain map is made up of arbitrary length segments with
the option
% of discontinuity in elevation
% Bit 1: Previous elevation point
% Bit 2: Next elevation point
% Bit 3: Distance along terrain

% Definition of 'Start_height':
% Height of start antenna in m

% Definition of 'End_height':
% Height of end antenna in m

% Add heights (in m) of start antenna and end antenna
% Definition of 'Start_Point' and 'End_Point':
% Bit 1: x-coordinate
% Bit 2: y-coordinate (with correction for the curvature of
Earth)
[terrain_map,Start_point] =
make_Start(terrain_map,Start_height);
[terrain_map,End_point] = make_End(terrain_map,End_height);

% Convert elevations and distances to Cartesian coordinates
with the
% origin centred on the transmit antenna
% Enhanced definition of 'terrain_map':
% Bit 3: x-coordinate (with the origin centred on the start
antenna)
% Bit 4: y-coordinate of previous elevation (with the origin
centred on the
% start antenna)
% Bit 5: y-coordinate of next elevation (with the origin
centred on the
% start antenna)
terrain_map = convert_Cart_Start(terrain_map);

% Find maximum angle between transmit antenna and elevation
points, and
% record index of entry corresponding to maximum angle
[max_angle1] = max_angle_Start(terrain_map,End_height);
max_angle1_deg = max_angle1*180/pi;

% Find maximum angle between receive antenna and elevation
points, and
```

```
% record index of entry corresponding to maximum angle
[max_angle2] = max_angle_End(terrain_map,Start_height);
max_angle2_deg = max_angle2*180/pi;

% Calculate Fresnel integral parameter
[v,h,Z_A,Z_B]=
calc_Fres_param(max_angle1,max_angle2,terrain_map,freq,c);

if v < 0
    v = -v;
end

% Perform change of variables
v = v*sqrt(2/pi);

% Calculate Fresnel integral
[C S] = fresnel_int(v);

% Perform change of variables
C = C*sqrt(pi/2);
S = S*sqrt(pi/2);

% Calculate propagation loss (in dBs) due to general
'effective'
% diffractive screen
[screen_loss]= calc_diff_loss(h,v,C,S);
diff_loss = real(screen_loss);

% Calculate path length
l1 = Z_A/cos(max_angle1);
l2 = Z_B/cos(max_angle2);
path_len = l1 + l2;
diff_td = calc_dsi_td(path_len,c);
if diff_loss == 0
    diff_td = 0;
end


% make_Start.m

% Constructs a two-element array 'Start_point' and adds it to
the map

function [map,Start_point] = make_Start(map,height)
% Definition of 'Start_Point':
%   Bit 1: x-coordinate
%   Bit 2: y-coordinate (with correction for the curvature of
Earth)
Start_point = [0 map(1,1)+height];
% Add to map
map(1,1) = Start_point(2);
map(1,2) = Start_point(2);


% make_End.m

% Constructs a two-element array 'End_point' and adds it to the
map

function [map,End_point] = make_End(map,height)
% Definition of 'End_Point':
```

```
%   Bit 1: x-coordinate
%   Bit 2: y-coordinate (with correction for the curvature of
Earth)
End_point = [map(length(map(:,1)),3)
map(length(map(:,1)),1)+height];
% Add to map
map(length(map(:,1)),1) = End_point(2);
map(length(map(:,1)),2) = End_point(2);


% convert_Cart_Start.m

% Converts elevations and distances in the matrix 'map' to
Cartesian
% coordinates with the origin centred on the start antenna

function [map] = convert_Cart_Start(map)

% Enhanced definition of 'map':
%   A terrain map is made up of arbitrary length segments with
the option
%   of discontinuity in elevation
%   Bit 1: Previous land elevation above sea level (in m)
%   Bit 2: Next land elevation above sea level (in m)
%   Bit 3: x-coordinate (with the origin centred on the start
antenna)
%   Bit 4: y-coordinate of previous elevation (with the origin
centred on
%   the start antenna)
%   Bit 5: y-coordinate of next elevation (with the origin
centred on the
%   start antenna)

% Process starting point (set as origin)
map(1,4) = 0;
map(1,5) = 0;
% Process remainder of elements in 'map'
for i = 2:length(map(:,1))
    % Add correction factor for curvature of the earth
    correction = curv_correctn(map(i,3));
    % Centre the Cartesian coordinate system on the starting
point
    % (the start antenna)
    map(i,4) = map(i,1)+correction-map(1,1);
    map(i,5) = map(i,2)+correction-map(1,1);
end


% max_angle_Start.m

% Finds maximum angle between start antenna and elevation
points, and
% records index of entry corresponding to maximum angle

function [max_angle1] = max_angle_Start(map,height)

% Enhanced definition of 'map':
%   A terrain map is made up of arbitrary length segments with
the option
%   of discontinuity in elevation
%   Bit 1: Previous land elevation above sea level (in m)
```

```
%   Bit 2: Next land elevation above sea level (in m)
%   Bit 3: x-coordinate (with the origin centred on the start
antenna)
%   Bit 4: y-coordinate of previous elevation (with the origin
centred on
%   the start antenna)
%   Bit 5: y-coordinate of next elevation (with the origin
centred on the
%   start antenna)

max_ang_idx1 = 1;
% Check previous elevation
max_angle1 = atan(map(2,4)/map(2,3));
% Check next elevation
temp_angle1 = atan(map(2,5)/map(2,3));
if temp_angle1 > max_angle1
    w = 1;
    max_angle1 = temp_angle1;
end
for i = 3:length(map(:,1))-1
    % Check previous elevation
    temp_angle1 = atan(map(i,4)/map(i,3));
    if temp_angle1 > max_angle1
        max_angle1 = temp_angle1;
        % Store index of entry corresponding to maximum angle
        max_ang_idx1 = i;
    end
    % Check next elevation
    temp_angle1 = atan(map(i,5)/map(i,3));
    if temp_angle1 > max_angle1
        max_angle1 = temp_angle1;
        % Store index of entry corresponding to maximum angle
        max_ang_idx1 = i;
    end
end
% Check final waypoint
i = length(map(:,1));
% Check previous elevation
temp_angle1 = atan((map(i,4)-height)/map(i,3));
if temp_angle1 > max_angle1
    max_angle1 = temp_angle1;
    % Store index of entry corresponding to maximum angle
    max_ang_idx1 = i;
end
% Check next elevation
temp_angle1 = atan((map(i,5)-height)/map(i,3));
if temp_angle1 > max_angle1
    max_angle1 = temp_angle1;
    % Store index of entry corresponding to maximum angle
    max_ang_idx1 = i;
end



% max_angle_End.m

% Finds maximum angle between end antenna and elevation points,
and
% records index of entry corresponding to maximum angle

function [max_angle2] = max_angle_End(map,height)

% Enhanced definition of 'map':
```

```
%   A terrain map is made up of arbitrary length segments with
the option
%   of discontinuity in elevation
%   Bit 1: Previous land elevation above sea level (in m)
%   Bit 2: Next land elevation above sea level (in m)
%   Bit 3: x-coordinate (with the origin centred on the start
antenna)
%   Bit 4: y-coordinate of previous elevation (with the origin
centred on
%   the start antenna)
%   Bit 5: y-coordinate of next elevation (with the origin
centred on the
%   start antenna)

max_ang_idx2 = length(map(:,1))-1;
max_angle2 = atan((map(length(map(:,1))-1,4)-
map(length(map(:,1)),4))/(map(length(map(:,1)),3)-
map(length(map(:,1))-1,3)));
for i = length(map(:,1))-2:-1:2
    % Check previous elevation
    temp_angle2 = atan((map(i,4)-
map(length(map(:,1)),4))/(map(length(map(:,1)),3)-map(i,3)));
    if temp_angle2 > max_angle2
        max_angle2 = temp_angle2;
        % Store index of entry corresponding to maximum angle
        max_ang_idx2 = i;
    end
    % Check next elevation
    temp_angle2 = atan((map(i,5)-
map(length(map(:,1)),5))/(map(length(map(:,1)),3)-map(i,3)));
    if temp_angle2 > max_angle2
        max_angle2 = temp_angle2;
        % Store index of entry corresponding to maximum angle
        max_ang_idx2 = i;
    end
end
% Check final waypoint
i = 1;
% Check previous elevation
temp_angle2 = atan((map(i,4)-height-
map(length(map(:,1)),4))/map(length(map(:,1)),3));
if temp_angle2 > max_angle2
    max_angle2 = temp_angle2;
    % Store index of entry corresponding to maximum angle
    max_ang_idx2 = i;
end
% Check next elevation
temp_angle2 = atan((map(i,5)-height-
map(length(map(:,1)),5))/map(length(map(:,1)),3));
if temp_angle2 > max_angle2
    max_angle2 = temp_angle2;
    % Store index of entry corresponding to maximum angle
    max_ang_idx2 = i;
end



% calc_Fres_param.m

% Calculates Fresnel integral parameter 'v' given the 2 maximum
angles
% ('max_angle1' and 'max_angle2') and the terrain map 'map'
```

```
function [v,h,Z_A,Z_B] =
calc_Fres_param(max_angle1,max_angle2,map,f,c)
% Determine point of intersection of the 2 lines corresponding
to the 2
% maximum angles
slope1 = tan(max_angle1);
slope2 = -tan(max_angle2);
y_intercept1 = map(1,4);
y_intercept2 = map(length(map(:,1)),4)-
map(length(map(:,1)),3)*(-tan(max_angle2));
% Calculate x-coordinate of point of intersection
if slope1 == slope2
    x_coord_int = map(length(map(:,1)),3)/2;
else
    x_coord_int = (y_intercept2-y_intercept1)/(slope1-slope2);
end
% Calculate Fresnel integral parameter
Z_A = x_coord_int;  % distance from Tx to peak
Z_B = map(length(map(:,1)),3)-Z_A;  % distance from Rx to peak
h1 = slope1*x_coord_int+y_intercept1;
h2 = slope2*x_coord_int+y_intercept2;
h_init = h1;
% Adjust value of height
% Find line that joins tops of Tx and Rx
slope = (map(length(map(:,1)),4)-
map(1,4))/map(length(map(:,1)),3);
y_h = slope*Z_A;
h = h_init - y_h;
beta = 2*pi*f/c;
v = h*sqrt(beta/2*(1/Z_A+1/Z_B));



% fresnel_int.m

% This function calculates an estimate of the Fresnel integrals
% Assumes 0 <= v <= infinity
% C(x) = integral from 0 to x of cos(pi/2*t^2) dt
% S(x) = integral from 0 to x of sin(pi/2*t^2) dt

function [C S] = fresnel_int(v)
if v >= 0
    % Calculate approximate Fresnel integrals
    f = (1+0.926*v)/(2+1.792*v+3.104*v^2);
    g = 1/(2+4.142*v+3.492*v^2+6.67*v^3);
    C = 0.5+f*sin(pi/2*v^2)-g*cos(pi/2*v^2);
    S = 0.5-f*cos(pi/2*v^2)-g*sin(pi/2*v^2);
else
    C = 0;
    S = 0;
end



% calc_diff_loss.m

% Calculates propagation loss (in dBs) due to general
'effective'
% diffractive screen

function [screen_loss] = calc_diff_loss(h,v,C,S)
exp_int = sqrt(pi/8)-sqrt(pi/8)*i-C+i*S;
exp_int_conj = conj(exp_int);
screen_loss = 1/sqrt(1/pi*exp_int*exp_int_conj);
```

```
% Convert to dBs
screen_loss = 20*log10(screen_loss);
% Below LOS, diffractive loss is 0 dB
if h < 0
    screen_loss = 0;
end
```

A.4 Multipath Loss Unit

```
% mult_loss_unit.m

% Multipath Loss Unit
% This Unit calculates the propagation loss in decibels to the
transmitted
% signals due to multipath and determines the x-coordinates of
the
% reflection points with the shortest corresponding path
lengths

function [mult_loss,refl_pt_x,mult_td] =
mult_loss_unit(terrain_map,f,c)

% Definition of 'terrain_map':
% A terrain map is made up of arbitrary length segments with
the option
% of discontinuity in elevation
% Bit 1: Previous elevation point
% Bit 2: Next elevation point
% Bit 3: x-coordinate (with the origin centred on the start
antenna)
% Bit 4: y-coordinate of previous elevation (with the origin
centred on the
% start antenna)
% Bit 5: y-coordinate of next elevation (with the origin
centred on the
% start antenna)

% Correct y_coordinates in 'terrain_map' for the curvature of
Earth
% Enhanced definition of 'terrain_map':
% Bit 6: y-coordinate of previous elevation
% (with correction for curvature of Earth)
% Bit 7: y-coordinate of next elevation
% (with correction for curvature of Earth)
terrain_map = elev_correctn(terrain_map);

% Find stationary points corresponding to valid path lengths
N = 100;     % number of points to check on terrain map
% Calculate the length of the segment interval to check
seg_int = calc_seg_int(terrain_map,N);
% Find reflection points
pts_paths = find_pts_paths(terrain_map,seg_int);
% Find stationary points
stat_pts = find_stat_pts(pts_paths,terrain_map);
clear pts_paths;
% Remove stationary points that lie outside the terrain map
stat_pts_map = trunc_to_map(stat_pts,terrain_map);
% Find path length of line-of-sight signal
path_length_LOS =
calc_path(terrain_map(1,3),terrain_map(length(terrain_map(:,1))
,3),terrain_map(1,4),terrain_map(length(terrain_map(:,1)),4));
```

```
R = -1;         % reflection coefficient
beta = 2*pi*f/c;
x_coord = [];
y_coord = [];
mult_loss = 0;
refl_pt_x = 0;
path_lens = [];
mult_td = -1;

if stat_pts_map(1,1) > 0
    for i = 1:length(stat_pts_map(:,1))
        x_coord(i) = stat_pts_map(i,2); % x-coordinate of
reflection point
        y_coord(i) = stat_pts_map(i,3); % y-coordinate of
reflection point
        r = sqrt(x_coord(i)^2+y_coord(i)^2);
        % Calculate electric field amplitude (V/m)
        E = R*1/r*exp(-j*beta*r);
        % Calculate power (W)
        P = abs(E)^2;
        % Convert to decibels
        P = 10*log10(P);
        mult_loss(i) = -P; % propagation loss in decibels due
to multipath
        refl_pt_x(i) = x_coord(i);    % x-coordinate of
reflection point
        path_lens(i) = stat_pts_map(i,4);   % path length of
reflection point
        % Calculate reflected path time delay
        mult_td(i) = calc_dsi_td(path_lens(i),c);
    end
end



% elev_correctn.m

% Corrects y-coordinate of elevations in 'map' due to the
curvature of
% Earth

function [map] = elev_correctn(map)

% Enhanced definition of 'map':
%   A terrain map is made up of arbitrary length segments with
the option
%   of discontinuity in elevation
%   Bit 1: Land elevation above sea level (in m)
%   Bit 2: Distance along terrain (in m)
%   Bit 3: x-coordinate (with the origin centred on the
transmit antenna)
%   Bit 4: y-coordinate of previous elevation (with the origin
centred on
%   the start antenna)
%   Bit 5: y-coordinate of next elevation (with the origin
centred on the
%   start antenna)
%   Bit 6: y-coordinate of previous elevation (with correction
for
%   curvature of Earth)
%   Bit 7: y-coordinate of next elevation (with correction for
curvature
%   of Earth)
```

```
for i = 1:length(map(:,1))
    map(i,6) = map(i,1)+curv_correctn(map(i,3));
    map(i,7) = map(i,2)+curv_correctn(map(i,3));
end


% calc_seg.int.m

% Calculates the length of the segment interval to check

function [seg_int] = calc_seg_int(map,N)
% Calculate the total path length from Tx to Rx
tot_path_len = 0;
for i = 2:length(map(:,1))
    path_len = calc_seg_len(map,i);
    tot_path_len = tot_path_len+path_len;
end
% Calculate the length of the segment interval to check
seg_int = tot_path_len/N;


% find_pts_paths.m

% Finds terrain reflection points and corresponding path
lengths

function [pts_paths] = find_pts_paths(map,seg_int)

% Definition of 'terr_pt':
%   Bit 1: x-coordinate
%   Bit 2: y-coordinate

% Definition of 'pts_paths':
%   Bit 1: Number of way-point to left of terrain reflection
point
%   Bit 2: x-coordinate of terrain reflection point
%   Bit 3: y-coordinate of terrain reflection point
%   Bit 4: Path length from start antenna to terrain reflection
point to
%   end antenna

pts_paths = 0;
terr_pt = double([0 0]);
m = 1;  % index for 'pts_paths' matrix
for a = 2:length(map(:,1))
    % Find the length of the segment to be searched
    seg_len = calc_seg_len(map,a);
    % Determine the number of points to check for this segment
    num_points = ceil(seg_len/seg_int);
    % Divide segment into (num_points-1) smaller segments
    for i = 1:num_points
        % Find the terrain reflection point
        terr_pt = find_terr_pt(terr_pt,a,map,num_points);
        % Store the number of the way-point to the left of the
terrain
        % reflection point
        pts_paths(m,1) = a;
        % Store the terrain reflection point
        pts_paths(m,2) = terr_pt(1);
        pts_paths(m,3) = terr_pt(2);
```

```
        % Calculate distance from transmitter to point to
receiver
        path_lengthStart =
calc_path(pts_paths(m,2),map(1,3),pts_paths(m,3),map(1,6));
        path_lengthEnd =
calc_path(pts_paths(m,2),map(length(map(:,1)),3),pts_paths(m,3)
,map(length(map(:,1)),6));
        path_length = path_lengthStart+path_lengthEnd;
        % Add to path lengths
        pts_paths(m,4) = path_length;
        m=m+1;
    end
end


% find_stats_pts.m

% Given three two-dimensional points, determines the location
of the
% stationary point, its path length, and the segment of 'map'
in which it
% lies

function [stat_pts] = find_stat_pts(pts_paths,map)

% Definition of 'stat_pts':
%   Bit 1: Number of way-point to right of stationary point
%   Bit 2: x-coordinate of stationary point
%   Bit 3: y-coordinate of stationary point
%   Bit 4: Path length from start antenna to stationary point
to end
%   antenna

stat_pts = zeros(length(pts_paths)-2,4);

for i = 1:length(pts_paths)-2
    x1 = pts_paths(i,2);
    x2 = pts_paths(i+1,2);
    x3 = pts_paths(i+2,2);
    f1 = pts_paths(i,4);
    f2 = pts_paths(i+1,4);
    f3 = pts_paths(i+2,4);
    % Test whether there is a minimum or maximum
    if (f2 < f1 & f2 < f3) | (f2 > f1 & f2 > f3)
        % Find stationary point x-coordinate and path length
        [stat_pts(i,2),stat_pts(i,4)] =
find_stat_pt(x1,x2,x3,f1,f2,f3);
        % Find way-point of which stationary point lies left in
'map'
        j = 1;
        while j <= length(map(:,1)) & j ~= 0
            if stat_pts(i,2) <= map(j,3) & stat_pts(i,2) > 0
                % 'stat_pt' x-coordinate lies in this segment
of 'map'
                stat_pts(i,1) = j;
                j = 0;
            else
                % Continue searching
                j = j+1;
            end
        end
        % Find stationary point y-coordinate
```

```
        stat_pts(i,3) =
find_y_terr(stat_pts(i,2),stat_pts(i,1),map);
    end
end


% trunc_to_map.m

% Removes points in 'stat_pts' that lie outside the scope of
'map'

function [stat_pts_map] = trunc_to_map(stat_pts,map)

% Definition of 'stat_pts_map':
%   Bit 1: Number of way-point to right of stationary point
%   Bit 2: x-coordinate of stationary point
%   Bit 3: y-coordinate of stationary point
%   Bit 4: Path length from Tx to stationary point to Rx

stat_pts_map = zeros(1,4);
j = 1;
for i = 1:length(stat_pts(:,1))
    if stat_pts(i,1) ~= 0
        % Point lies inside the scope of 'map', so check
whether point
        % causes ray path to pass through terrain
        isValid = check_intn([stat_pts(i,2)
stat_pts(i,3)],stat_pts(i,1)-1,map);
        if isValid == 1
            stat_pts(i,:);
            % Ray path does not pass through terrain, so
eliminate spurii
            % Check whether stationary point lies on a corner
            x1 = map(stat_pts(i,1)-1,3);
            y1 = map(stat_pts(i,1)-1,7);
            x2 = stat_pts(i,2);
            y2 = stat_pts(i,3);
            x3 = map(stat_pts(i,1),3);
            y3 = map(stat_pts(i,1),7);
            isCorner = check_corner(x1,y1,x2,y2,x3,y3);
            if isCorner == 0
                % Stationary point does not lie on a corner, so
check
                % whether angle of incidence equals angle of
reflection
                x1 = map(1,3);
                y1 = map(1,7);
                x2 = stat_pts(i,2);
                y2 = stat_pts(i,3);
                x3 = map(stat_pts(i,1)-1,3);
                y3 = map(stat_pts(i,1)-1,7);
                x4 = map(length(map(:,1)),3);
                y4 = map(length(map(:,1)),7);
                x5 = map(stat_pts(i,1),3);
                y5 = map(stat_pts(i,1),7);
                areEqual =
incid_refl(x1,y1,x2,y2,x3,y3,x4,y4,x5,y5);
                if areEqual == 1
                    % Angle of incidence equals angle of
reflection, so
                    % store the point
                    stat_pts_map(j,:) = stat_pts(i,:);
```

```
                    j = j+1;
                end
            end
        end
    end
end


% calc_path.m

% Calculates the path length between two two-dimensional points

function [path_length] = calc_path(x1,x2,y1,y2)
path_length = sqrt((x1-x2)^2+(y1-y2)^2);


% calc_dsi_td.m

% Calculates time delay of a DSI signal

function [delay] = calc_dsi_td(distance,c)
% Calculate time delay
delay = (distance)/c;
```

A.5 Depolarisation Loss Unit

```
% calc_trans_slope.m

% Calculate transverse slope of terrain at reflection point(s)

function [trans_slope] =
calc_trans_slope(submatrix,slope,refl_pt_x)

theta = atan(slope);    % angle in radians
x = refl_pt_x*cos(theta);   % x-coordinate of reflection point
y = refl_pt_x*sin(theta);  % y-coordinate of reflection point

trans_dist = 100;  % distance on either side of reflection
point (in m)

x_dist = trans_dist*cos(pi/2-theta);
y_dist = trans_dist*sin(pi/2-theta);

% Calculate coordinates of two transverse points on either side
of
% reflection point
x1 = x-x_dist;
x2 = x+x_dist;

if slope > 0
    y1 = y-y_dist;
    y2 = y+y_dist;
else
    y1 = y+y_dist;
    y2 = y-y_dist;
end

% Look up elevations of two transverse points in submatrix
cols = 1:length(submatrix(1,:));
```

```
rows = 1:length(submatrix(:,1));
post_spacing = 90;  % originally 900 m (for 30 arc seconds)

% Look up elevation of first point
c1 = x1/post_spacing;
if c1 < 1
    c1 = 1;
end
r1 = y1/post_spacing;
if r1 < 1
    r1 = 1;
end
elev1 = interp2(cols,rows,submatrix,c1,r1);  % plays up when c1
or r1 < 1

% Look up elevation of second point
c2 = x2/post_spacing;
if c2 < 1
    c2 = 1;
end
r2 = y2/post_spacing;
if r2 < 1
    r2 = 1;
end
elev2 = interp2(cols,rows,submatrix,c2,r2);  % plays up when c2
or r2 < 1

% Calculate transverse slope
elev1 = double(elev1);
elev2 = double(elev2);
trans_slope = abs((elev2-elev1)/(2*trans_dist));



% depol_loss_unit.m

% Depolarisation Loss Unit
% This Unit calculates the power in the horizontal component of
a
% vertically polarised electric field reflected from a sloping
surface,
% given the transverse gradient of the sloping surface

function [depol_loss] = depol_loss_unit(slope)

E_i = 1;                    % incident electric field magnitude
(in V/m)
R_V = -1;                   % vertical polarisation reflection
coefficient

% Calculate angle made by slope with horizontal
alpha = atan(slope);

% Calculate magnitude of horizontal component of reflected
electric field
E_r_h = R_V*2*alpha*E_i;

% Calculate power of horizontal component of reflected electric
field
P_r_h = E_r_h^2;
P_i_v = E_i^2;
P_r_h = 4*alpha^2*P_i_v;
```

```
% Convert to decibels
P_r_h = 10*log10(P_r_h);

if P_r_h < -1000
    P_r_h = 0;
end

depol_loss = -P_r_h;
```

Bibliography

1. Acker, A. E. (1988). How to Speak Radar: Basic Fundamentals and Applications of Radar, Varian Associates.
2. Willis, N. J. (1995). Bistatic Radar. Radar Handbook. M. I. Skolnik, McGraw-Hill, Inc.
3. Howland, P. (2005). "Editorial: Passive radar systems." IEE Proceedings, Radar, Sonar and Navigation **152**(3): 105-106.
4. Griffiths, H. D. (2003). From a different perspective: principles, practice and potential of bistatic radar. Proceedings of the IEEE Conference on Radar, Adelaide.
5. Griffiths, H. D. and C. J. Baker (2003). Measurement and analysis of ambiguity functions of passive radar transmissions. Proceedings of the IEEE Conference on Radar, Adelaide.
6. Saini, R. and Cherniakov, M. (2005). "DTV signal ambiguity function analysis for radar application." IEE Proceedings, Radar, Sonar and Navigation **152**(3): 133-142.
7. Griffiths, H. D. and Baker, C. J. (2005). "Passive coherent location radar systems. Part 1: Performance prediction." IEE Proceedings, Radar, Sonar and Navigation **152**(3): 153-159.
8. Griffiths, H. D., Al-Ashwal, W.A., Ward, K.D., Tough, R.J.A., Baker, C.J. and Woodbridge, K. (2010). "Measurement and modelling of bistatic radar sea clutter." IET Radar Sonar Navigation **4**(2): 280-292.
9. Howland, P. (2005). "Editorial: Passive radar systems." IEE Proceedings, Radar, Sonar and Navigation **152**(3): 105-106.
10. Willis, N. J. and Griffiths, H. D. (ed.) (2007). Advances in Bistatic Radar, Scitech Pub. Inc.
11. Griffiths, H. D. and Baker, C. J. (2005). "Passive coherent location radar systems. Part 2: Waveform properties." IEE Proceedings, Radar, Sonar and Navigation **152**(3): 160-168.
12. Howland, P. E., Maksimiuk, D. et al. (2005). "FM radio based bistatic radar." IEE Proceedings, Radar, Sonar and Navigation **152**(3): 107-115.
13. Tan, D. K. P., Sun, H. et al. (2005). "Passive radar using Global System for Mobile communication signal: theory, implementation and measurements." IEE Proceedings, Radar, Sonar and Navigation **152**(3): 116-123.
14. He, X., Cherniakov, M. et al. (2005). "Signal detectability in SS-BSAR with GNSS non-cooperative transmitter." IEE Proceedings, Radar, Sonar and Navigation **152**(3): 124-132.
15. Morabito, A. N., Meyer, M. G. et al. (2005). "Improved computational performance for distributed passive radar processing through channelised data." IEE Proceedings, Radar, Sonar and Navigation **152**(3): 179-184.
16. Tobias, M. and Lanterman, A. D. (2005). "Probability hypothesis density-based multitarget tracking with bistatic range and Doppler observations." IEE Proc.-Radar Sonar Navig. **152**(3): 195-205.
17. Hoyuela, C. M., Terzuoli, A. J. and Wasky, R. P. (2005). "Determining possible receiver locations for passive radar." IEE Proc.-Radar Sonar Navig. **152**(3): 206-214.

18. Xiu, J.-J., He, Y., Wang, G.-H., Xiu, J.-H. and Tang, X.-M. (2005). "Constellation of multisensors in bearing-only location system." IEE Proc.-Radar Sonar Navig. **152**(3): 215-218.
19. Li, W.-C., Wei, P. and Xiao, X.-C. (2005). "TDOA and T2/R radar based target location method and performance analysis." IEE Proc.-Radar Sonar Navig. **152**(3): 219-223.
20. Kulpa, K. S. (2005). "Multi-static entirely passive detection of moving targets and its limitations." IEE Proceedings, Radar, Sonar and Navigation **152**(3): 169-173.
21. Kulpa, K. S. and Czekala, Z. (2005). "Masking effect and its removal in PCL radar." IEE Proceedings, Radar, Sonar and Navigation **152**(3): 174-178.
22. Lesturgie, M. (2005). "Use of dynamic radar signature for multistatic passive localisation of helicopter." IEE Proceedings, Radar, Sonar and Navigation **152**(6): 395-403.
23. Inggs, M., Paichard, Y. and Lange, G. (2009). Passive Coherent Location System Planning Tool. 2009 International Radar Conference "Surveillance for a Safer World" (RADAR 2009), Bordeaux, France.
24. Wan, H., Li, S. and Wang, Z. (2006). Direct Path Interference Cancellation in FM Radio-Based Passive Radar. ICSP.
25. Howland, P. E., Griffiths, H.D. and Baker, C.J. (2008). Passive Bistatic Radar. Bistatic Radar: Emerging Technology. M. Cherniakov, Wiley.
26. Saini, R., Cherniakov, M. et al. (2003). Direct Path Interference Suppression in Bistatic system: DTV Based Radar. Proceedings of the IEEE Conference on Radar, Adelaide.
27. Yardley, H. (2007). "Bistatic Radar Based on DAB Illuminators: The Evolution of a Practical System." IEEE A&E Systems Magazine **November**: 13-16.
28. Airiau, O. and Khenchaf, A. (1999). "Simulation of a complete moving polarimetric bistatic radar: Application to the maritime environment." IEEE 1999 International Geoscience and Remote Sensing Symposium. IGARSS'99 (Cat. No.99CH36293): 2751-2753 vol.2755.
29. Scott, I. (2001). "Development of a complete radar system model." Proceedings of the 2001 IEEE Radar Conference (Cat. No.01CH37200): 35-40.
30. Han, L.-J., Chen, Z.-M. et al. (2007). Modeling of varying geometrical scenarios of bistatic radar. Proceedings of 2007 International Symposium on Intelligent Signal Processing and Communication Systems.
31. Liu, N., Zhang, L. et al. (2008). Clutter modeling and analysis for spaceborne bistatic radar. Institution of Engineering and Technology International Conference on Radar Systems 2007.
32. Geng, X., Yan, H. and Wang, Y. (2008). "A Two-Dimensional Spectrum Model for General Bistatic SAR." IEEE Transactions on Geoscience and Remote Sensing **46**(8): 2216-2223.
33. Du, L., Wang, Y.-P. et al. (2007). "Analytic modeling and three-dimensional imaging of downward-looking SAR using bistatic uniform linear array antennas." 2007 1st Asian and Pacific Conference on Synthetic Aperture Radar: 536-540.
34. Franceschetti, G., Iodice, A., Perna, S. and Riccio, D. (2006). "Efficient Simulation of Airborne SAR Raw Data of Extended Scenes." IEEE Transactions on Geoscience and Remote Sensing **44**(10): 2851-2860.

35. Villard, L., P. Borderies, et al. (2006). "Bistatic synthetic aperture radar simulation for forests including border effects." Proceedings of 2006 CIE International Conference on Radar: 1339-1342 vol.1332.
36. Gebhardt, U., Loffeld, O. et al. (2006). "Bistatic spaceborne/airborne experiment: geometrical modeling and simulation." 2006 IEEE International Symposium on Geoscience and Remote Sensing: 1884-1887.
37. Comblet, F., Khenchaf, A. et al. (2006). "Bistatic synthetic aperture radar imaging: theory, simulations, and validations." IEEE Transactions on Antennas and Propagation **54**(11): 3529-3540.
38. Wu, Y., Wang, H. et al. (2006). "Study and simulation on bistatic SAR." 2006 7th International Symposium on Antennas, Propagation & EM Theory: 4 -4.
39. Comblet, F., Pellen, F. et al. (2005). "Bistatic SAR: theory and simulation." 2005 IEEE Antennas and Propagation Society International Symposium (IEEE Cat. No. 05CH37629) **2A**: 664-667.
40. Loffeld, O., Nies, H. et al. (2004). "Models and useful relations for bistatic SAR processing." IEEE Transactions on Geoscience and Remote Sensing **42**(10): 2031-2038.
41. Hawkins, R. K., Gibson, J.R., Saper, R. and Hilaire, M. (2003). "A Tool for Bistatic SAR Geometry Determinations." Advances in Space Research **32**(11): 2311-2318.
42. Paichard, Y., Brooker, M. and Inggs, M. (2010). "Signal Level Simulator for Netted Text Radar Waveforms Evaluation." IEEE A&E Systems Magazine (March): 27-29.
43. Brooker, M. and M. Inggs (2011). "A Signal Level Simulator for Multistatic and Netted Radar Systems." IEEE Trans. AES **47**(1): 178-186.
44. Weiss, A. (2012). A Flexible and Reliable Radar Simulator in Matlab OOP for Optimizing Tracking Algorithms. EUROCAST 2011, Part 1, LNCS 6927. Moreno-Diaz, R. et al.**:** 472-476.
45. Berry, P. E., Currie, G. et al. (2011). A Generic Phased Array Radar Model for Detailed Radar Performance Assessment. 19th International Congress on Modelling and Simulation, 12-16 December 2011, Perth, Australia.
46. Birta, L. G. & Arbez, G. (2007). Modelling and Simulation: Exploring Dynamic System Behaviour. London, Springer-Verlag.
47. Levanon, N. (1988). Radar Principles, John Wiley and Sons.
48. Wikipedia entry for "University of Bath" [Online] Available: www.wikipedia.org/wiki/University_of_Bath [Nov 17, 2008],
49. "mb21 UK Broadcast Transmission" website [Online] Available: www.tx.mb21.co.uk/gallery/index.php [Nov 17, 2008].
50. Shuttle Radar Topography Mission detailed elevation models [Online] Available: ftp://e0srp01u.ecs.nasa.gov/srtm/version2/SRTM3 [Mar 23, 2009].
51. Wikipedia entry for "Mount Lofty" [Online] Available: www.wikipedia.org/wiki/Mount_Lofty [Jun 5, 2012].
52. Saunders, S. R. (1999). Antennas and Propagation for Wireless Communication Systems, John Wiley and Sons, Ltd.
53. Coleman, C. (2004). An Introduction to Radio Frequency Engineering, Cambridge University Press.

54. Abramowitz, M. E. and Stegun , I. E. (1970). Handbook of Mathematical Functions, Dover Publications, Inc.
55. Bullington, K. (1947). "Radio Propagation at Frequencies Above 30 Megacycles." Proceedings of the IRE - Waves and Electrons Section **35**(10): 1122-1136.
56. Blaunstein, N. (2000). Radio Propagation in Cellular Networks, Artech House.
57. Ong, L. C. and Constantinou, C. C. (1996). "Diffraction over an infinitely wide plateau." IEE Proc. - Microw. Antennas Propag. **143**(1): 94-96.
58. Yourgrau, W. and M., S. (1968). Fermat's Principle of Least Time. Variational Principles in Dynamics and Quantum Theory, Dover Publications, Inc.**:** 11-18.
59. Bhattacharyya, A. K. and D. L. Sengupta (1991). Radar Cross Section Analysis and Control, Artech House, Inc.
60. Coleman, C. and Yardley, H. (2008). "Passive bistatic radar based on target illuminations by digital audio broadcasting." IET Radar Sonar Navigation **2**(5): 366-375.
61. Voors, A. (2011). "Numerical Electromagnetics Code (4nec2)", v. 5.8.4.
62. Lawrence Livermore Laboratory (1996). NEC-2 Manual, Part III: User's Guide, Lawrence Livermore Laboratory.
63. Knott, E.F., Shaeffer, J.F. and Tuley, M.T. (2004) Radar Cross Section, Raleigh, N.C., SciTech Publishing, Inc.
64. Stutzman, W. L. and Thiele, G. A. (1998). Antenna Theory and Design, John Wiley and Sons, Inc.
65. UK Free-TV "Bath (Bath and North East Somerset, England) DAB Transmitter" [Online] Available: http://www.ukfree.tv/dabtx.php?tx=ST769655 [Jun 1, 2012].
66. Levy, M. F. (1990). "Parabolic equation modelling of propagation over irregular terrain." Electronics Letters **26**(15): 1153-1155.
67. Galloway, P. (2009) "A Network Application Interface for RCS Calculations." ARMMS RF and Microwave Society, 23-24 November 2009, Northamptonshire, UK.
68. Coleman, C. (2009). Mitigating the effect of direct signal interference in passive bistatic radar. Radar Conference - Surveillance for a Safer World. Bordeaux**:** 1-4.